CANADIAN THESES

THÈSES CANADIENNES

NOTICE

The quality of this microfiche is heavily dependent upon the quality of the original thesis submitted for microfilming. Every effort has been made to ensure the highest quality of reproduction possible.

If pages are missing, contact the university which granted the degree.

Some pages may have indistinct print especially if the original pages were typed with a poor typewriter ribbon or if the university sent us an inferior photocopy.

Previously copyrighted materials (journal articles, published tests, etc.) are not filmed.

Reproduction in full or in part of this film is governed by the Canadian Copyright Act, R.S.C. 1970, c. C-30. Please read the authorization forms which accompany this thesis.

AVIS

La qualité de cette microfiche dépend grandement de la qualité de la thèse soumise au microfilmage. Nous avons tout fait pour assurer une qualité supérieure de reproduction.

S'il manque des pages, veuillez communiquer avec l'université qui a conféré le grade.

La qualité d'impression de certaines pages peut laisser à désirer, surtout si les pages originales ont été dactylographiées à l'aide d'un ruban usé ou si l'université nous a fait parvenir une photocopie de qualité inférieure.

Les documents qui font déjà l'objet d'un droit d'auteur (articles de revue, examens publiés, etc.) ne sont pas microfilmés.

La reproduction, même partielle, de ce microfilm est soumise à la Loi canadienne sur le droit d'auteur, SRC 1970, c. C-30. Veuillez prendre connaissance des formules d'autorisation qui accompagnent cette thèse.

THIS DISSERTATION HAS BEEN MICROFILMED EXACTLY AS RECEIVED

LA THÈSE A ÉTÉ MICROFILMÉE TELLE QUE NOUS L'AVONS REÇUE

Buckling of Glass-Reinforced Plastic Filament-Wound Pressure Vessels Under Hydrostatic External Pressure

Paul Ouellette

A Thesis

in

The Department

of

Mechanical Engineering

Presented in Partial Fulfillment of the Requirements
for the Degree of Master of Engineering at
Concordia University
Montréal, Québec, Canada

September 1985

ABSTRACT

Buckling
of Glass-Reinforced Plastic Filament-Wound
Pressure Vessels
Under Hydrostatic External Pressure

Paul Ouellette

In the wake of developments in the aerospace, aviation, and automotive fields, industry in general has discovered the advantages that composite structures can provide. One of the earlier users of composite shells was the tank and pressure vessel fabricating industry. A widely used composite in this sector is plastic reinforced with glass fibers because of its combination of strength, corrosion resistance, and cost competitiveness. Along with increasing use has come the incentive to establish norms for the design of these structures. It is the purpose of the present work to examine some design rules and guidelines for glass-reinforced plastic filament-wound cylindrical shells subjected to hydrostatic external pressure tending to produce buckling. Experimental results are obtained on 4 tubes about 0.9 m long, with a radius of about 0.14 m. Two of these tubes have corrosion barriers while the others have only the filament-wound structural layers. The experimental results include an imperfection survey on the tubes (which

were produced with commercial techniques and equipment), and buckling pressure. Three procedures for predicting the buckling pressure are selected for comparison with the observations. These are: an analysis first presented by Cheng and Ho in 1963, the French Standard, and an ASME Draft Proposal. The latter two are simpler, but all virtually require computer coding in practice. The Proposal gives the most conservative design pressure, while the other two allow for higher pressures, i.e. the possibility of a less expensive product. It is interesting that the ultimate collapse pressures are about three times higher than the identified buckling pressures, providing an added margin of safety with these structures.

ACKNOWLEDGEMENT

I want to thank Professor S.V. Hoa, my supervisor, for pointing out this topic. Thanks to his enthusiasm on the subject of Composite Materials and his ready availability to discuss related matters, my work was made more pleasant. I also thank Chairman T.S. Sankar who, together with Professor Hoa, helped to secure finiancial assistance for me over the last three years, in large part from the Quebec government's FCAC programme.

The tubes were fabricated by C P F Dualam Ltd., Montréal Nord, and their cooperation is greatly appreciated.

I am also indebted to the technical staff of Mechanical Engineering for their help in the material set-up for the experiments.

TABLE OF CONTENTS

LIST OF TABLES

LIST OF FIGURES

LIST OF APPENDICES

I:1.0 INTRODUCTION

"(a) What is the question?

"(b) What was done about it?

"(c) What was learned?"[1]*

This thesis will attempt to follow this simple and elegant outline of what an engineering document should answer. Thus, three different sections will deal with these three queries.

The present section will expose the answer to the first question and outline the motivation for asking it. In doing so, the literature on the topic will be discussed briefly, and the relevant work done by others will be brought together to form the base upon which the present investigation will build.

The second section will be concerned with the experimental techniques and analytical approaches used to try to answer question (b) above.

The third and final section will examine the results flowing from the work described in the second section. The

---

* Numbers in brackets designate References at the end of this thesis.

knowledge gained in the course of the study will be discussed with the aim of assessing practical applications. The shortcomings of the work will be mentioned in the hope that future efforts will benefit therefrom.

I.1.1 "What is the question?"

The work undertaken here tries to answer the question:

> Among the buckling design procedures available, which one(s) give(s) results combining both ease of application and good agreement with experimental data for the loads and materials which concern us here?

This question can conveniently be divided into three parts.

Part 1. Buckling design procedures may be simply expressed in a few equations, or they may require relatively complex and extensive computations best handled by a digital computer. The latter case may include complex codes which "...require much sophisticated knowledge of computer analysis and shell behavior."[2] Obviously, "ease of application" and "good agreement with experimental data" will mean different things to different people. It is hoped that readers will be able to come to a tacit consensus on what "good agreement" should mean after having read this Introduction. As for "ease of application", readers should keep in mind that those for whom these results might be

useful may, at best, have access to small personal computers. The necessity for greater sophistication should thus be understood to imply "difficulty of application".

Part 2. The procedures will only apply to hydrostatic buckling loads. These are loads which are uniform over the entire surface of the vessel. Such a vessel would be subjected to a pressure difference, with the external pressure being greater than the internal pressure.

Part 3. The materials of which our test structures are made are a specific class of composite. The reinforcement is continuous glass roving and the matrix in which it is imbedded is plastic. The shells are made by a process called filament winding. More will be said on this subject in Section II. (The interested reader will find much information on materials and fabrication methods in [3].) Having defined the question, Figure 1 will help situate this work in the broader field of Stability Analysis.

The purpose of this thesis then is to briefly consider the work done over the last one hundred thirty years, but more particularly over the last twenty-five to thirty years when composite shells started to be used in various applications. The information thus gathered will be used to address the specific technical problem of filament-wound

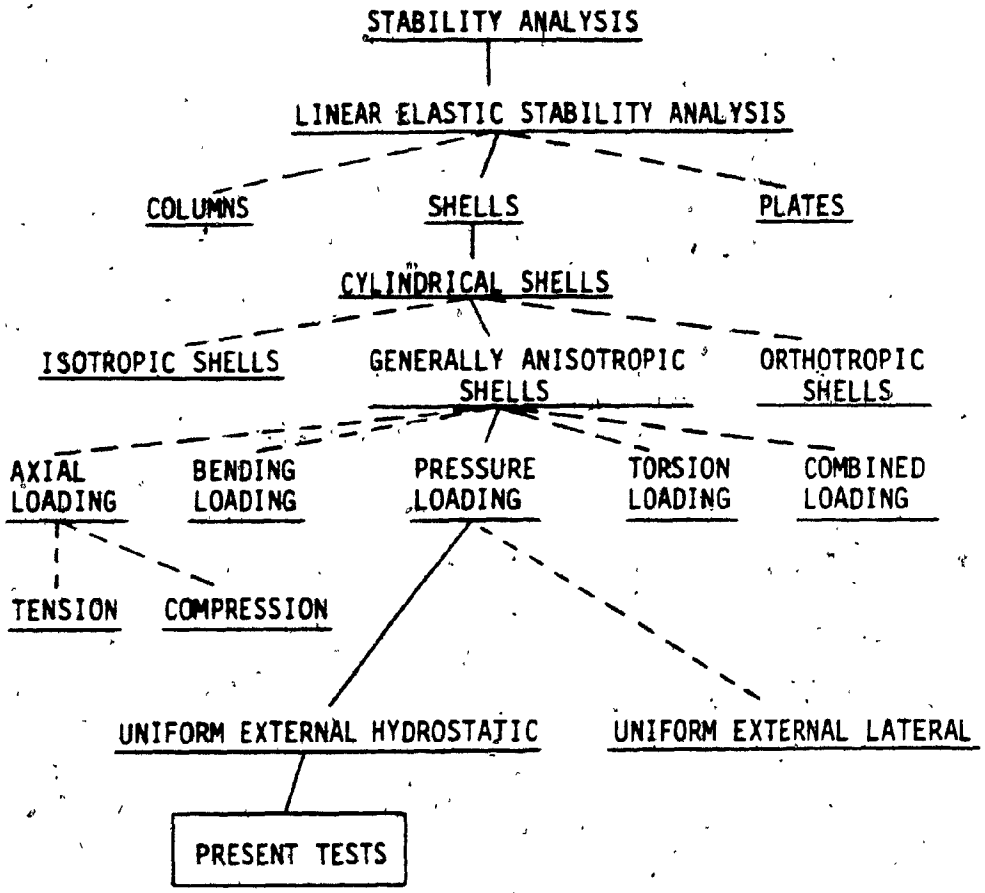

Figure 1. The situation of the present topic in the broad field of Stability Analysis.

glass fiber reinforced plastic vessels subjected to hydostatic pressure buckling loads.

I.1.2 Motivation for the question

When a fabricator must supply a pressure vessel to an end-user, he usually must comply with certain specifications. In some cases, the end-user will refer to standards which are voluntary industry standards or which may be legal requirements. In either case, the designer has guidelines to determine the parameters of the vessel. In the absence of such standards, the parties must reach an agreement on the appropriate design, a process which can cause delays and misunderstandings.

The design of filament-wound composite pressure vessels against buckling failure is one instance where standards do not exist in North America. ASME Section X on Fiberglass Reinforced Plastic Pressure Vessels [4], Part G-121(c) specifically excludes "...vessels having an internal or external operating pressure not exceeding 15 psig (100 kPa) with no limitation on size." While article D-3 specifies mandatory rules for qualifying vessels under external pressure, no formulas are provided for design. A design can only be qualified by testing one vessel to destruction according to a specified loading schedule. When only one

vessel is required by the end-user, this becomes an expensive proposition.

There is a draft proposal which has just been circulated to members of Subcommittee X on FRP Vessels. This is not yet a standard. It was developed by the Reinforced Thermoset Plastic Committee of the ASME and it covers containers, including those made by filament-winding, at up to full vacuum. This proposal will be considered in Section II.2.2.1.

British Standard BS 4994 1973, Vessels and Tanks in Reinforced Plastics [5], deals specifically with glass-mat and woven roving reinforcements, but not with filament-wound structures. The design method requires that the material extensibility be known for all layers, and only values for chopped strand mat and woven roving cloth are standardized in Table 2 of the code. External pressures up to 1.0 bars are considered in the standard, which is thus sufficient for conditions up to full vacuum. Because filament-wound materials are not specifically included, this standard will not be used here. Furthermore, no explicit equations for critical pressure are given, since the procedure is based on a try-and-check iterative method.

There is a French standard which deals with filament-wound vessels subjected to buckling loads, viz.

Code de construction des appareils chaudronnes en plastique armé [6], which was published in December 1976. Article 3.11 is specifically directed to cases of vessels under external pressure or vacuum, and it gives design formulas. This Standard will be considered in Section II.2.2.2.

Since an appropriate code has not yet been adopted by the ASME, more data would be useful. In a review article of 1981, the author could write on the buckling of composite shells : "Additional observations of experiments and measurement [of geometric imperfections] on practical structures are required ...."[7]

I.2.1 Literature Survey

I.2.1.1 General

According to [8], the first experiments in tube buckling were reported by W. Fairbairn in 1858, subsequent to "... the great increase in the number of boiler-explosions ...." The theory of elasticity, developed after 1820, was applied to shells for the first time in 1874.[9] After some experimental investigations by Lilly in 1908, Lorenz and Timoshenko independently analyzed shells under uniform axial compression around 1910.[10,11] The classical critical buckling stress formula for this loading

case resulted from this work. In 1911, Lorenz investigated the buckling of cylindrical shells under uniform lateral pressure.[11] By 1914, von Mises and Southwell reported on the problem of thin shells buckling under axial compression and lateral pressure.[10,11] In 1929, Von Mises published results for thin shells buckling under combinations of axial compression and lateral pressures, and he presented a formula for calculating the critical pressure in the case of a closed shell under uniform external pressure. This formula gave reasonably accurate predictions for thin vessels buckling within their elastic domain.[11]

After the mid 1920's, experiments were performed on shells much thinner than had previously been used. As a result, investigators found very large discrepancies between predicted critical loads and actual buckling loads. In 1932, Flügge analyzed thin shells and took into consideration the actual pre-buckling shape due to end constraints and included idealized axial and circumferential shape imperfection patterns.[10] At the same time, Donnell was doing work in which he used assumed shape imperfections and large deflection theory. These attempts succeeded in closing the gap somewhat between theory and experiments. These and many other investigations have shown that shells under axial compression are very sensitive to shape imperfections, thickness variations, boundary conditions, and loading methods.[12] (Indeed, Fairbairn, one hundred and

thirty years ago, had reported on the difference in boiler tubes made with lap joints versus tubes made with butt joints which were 50% stronger.[8])

For the case of lateral pressure, Donnell, in 1956 [13], published results tending to explain the lesser sensitivity of this load case (which experimenters had already discovered). Twelve years later, a paper was published showing that, for values of Z (Batdorf's parameter) between 100 and 1000, the hydrostatically loaded cylinder is intermediate in imperfection sensitivity between the axially loaded and laterally pressurized cylinder.[14]

I.2.1.2 Anisotropic Shells

The first reference found to shells of anisotropic materials dates from 1924, by Shtaerman, in which specially orthotropic shells of revolution under axisymmetric static loads were analyzed.[15] There is a relatively large body of Soviet work on this subject, dating from the 1930's on. The reader who can consult these publications in Russian should see the review article by Ambartsumian.[16] In 1932, Flügge treated an anisotropic shell problem using small-deflection theory.[17] During the 1940's, workers at the Forest Products Lab (USA) performed experimental and theoretical studies of thin plywood shells subjected to various buckling loads.[18] Starting in the 1950's, filament-wound shell

structures were used as rocket motor casings. Since the aerospace industries were the first to use polymer composite structures extensively, and since the shells they made were subjected mostly to axial compression due to rocket thrust and accelerations, it is not surprising that most of the work during this period considered buckling in axial compression. Concurrently, several theoretical treatments of orthotropic shells subjected to buckling were produced.[18] Among these, one used Flügge's linear analysis for the case of orthotropic cylinders under various loadings and simple supports.[19] In 1963, two papers were published by the same co-authors.[20,21] They gave the analysis for general laminated anisotropic shells under combined loadings and for four simple and four clamped end conditions. Flügge's linear analysis was adopted, with a procedure due to Donnell for satisfying the boundary conditions. Others have used Donnell's shell equations.[22] These two types (Flügge and Donnell) were compared in [23] and negligible differences were reported for the system studied. In [24], the results of [21] are compared with results obtained using Donnell's equilibrium equations with a solution method due to Batdorf. Again, for the plywood, three layer shells considered, good agreement for simply supported boundary conditions was found, especially for length-to-radius ratios less than 20. In [25], an analysis very much like that in [20] was done in which four simple support and four clamped support conditions were considered, although the shell was

restricted to orthotropic behaviour. Buckling loads were included in a 1968 report devoted to mechanical behavior of some filament-wound cylinders.[26] The ratio of experimental critical lateral pressure to the predicted value varied from 0.79 to 0.98 for the orthotropic boron-epoxy and glass-epoxy systems tested. A review report from 1981 evaluates the state-of-the-art in buckling of composite structures.[27] Plates and shells are treated. The main conclusions are: a) transverse shear effects are important for large ratios of E_{11}/E_{22}, and at high temperatures; b) differences in tensile and compressive moduli have little effect on critical loads for practical materials; c) the well known non-linear stress-strain behaviour in shear of composite materials seems to have little effect except perhaps at high temperatures; d) coupling between extension and bending should not be neglected for general laminate constructions.

II.1.0 EXPERIMENTAL PROGRAM

An experimental program was designed to generate some data for comparison with various predictive methods which will be described in Section II.2. The program consisted of four phases: first, the fabrication of the tubes using materials and practices common to suppliers of good quality pressure vessels to the chemical and pulp-and-paper industries; second, the inspection of the tubes and the recording of initial imperfections; third, the testing of the tubes to destruction; fourth, cutting samples from the failed tubes to determine glass content and to verify the wall construction and thickness. These four phases will now be addressed individually.

II.1.1 Fabrication of the Tubes

Four polymer composite tubes were made for the experimental program by CPF Dualam Ltd. They were made with materials typically used in many pressure vessel applications. The polymer matrix is a vinyl ester marketed by Dow Chemical Canada Ltd. under the name Derakane 411. Useful mechanical and physical properties are given in Table 1. The resin is activated and cured with 1% MEK Peroxide (max.) and 0.2 to 0.3% Cobalt Naphthenate. The reinforcement consisted of glass roving supplied by Fiberglas Canada under the designation E-Cr roving.

TABLE 1. Some mechanical and physical properties of the resin.

	Tensile Modulus, E (GPa)	Shear Modulus, G (GPa)	Poisson's Ratio, ν	Specific Gravity
Dow Derakane 411	3.45 *	1.28 **	0.35 ***	1.13

*Manufacturer's data.
** $G = E/[2(1+\nu)]$
*** Approximate value assumed.

TABLE 2. Some mechanical and physical properties of the glass.

	Tensile Modulus, E (GPa)	Shear Modulus, G (GPa)	Poisson's Ratio, ν	Specific Gravity
Fiberglas Can. E-Cr roving	77.2*	30.9**	0.25*	2.72*

*From: Rosenow, M.W.K., "Wind Angle Effects on Glass Reinforced Polyester Filament Wound Pipe", Thesis (Fiberglas Canada.)
** $G = E/(2(1+\nu))$

TABLE 3. Some mechanical properties of rigid PVC pipe.

	Tensile Modulus, E (GPa)	Shear Modulus, G (GPa)	Poisson's Ratio, ν
Harvel Co. PVC pipe	2.76*	1.00**	0.38***

*ASTM D 1784-65T, Type 1, Grade 1 pipe.
**$G = E/(2(1+\nu))$
***_____, Handbook of PVC Pipe Design and Construction, Uni-Bell Plastic Pipe Assoc., Dallas, 1977.

Applicable mechanical and physical properties are given in Table 2. Two of the tubes had a poly-vinyl chloride (PVC) liner which is often used to protect the structural layers of a vessel against corrosive contents. The PVC was supplied in the form of extruded pipe by Harvel Plastics. Applicable mechanical properties are given in Table 3. Note that all three constituents above are considered isotropic.

The tubes were made using the process of 'wet' filament-winding. This consists of winding continuous lengths of glass roving in the form of a band about 100 mm wide unto a rotating mandrel. The band is made up of many individual rovings each pulled from its own spool. The rovings are dipped into a bath of prepared resin and are then gathered into a band. The band and resin bath are carried back and forth along the tube length on a trolley. As the band is laid on the rotating mandrel it forms a helix. The relative speeds of mandrel rotation and trolley feed are adjusted to give the required winding angle (which is expressed with respect to the tube axis). The tube thickness is controlled by the total number of passes of the trolley. When the winding process is finished, the tube is cured on its mandrel (at ambient conditions in this case).

All four tubes were prepared on PVC pipes which served as the mandrels. For two of the tubes, a release film was put on the pipe before winding so that the tube could be

taken off the PVC pipe. For the other two, no release film was used; on curing, the PVC pipe became consolidated into the structure as the corrosion liner.

After curing, the tubes were cut to length and flanges were built up at the ends. The flanges were of glass mat and woven roving construction, while the covers were of glass mat; both were impregnated with the same resin used for the winding process.

II.1.2 Inspection of the Tubes

This second phase of the experimental program can be divided into two parts: first, the tubes were visually inspected for gross damage, delaminations, and surface flaws, and measures of winding angles and wall thickness were made; second, the initial outer surface imperfections were recorded.

Part 1. No gross damage or delaminations were observed. Lined tube 1 had two shallow scratches on its outer surface each about 10 mm long. Lined tube 2 had two inclusions of what appeared to be thread-like material at two locations near the outer surface. Some surface flaws were found on the inside surface of unlined tubes 3 and 4. The flaws were oriented in the direction of the reinforcement. Presumably, these were due to air bubbles

trapped during winding operations.

Winding angles can most accurately be measured after the tube has been tested, and cracking and ruptured rovings are evident. However, to check if destruction could affect the measured angles, tube 2 was measured before and after destruction. Both measures were the same when the helical crack pattern was taken to represent the winding angle. Thereafter, the cracking pattern produced by testing to failure was used to determine the angles for all tubes.

Wall thickness measurements were made using a Polygauge Model "C" thickness sensor. Its functioning is based on the non-magnetic property of the composite. The sensor was calibrated on a virtually flat plate (radius of curvature of 900 mm) cut out from a previously burst vessel. The sensor readings were compared to micrometer readings. The sensor readings were from 0.986 to 1.018 of the micrometer readings. (See Appendix 1 for calibration data.) Considering the non-uniformity normally encountered in the wall thickness of such structures, this accuracy is considered sufficient. The sensor thickness values were corrected for the curvature of the tubes. Table 4 lists the information gathered on the four tubes.

Part 2. As mentioned in the first section, initial shape imperfection of fabricated shell structures has been

TABLE 4. Geometric data on four tubes.

	Tube 1	Tube 2	Tube 3	Tube 4
Uncorrected total thickness [1] (mm)	6.5	6.4	3.5	3.4
Corrected total thickness, t [2] (mm)	5.8	5.7	2.8	2.7
PVC liner thickness, t_1 (mm)	4.76	4.76	N.A.	N.A.
Filament winding thickness, $(t-t_1)$ (mm)	1.04	0.94	2.8	2.7
Number of filament wound layers [3]	2	2	6	6
Winding angle (degree)	54	63	54	63
Mean inside radius, R_1 [4] (mm)	133	133	137	136
Radius to mid-surface, $(R=R_1+(t/2))$ (mm)	136	136	138	137
Tube length [5] (mm)	864	864	876	868

1. Measured at mid-length; 4 readings: C.O.V. = 3.3%, 2.7%, 6.4%, 4.4% for tubes 1,2,3,4, respectively.
2. Subtract 0.7mm from sensor readings to compensate for tube curvature.
3. One filament wound layer is about 0.5mm thick.
4. Measured at the end of the tube.
5. Excluding flanges which were about 20mm thick.

identified as one of the principal reasons for the discrepancy between experimental and predicted critical loads. While this effect is most serious for axial compression, it was decided that some data on the imperfection patterns produced by a filament-winding technique might prove useful. This is especially so, since no such information seems to have yet been published.

Accordingly, a set-up was prepared using a lathe to mount the tubes. Figure 2 shows a top view of the rig with the instrumentation shown in block form. One end of the tube is held in a 3-jaw chuck. A flat metal plate in the shape of a truncated cone slips partially into the other end. A center hole in the plate accepts the live center of the lathe tail-stock. The end plate is positioned perpendicular to the lathe bed, and the live center is locked, holding the tube in a nominally axial position with respect to the lathe spindle. A rotary potentiometer is fixed to the spindle to measure circumferential position. A linear potentiometer is fixed in the tool holder and measures radial displacement due to surface imperfections. The rotary pot drives the X-axis of an X-Y recorder while the linear pot drives the Y-axis. (See Appendices 2 and 3 for calibration data on the rotary and linear potentiometers, respectively.)

Eight circumferential scans and eight axial scans were

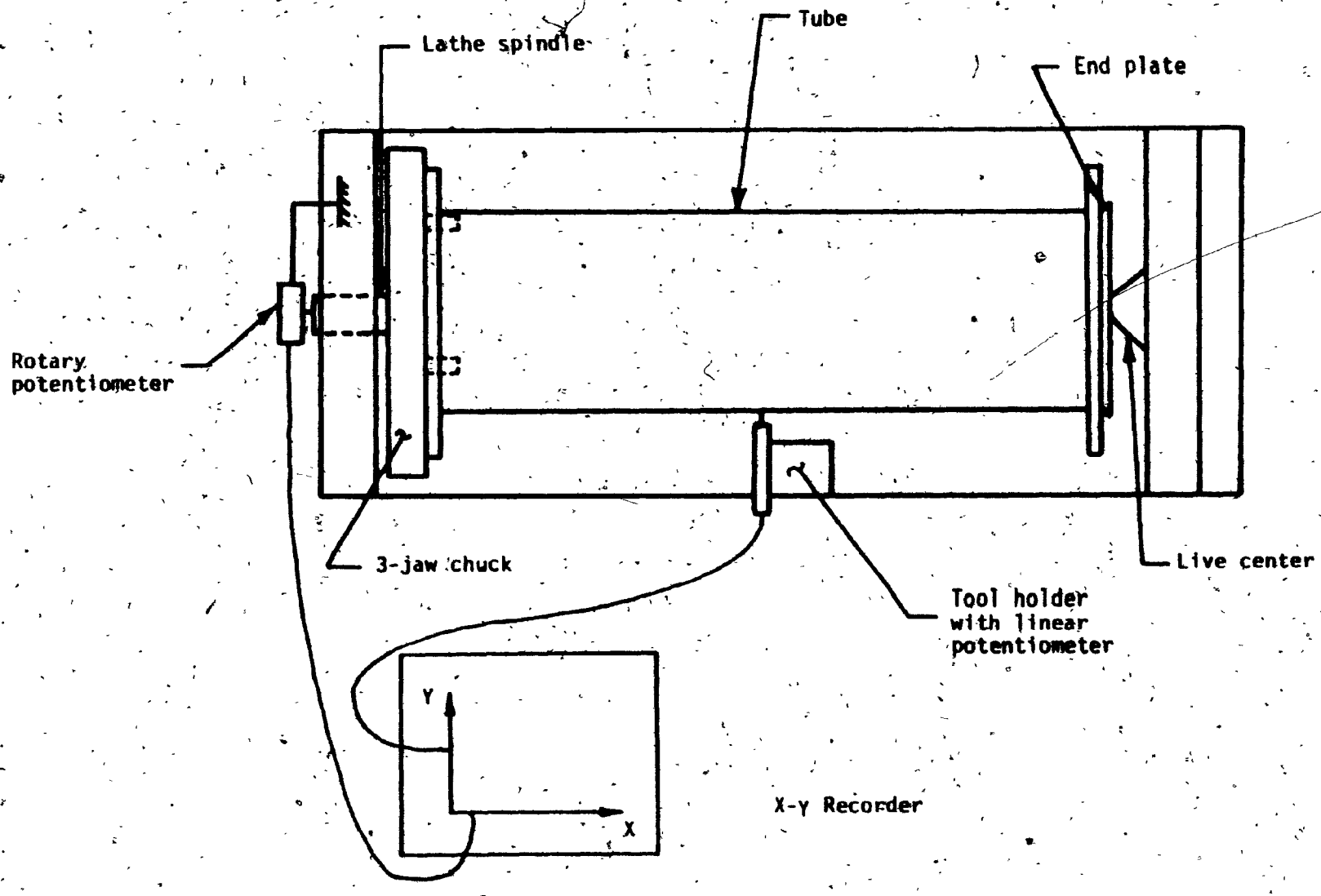

Figure 2. Set-up for initial imperfection recording.

recorded for each tube. Figure 3 shows the developed surface of a tube without the flanges and the traces of the scans. Continuous matched readout of circumferential position vs radial displacement was possible for scans around the tubes. However, for scans along the tube length no transducer was available for a readout of the axial position, and the tool holder could not be independently fed longitudinally at a known constant speed. Axial scans were generated by setting the recorder X-axis to time, and manually feeding the tool holder with its attached linear pot along the length of the tube. This method can only give an approximate correlation between axial position and radial displacement, although the relative radial displacement magnitudes are correct.

After the instruments were suitably calibrated, the scans were recorded, and they are shown in Figures 4 to 11. The circumferential scans of tube 3 and tube 4 show a clear pattern. This was less evident for tube 1, and not at all evident for tube 2. Therefore a spectral analysis was made to see if patterns could be extracted from the circumferential scans of these two tubes.

The set-up of Figure 2 was used, except that the output from the radial pot was directed to an FFT analyzer while the tubes were rotated at a nominal 30 rpm on the lathe. As a check on the method, scan 5 from tube 3, and scan 3 from

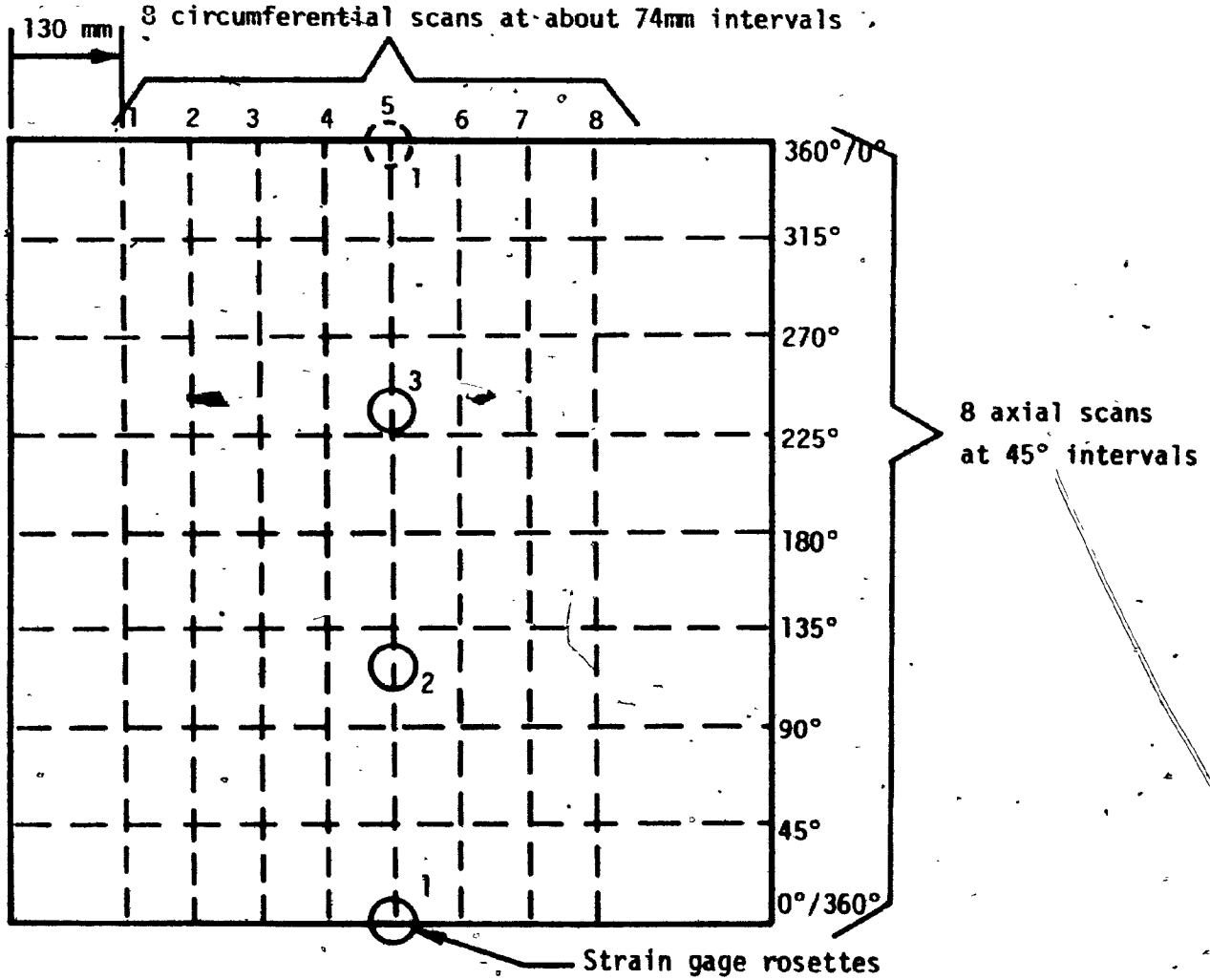

Figure 3. Developed surface of typical tube showing scan lines and strain gage positions.

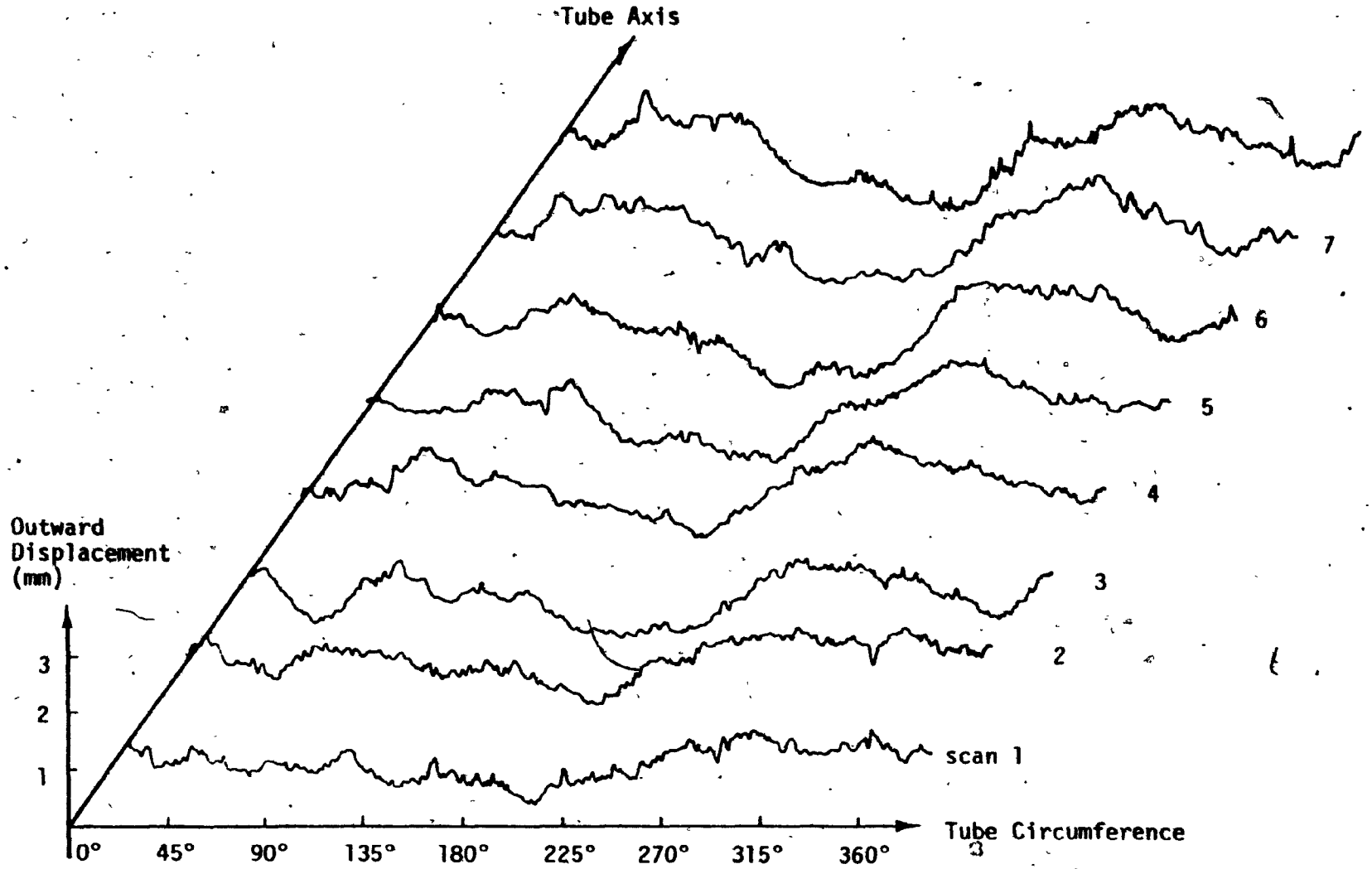

Figure 4. Circumferential scans of tube 1. Two wave-lengths can be discerned.

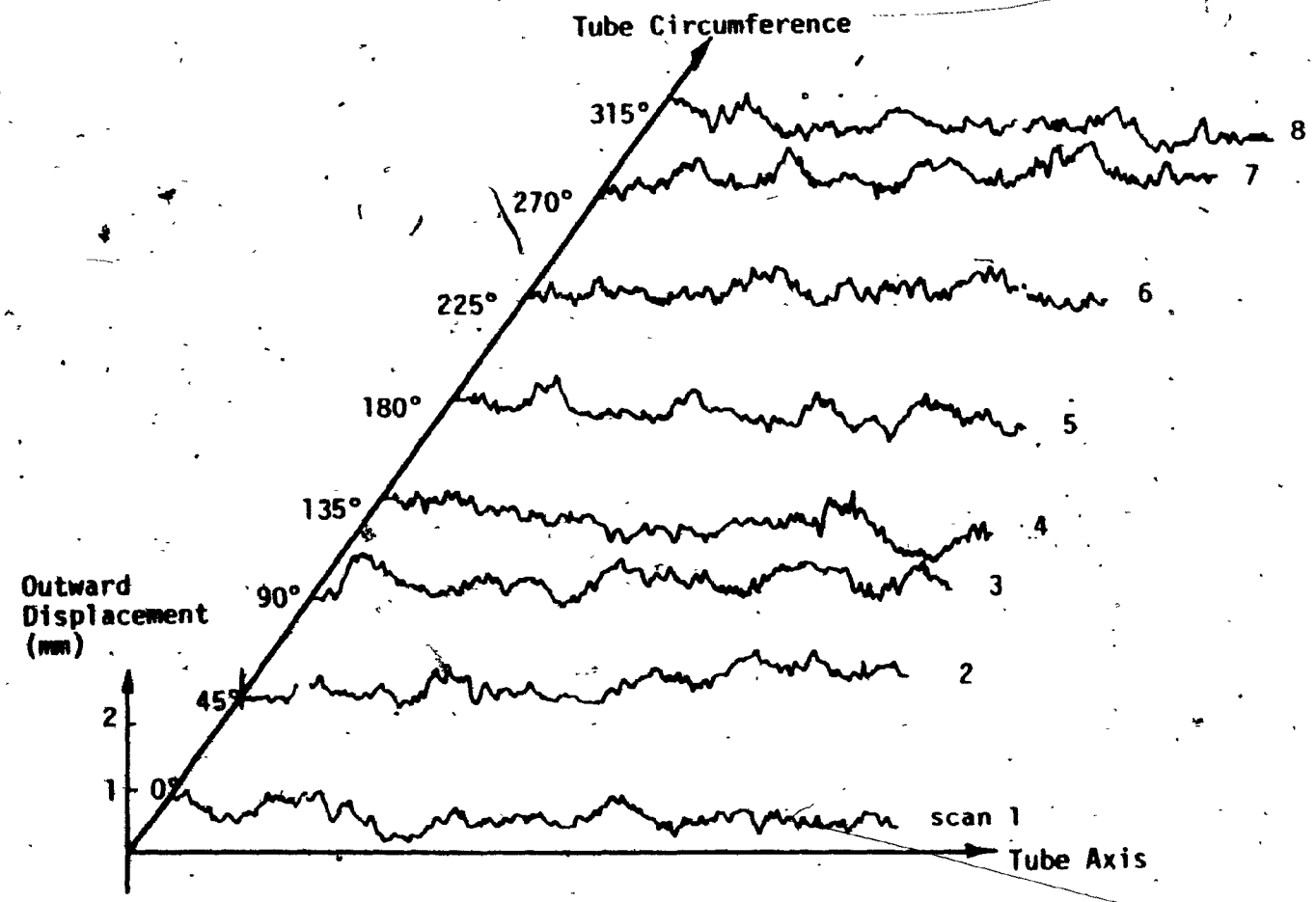

Figure 5. Axial scans of tube 1. No clear wave pattern can be identified.

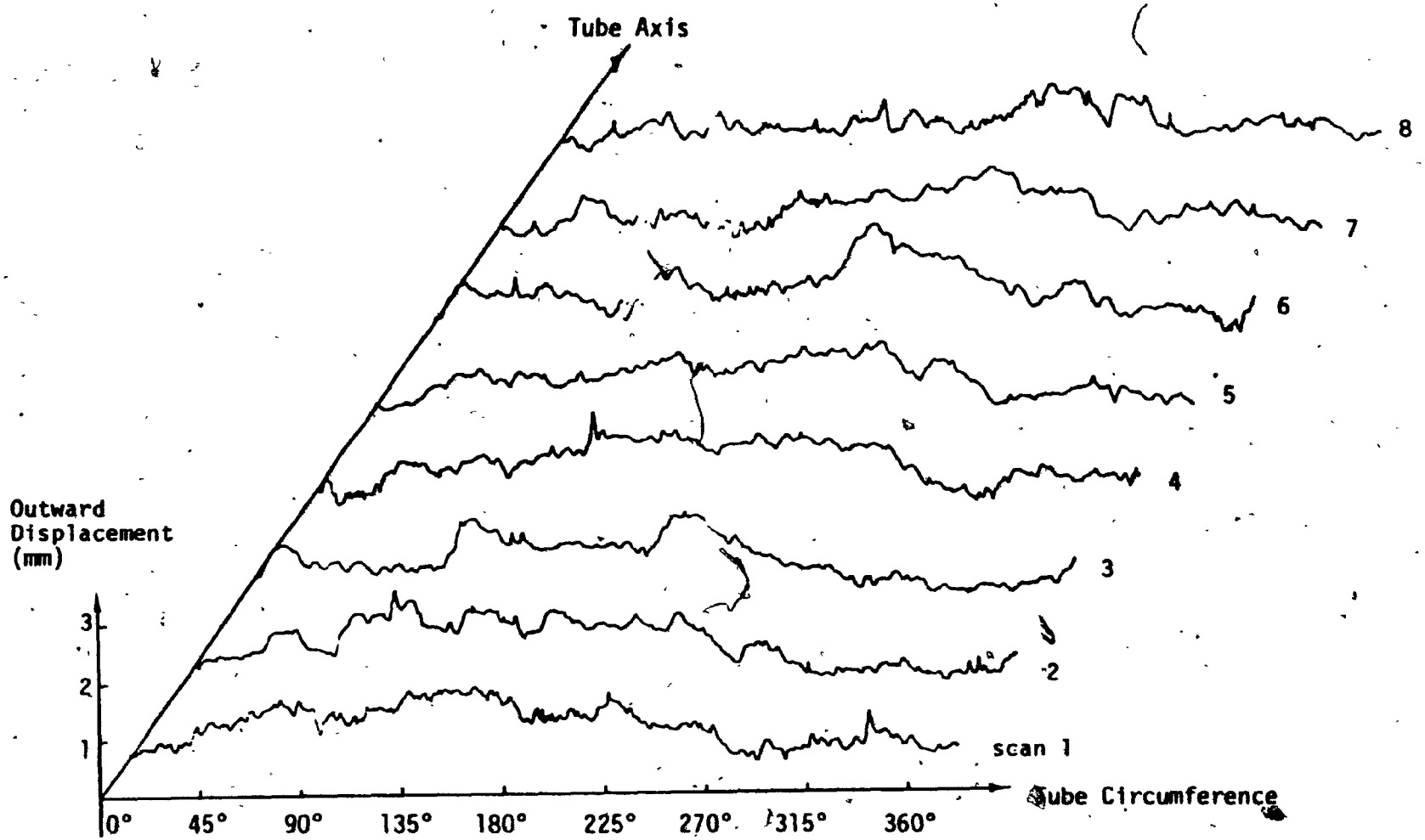

Figure 6. Circumferential scans of tube 2. No clear pattern can be seen.

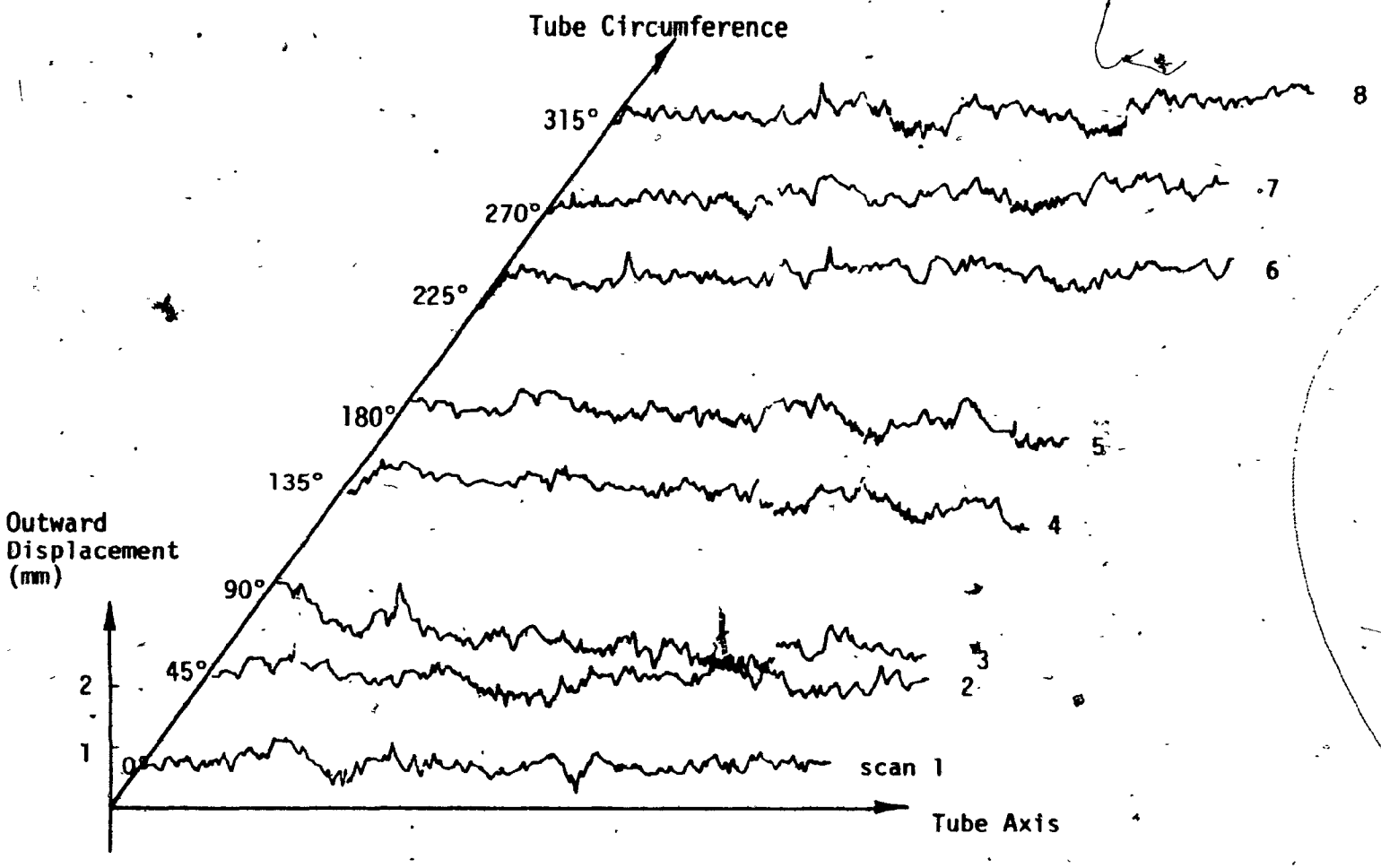

Figure 7. Axial scans of tube 2. Similar to random imperfections of tube 1.

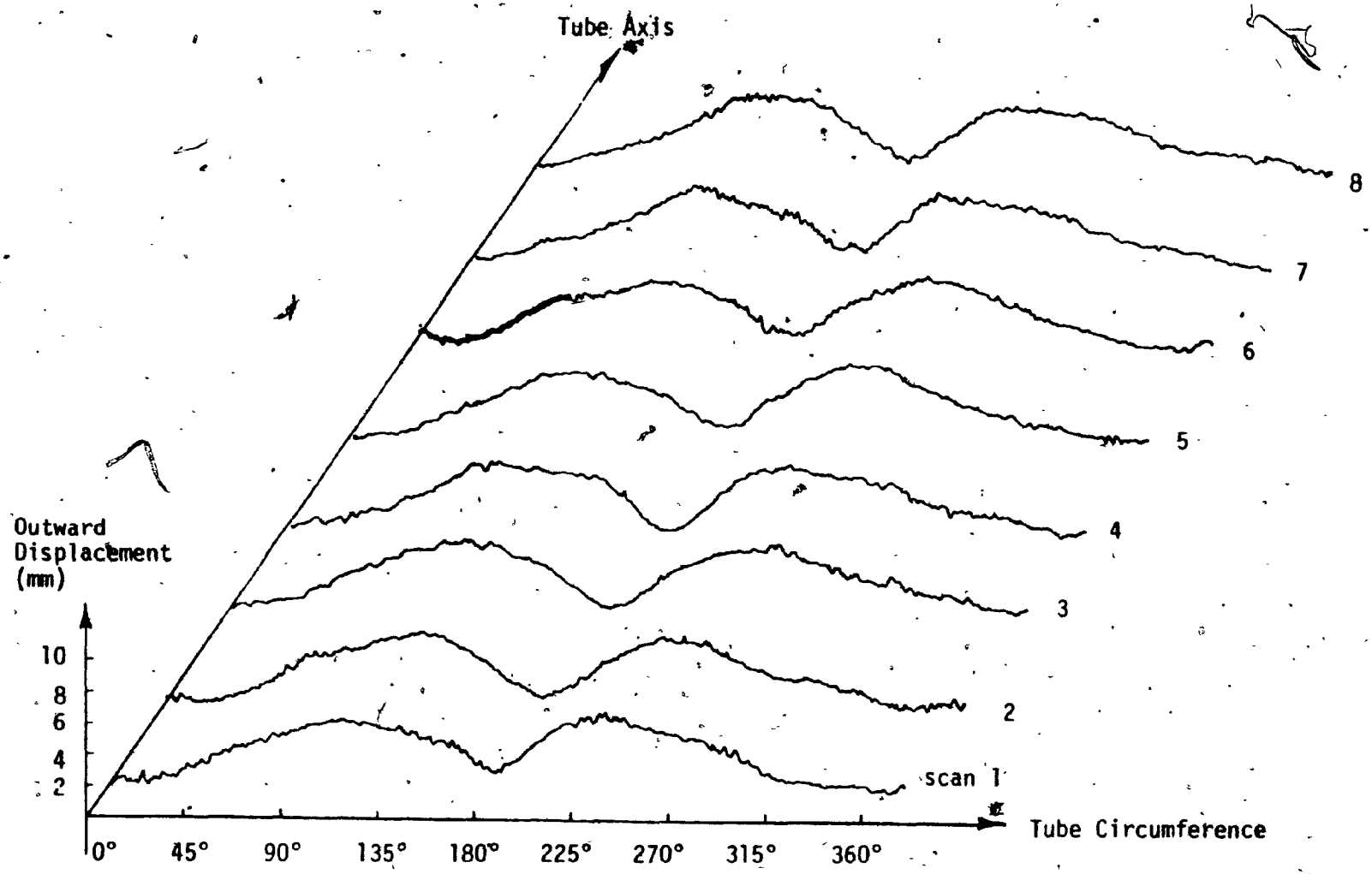

Figure 8. Circumferential scans of tube 3. Two wave-lengths are evident.

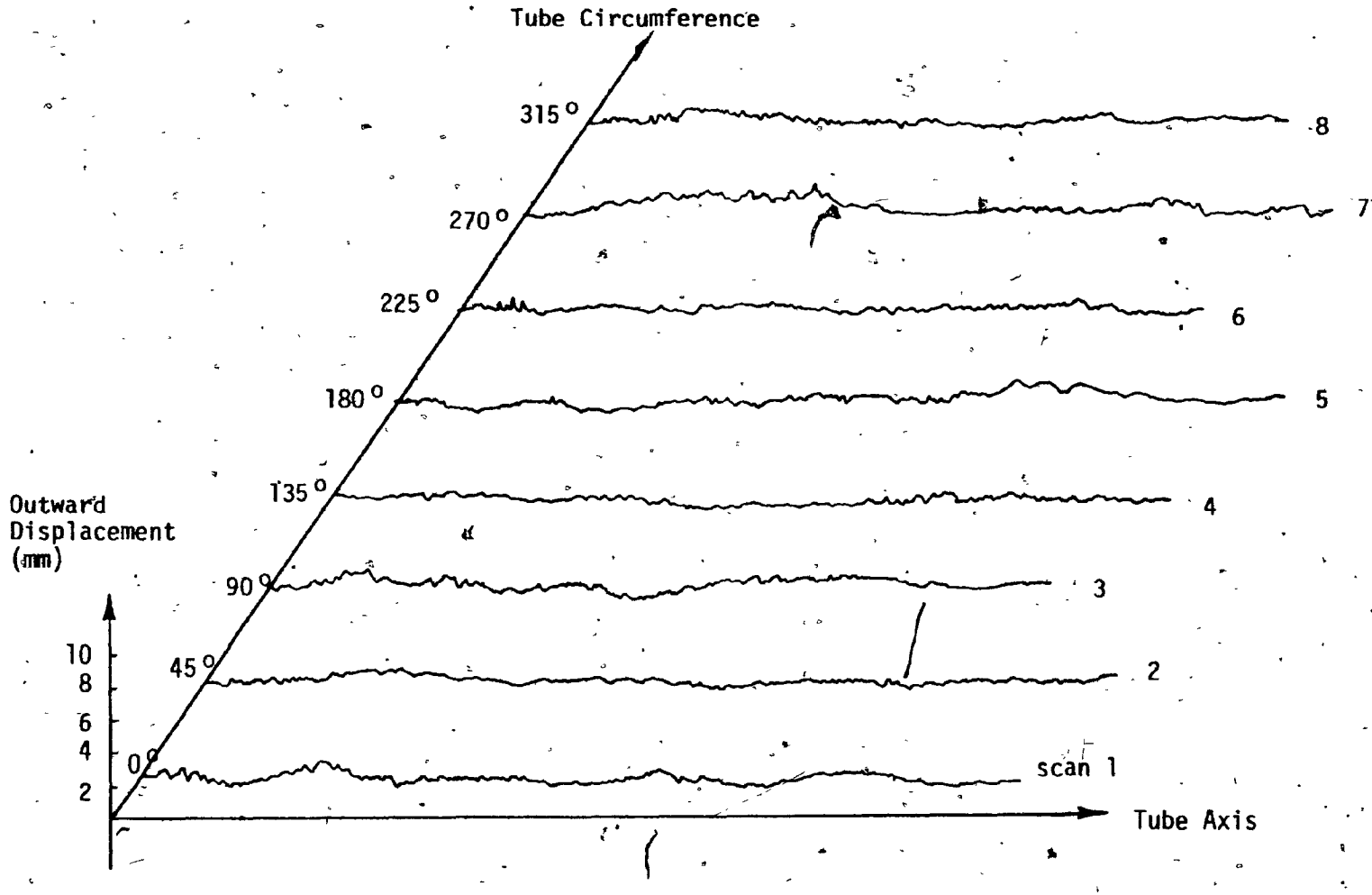

Figure 9. Axial scans of tube 3. The amplitudes are much smaller than those recorded in circumferential scans. No pattern is evident.

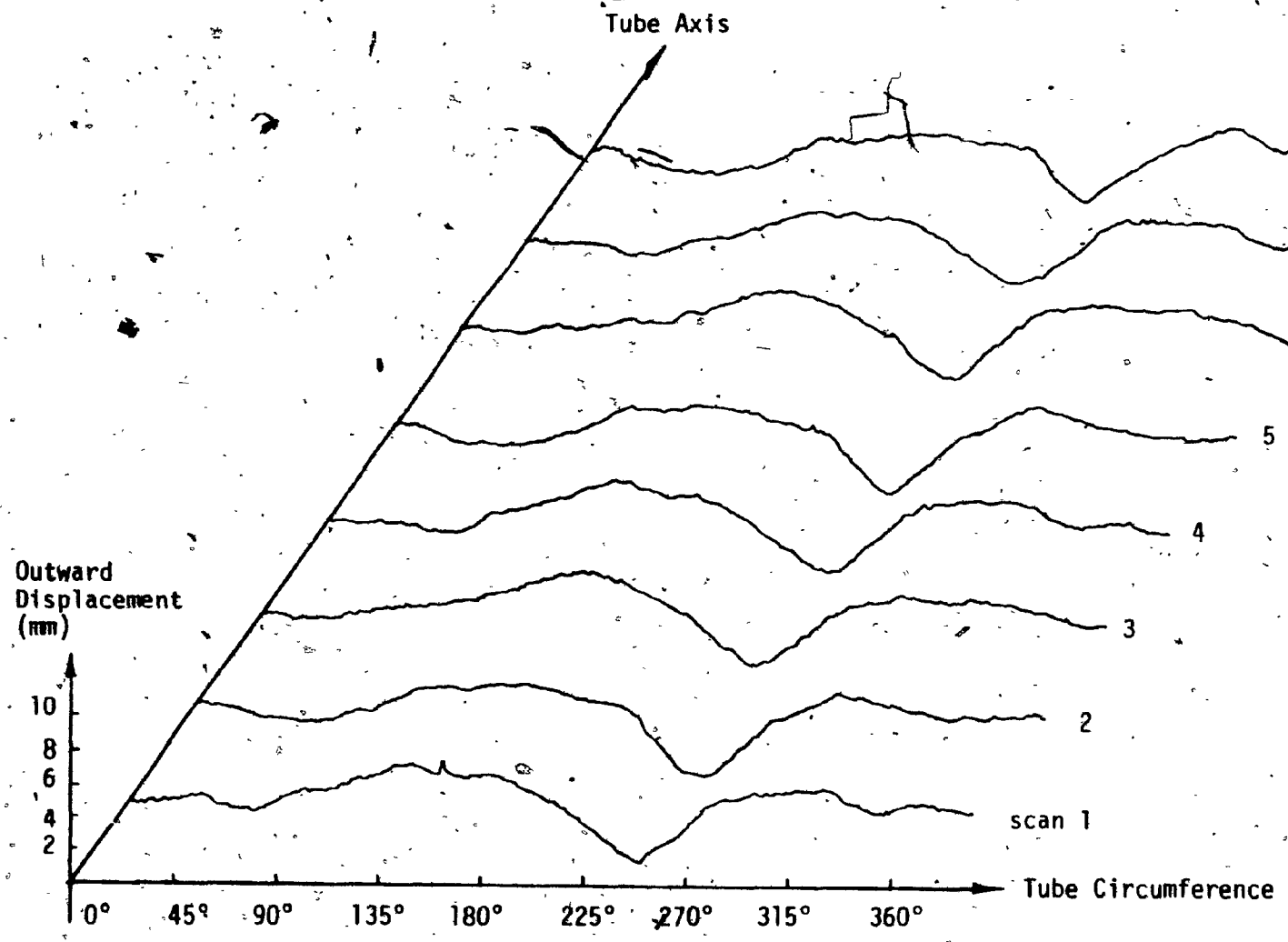

Figure 10. Circumferential scans of tube 4. The two wave-length pattern is the same as for tube-3, and amplitudes are similar.

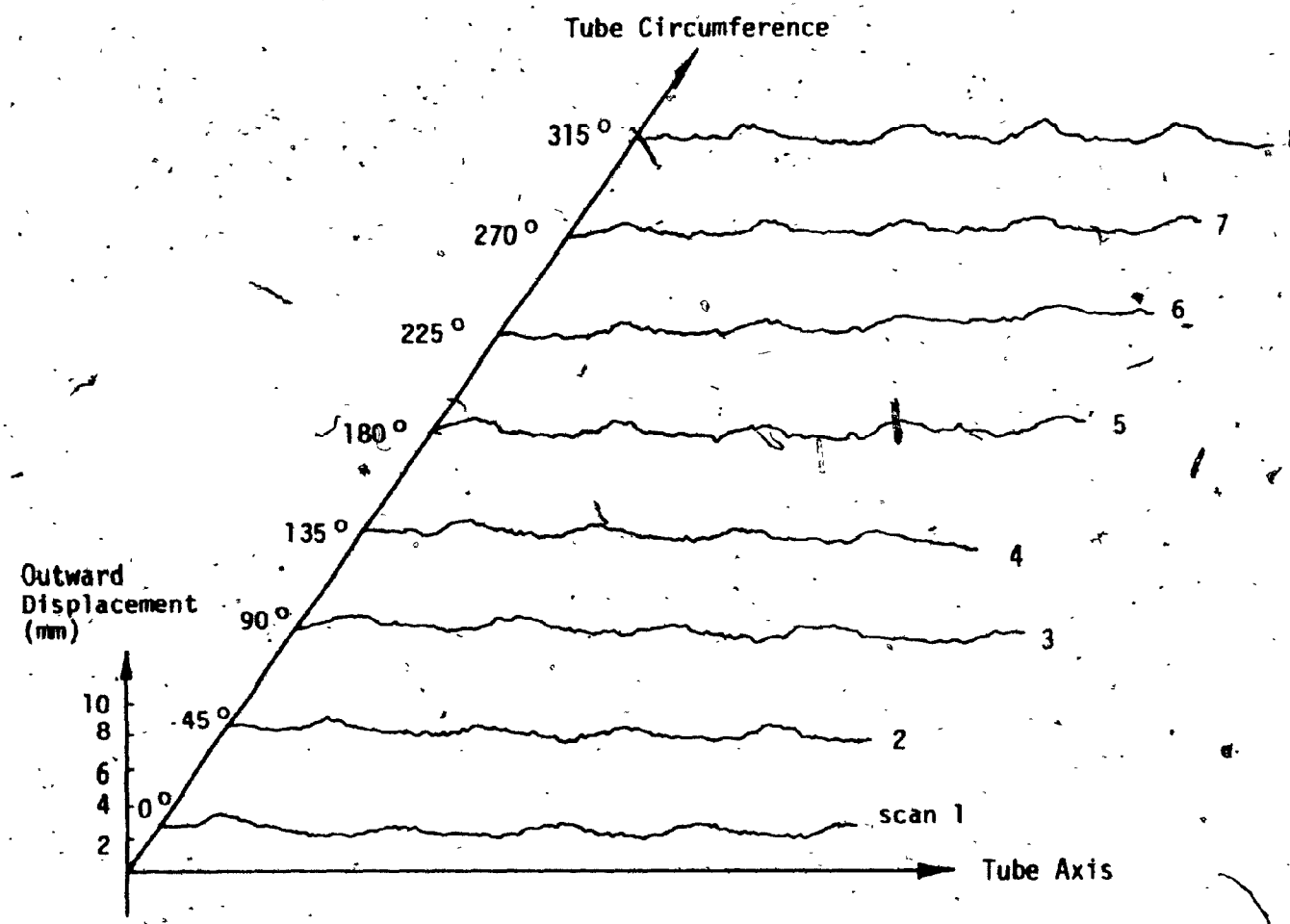

Figure 11. Axial scans of tube 4. Again the amplitudes of imperfections are considerably smaller than in the circumferential scans.

tube 4 were recorded since these give a clear imperfection pattern. Figure 12 shows the result for the former and Figure 13 shows the result for the latter. Both have principal peaks at 64.5 cycles per minute (CPM), corresponding to two wave-lengths around the circumference. Comparison with Figures 8 and 10 confirm the procedure. Accordingly, a complete set of circumferential scans were recorded on tubes 1 and 2. The results are displayed in Figures 14 and 15. Since the pattern with the largest amplitude is by far the most important [28], we may concentrate on the highest peaks.

The first peak at 31.5 CPM is probably due to the fact that the tubes are not perfectly axial with respect to the lathe spindle. The second peak at 64.5 CPM represents two waves per revolution of the tubes, and this corresponds to an elliptical shape. These are seen to be the major patterns in tube 1, and indeed we can make out the two waves in Figure 4, in retrospect. Tube 2 shows no clearly predominant pattern from Figure 6, and the spectrum of Figure 15 shows that, apart from the peak at 31.5 CPM, there are only relatively low peaks at 64.5 CPM, 129 CPM, and 258 CPM representing an elliptical shape, a four-lobe pattern, and an eigth-lobe pattern, respectively.

Figures 4 to 11 can be used to determine the size of the imperfections, as well as the general shape patterns,

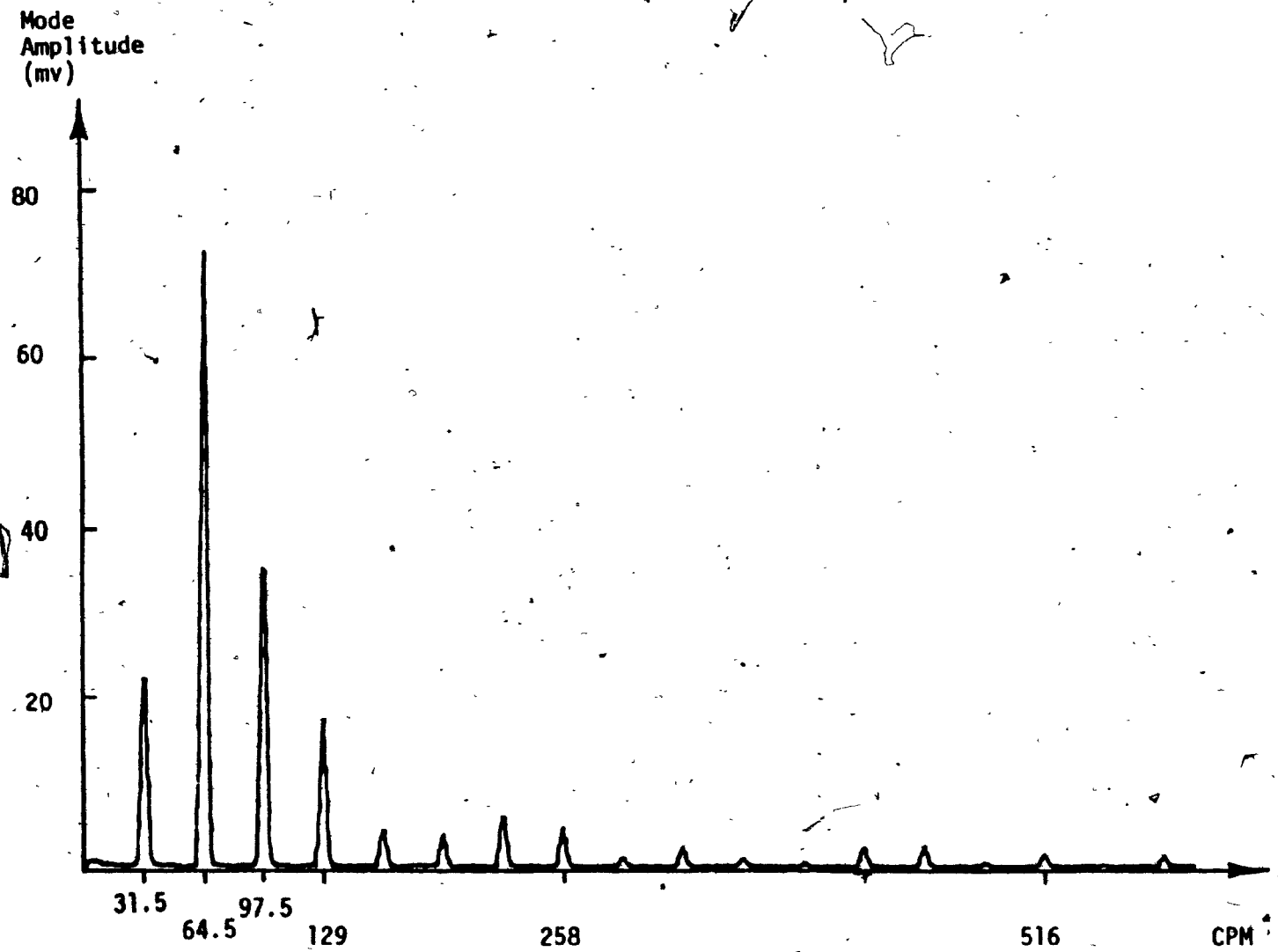

Figure 12. FFT analysis of scan 5 on tube 3, confirming the pattern observed.

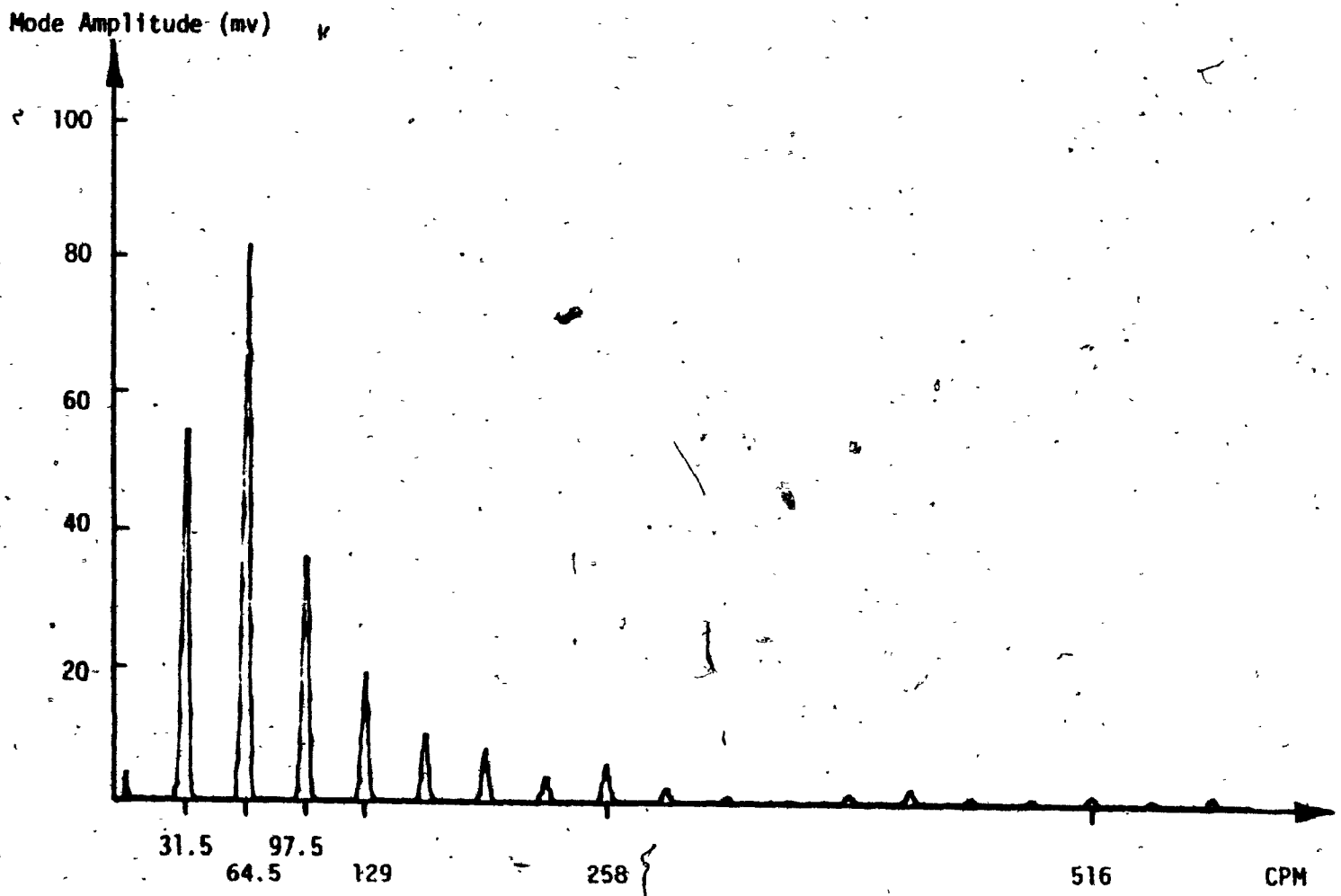

Figure 13. FFT analysis of scan 3 on tube 4, confirming the pattern observed.

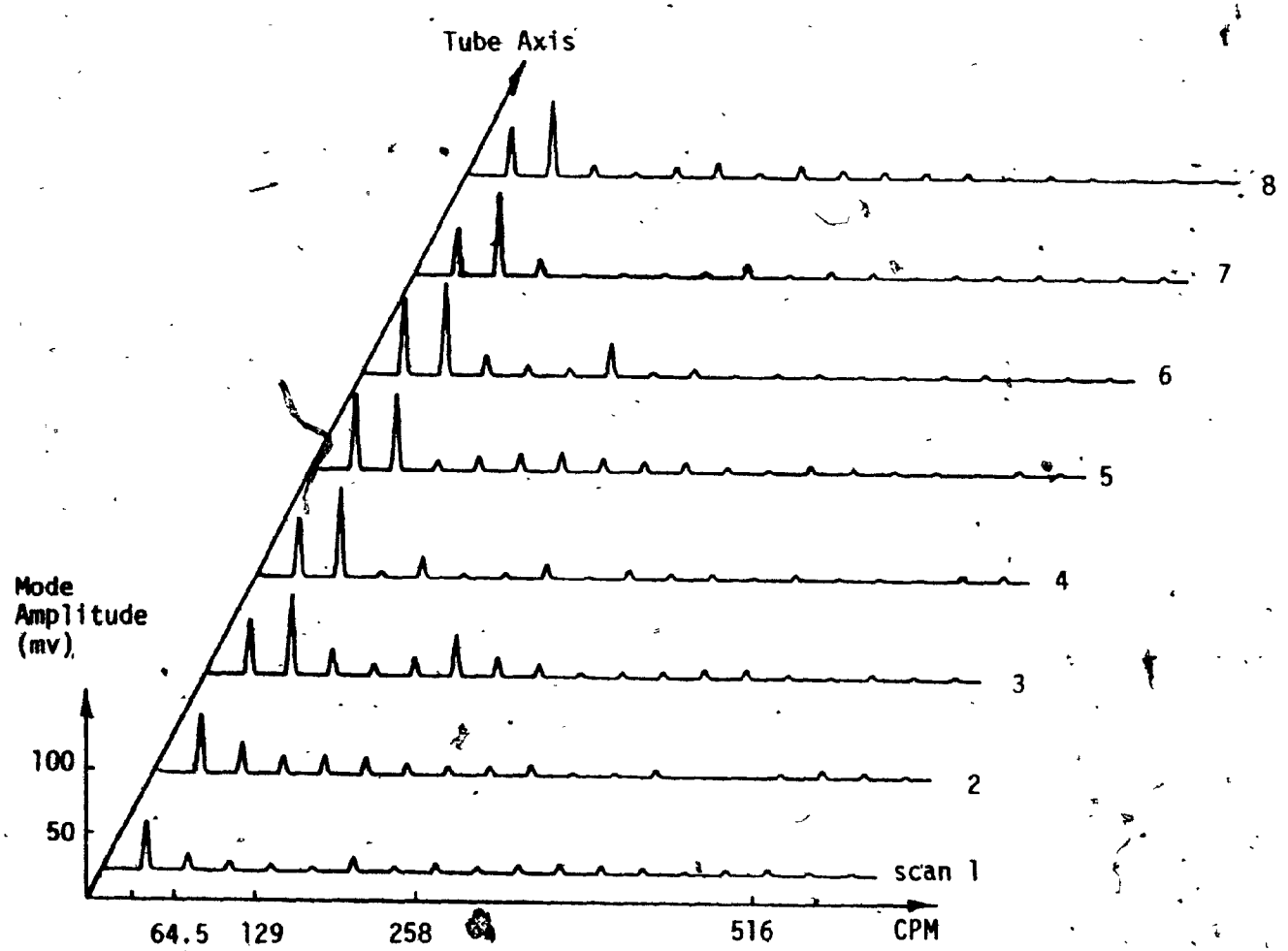

Figure 14. FFT analysis of circumferential scans on tube 1, showing a predominance of 2, and the presence of 6-wave modes.

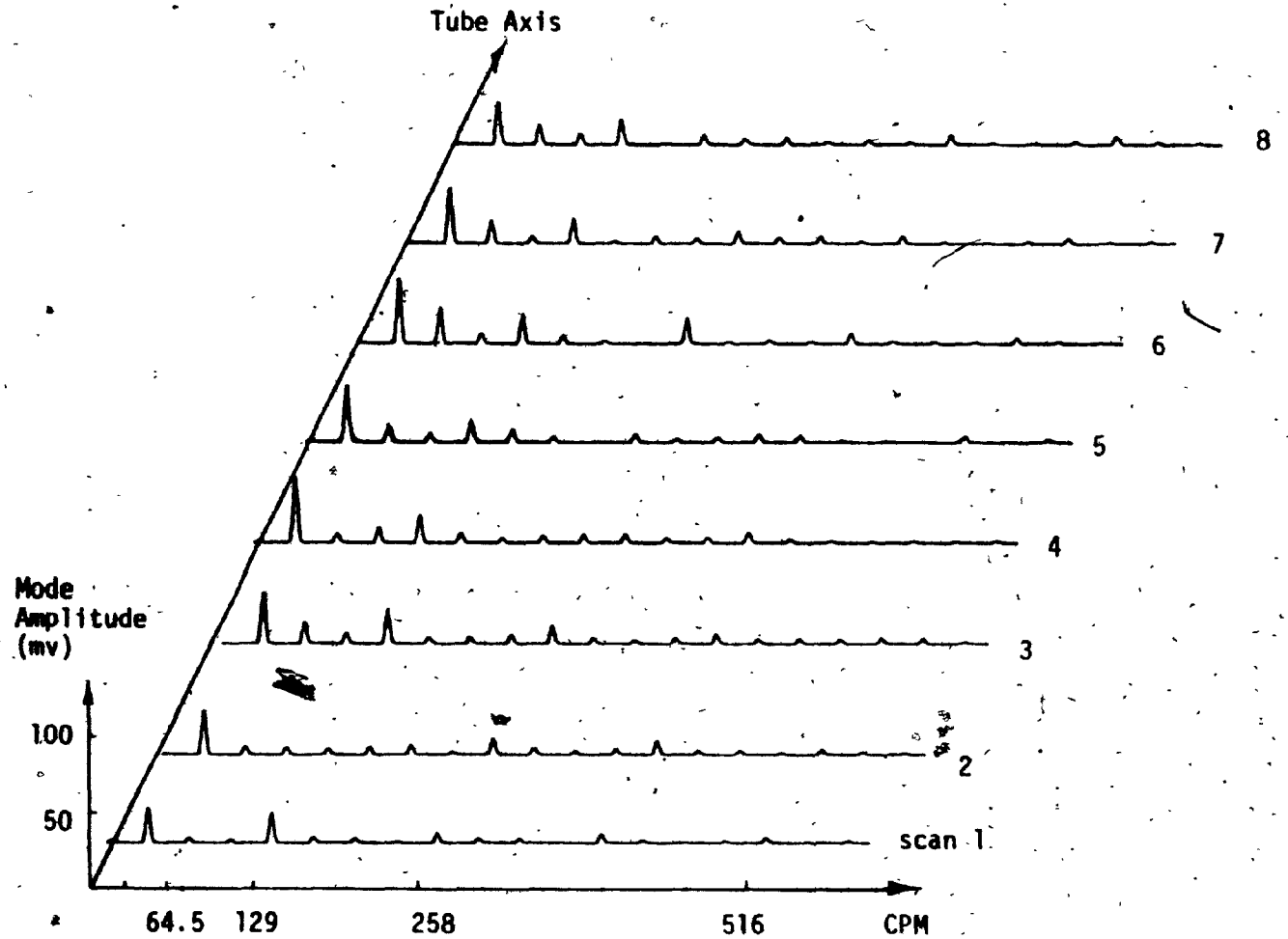

Figure 15. FFT analysis of circumferential scans on tube 2, showing the presence of 2, 4, and 8-wave modes at various scan positions.

and these data are brought together in Table 5.

II.1.3 Buckling Test on the Tubes

Each tube was instrumented with three strain gage rosettes at its mid-length about 120° apart (see Figure 3). Each rosette had three gages positioned as shown in Figure 16, which also gives the gage numbering scheme used for all the tubes. The gages were MM type CEA-6-250UR-120, bonded with M-Bond 200 adhesive to the outside surface.

The first tube tested was unlined tube 3. It was decided to test this tube first by pulling vacuum only. In order to do this, one of the covers was drilled and tapped to accept the line from a vacuum pump. The tube was stood on end and the set-up was made as shown in Figure 17. The linear pot used in the imperfection measurements was set to measure end deflection as vacuum was applied to the tube. A differential pressure transducer was used to drive the Y-axis of an X-Y recorder while the linear pot drove the X-axis. (See Appendix 4 for pressure transducer calibration data.) The nine strain gages and the pressure transducer were also monitored with a data logger. (See Appendix 5 for data logger strain recording verification.)

The test started with the vent valve open to atmosphere and followed the sequence: turn on and zero the

Table 5. Initial Imperfections of the tubes.

	Tube 1	Tube 2	Tube 3	Tube 4
Imperfection Pattern (circum. wave-length)	major: 2 minor: 6	major: ___ minor: 2,4,8	major: 2 minor: ___	major: 2 minor: ___
Max. circum. Imperfection Envelope, Δ_α (mm)	2.1	1.9	5.5	6.1
Max. relative Circum. imp. Envelope, (Δ_α/t)	0.36	0.33	1.96	2.26
Max. axial Imperfection Envelope, Δ_β (mm)	1.1	1.5	2.4	2.4
Max. relative Axial imp. Envelope, (Δ_β/t)	0.19	0.26	0.86	0.89

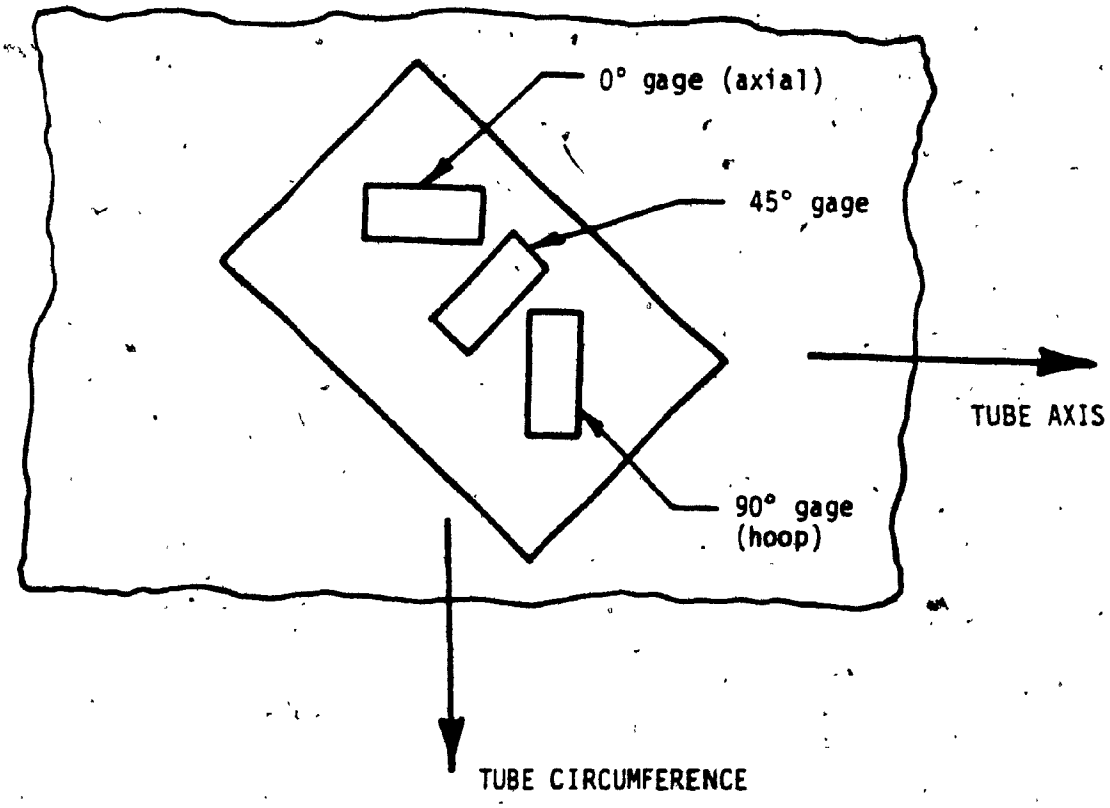

Rosette position*	Axial gage #	45° gage #	Hoop gage #
1	1	2**	3
2	4	5**	6
3	7	8**	9

* See Figure 3 for position on developed cylinder.
** These gages were disconnected for tests in the pressure chamber.

Figure 16. Position and numbering scheme of strain gage rosettes.

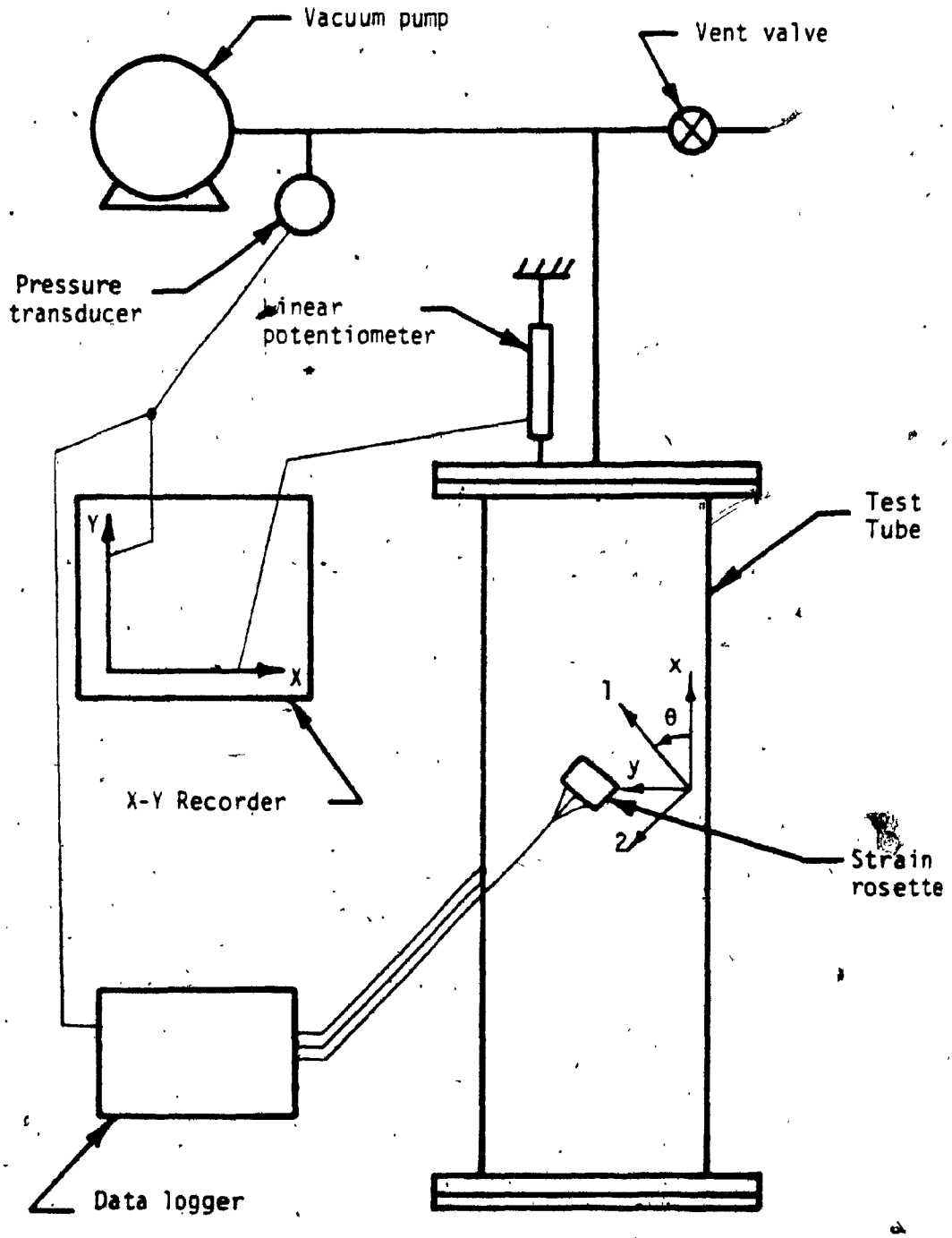

Figure 17. Tube 3 set up for vacuum testing.

instrumentation; turn on the vacuum pump; close the vent valve slowly, applying the vacuum to the tube. Vacuum was pulled to about 95 kPa, and no buckling was evident. The plot of end deflection vs vacuum, and strain vs vacuum are seen to be approximately linear in Figures 18 and 19, respectively. The initial vertical plateau in Figure 18 and the initial horizontal plateau in 19 are due to the inappropriate method of applying the vacuum, and so the data in these two figures should only be used qualitatively, indicating the linearity of strains and end deflection under vacuum, and that no buckling is evident.

To increase the external hydrostatic pressure it was necessary to place the tube in a steel pressure chamber. This required that some changes be made in the instrumentation of the tubes. First, the end deflection could no longer be measured. Second, only six strain gages could be monitored. All the 45^0 gages were disconnected, but the same gage numbering scheme was retained. Unfortunately visual observation was no longer possible. Figure 20 is a reproduction of the set-up which was used thereafter; it shows the pressure chamber with its door open and the data logger.

Tube 3 was now put in the pressure chamber with its contained air at atmospheric pressure, and the drilled and tapped hole in one of its covers was stoppered with a brass

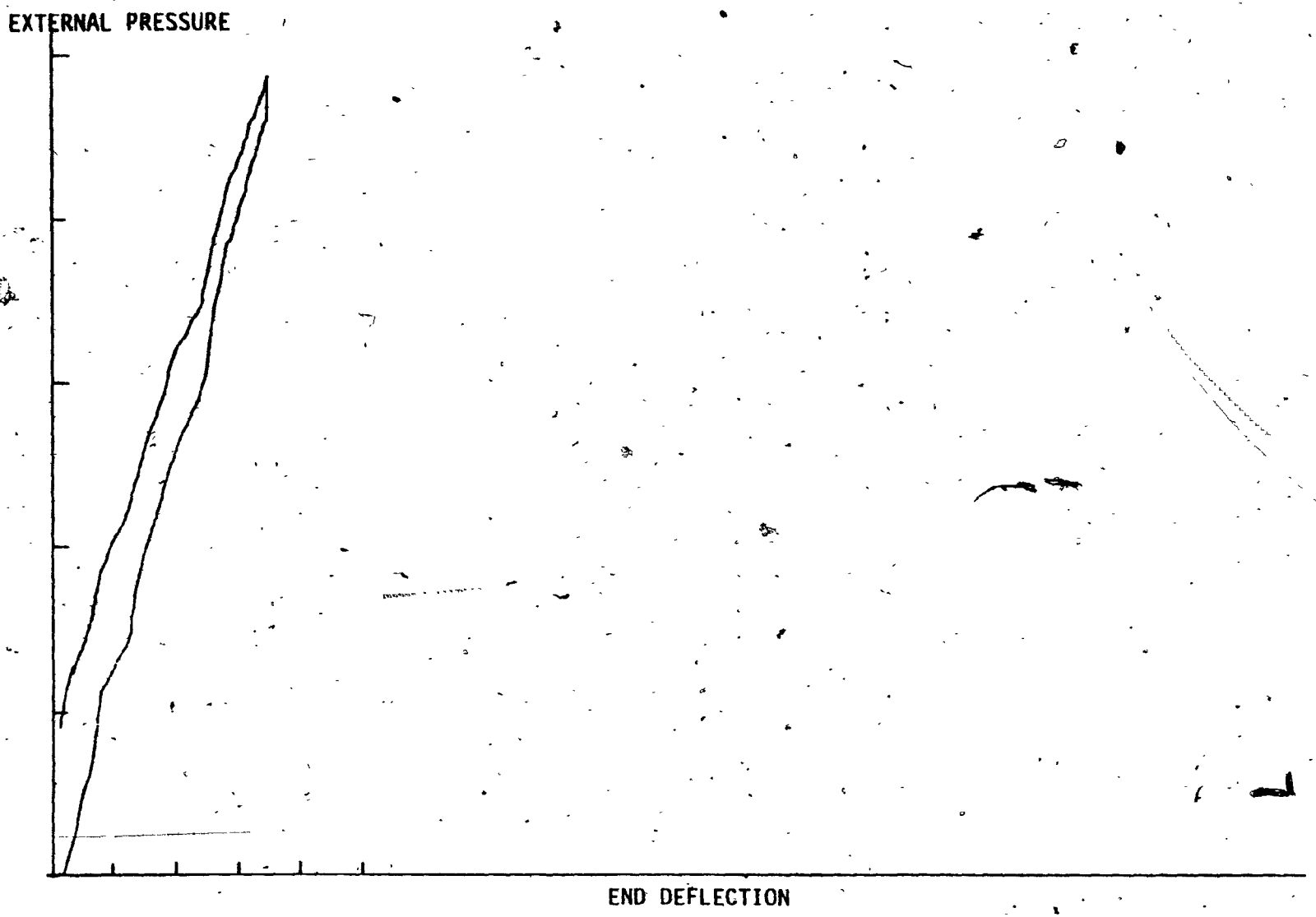

Figure 18. Plot of end deflection vs external pressure for tube 3 under vacuum only.

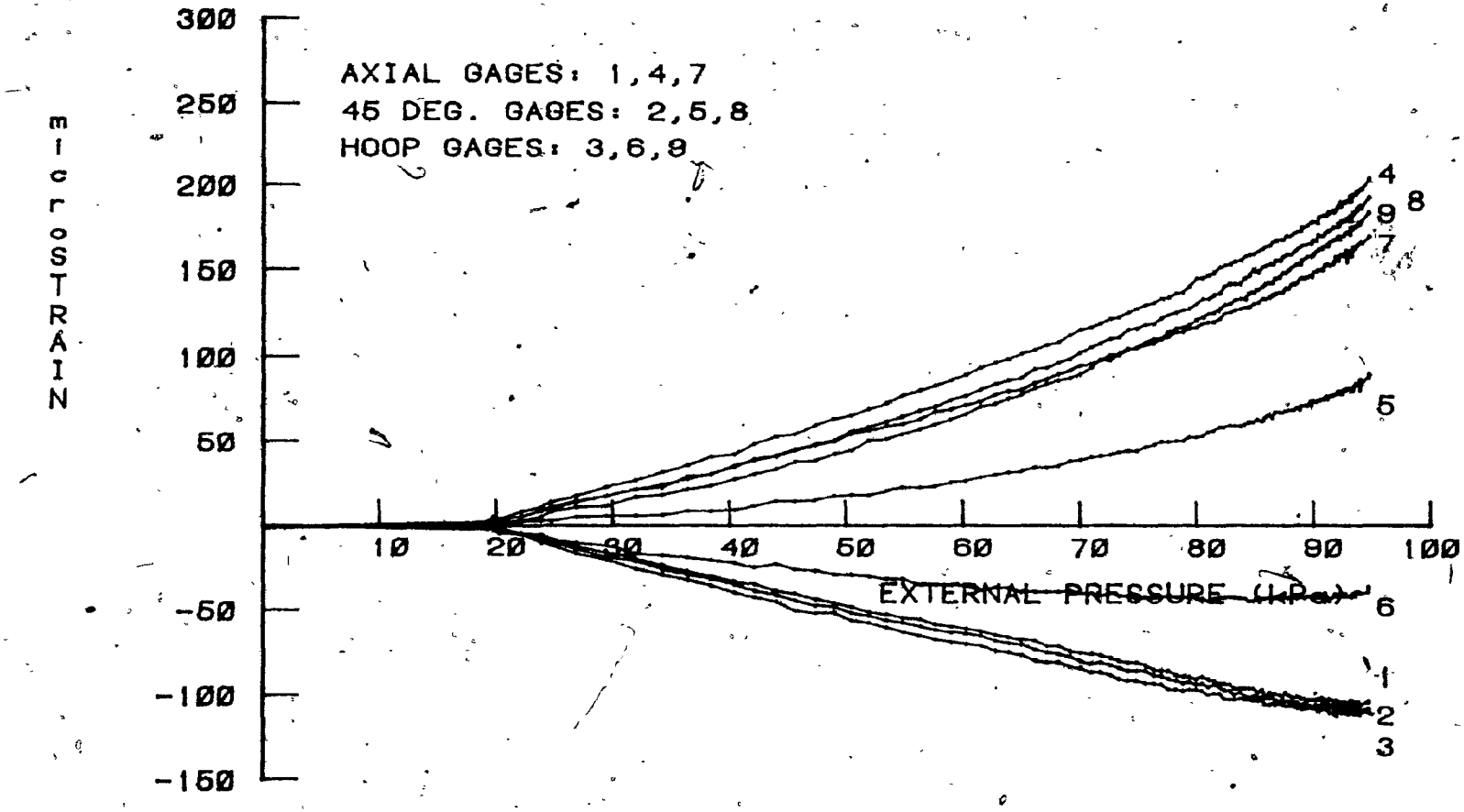

Figure 19. Test of tube 3 under vacuum only.

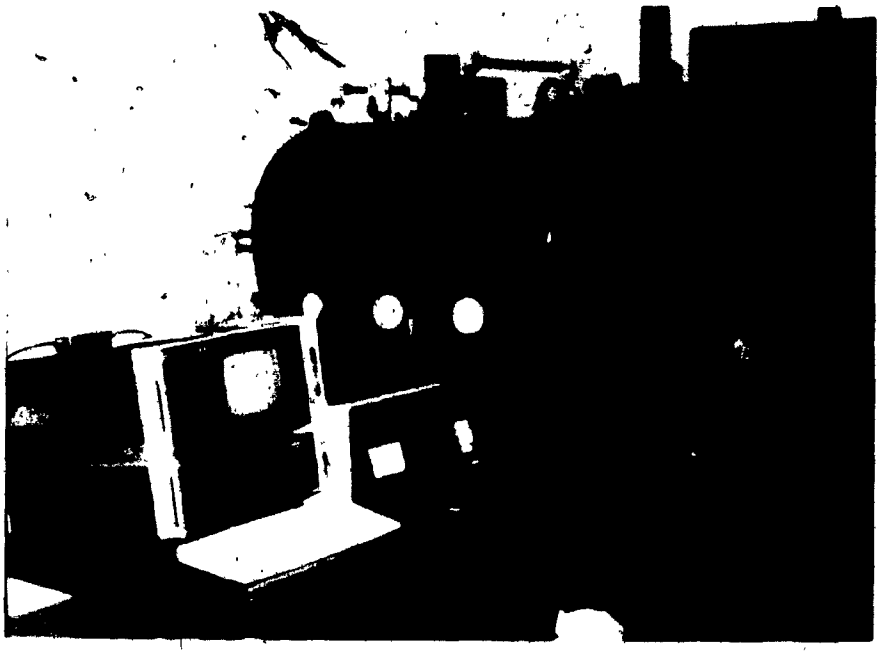

Figure 20. All four tubes were tested to destruction in the pressure chamber; data logger is shown in foreground.

plug. Air from a utility line at 8.8 atmospheres was slowly let into the chamber. Strains and pressure were recorded with the data logger. At a net external pressure of 250 kPa the test was stopped, the pressure released, and the tube examined for damage. The results of this second run on tube 3 are shown in Figure 21. The residual strains are small and there was no visible damage.

Once more the same tube was pressurized, this time to destruction. Failure was sudden and catastrophic, producing a loud explosive noise. Failure was accompanied by a sudden pressure drop and by the destruction of strain gages. The plotted data from the final run on tube 3 is shown in Figure 22.

Unlined tube 4 was tested to destruction in a single run, and the results are displayed in Figure 23.

Tubes 1 and 2 had liners, and the necessary buckling pressure was expected to be higher than for tubes 3 and 4. To prevent possible leaks to the inside of the tubes tacky-tape was used to seal the end closures. All other conditions were unchanged. Each tube was tested to destruction in a single run. The data are plotted in Figures 24 and 25.

All the above testing was done at about 21° C. and 30%

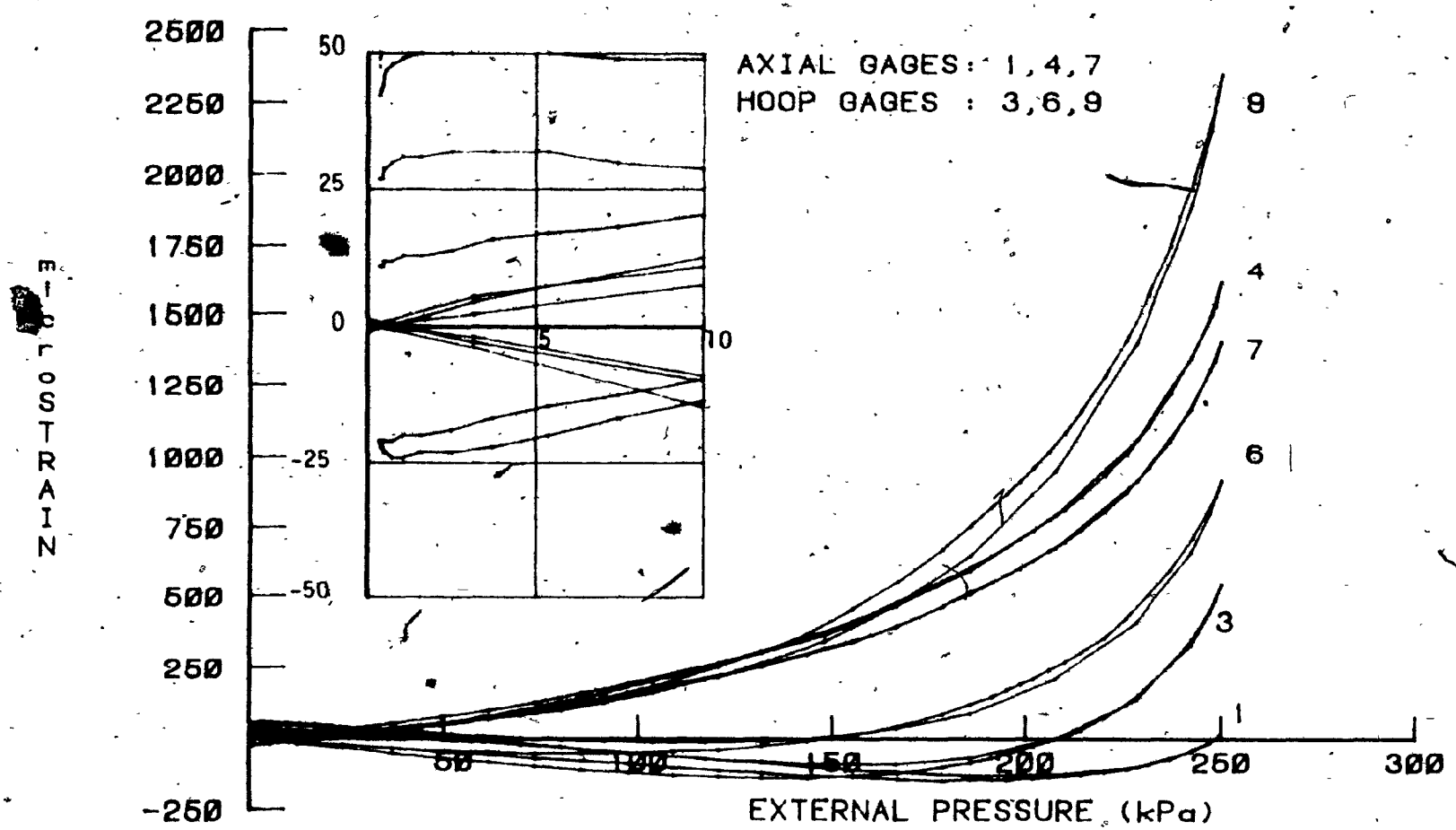

Figure 21. Test of tube 3, loading and unloading (2nd run)

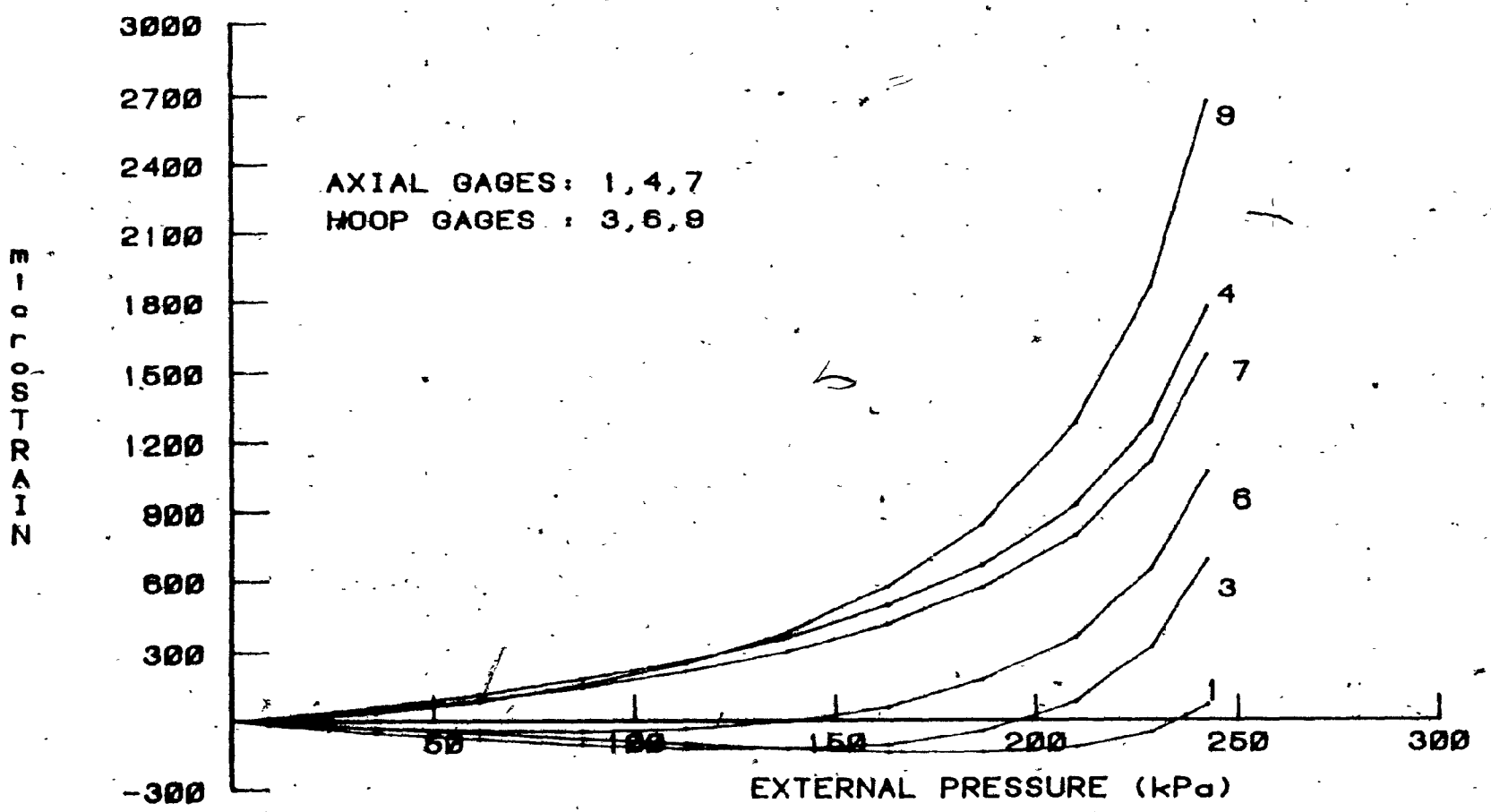

Figure 22. Test of tube 3, to failure (3rd run)

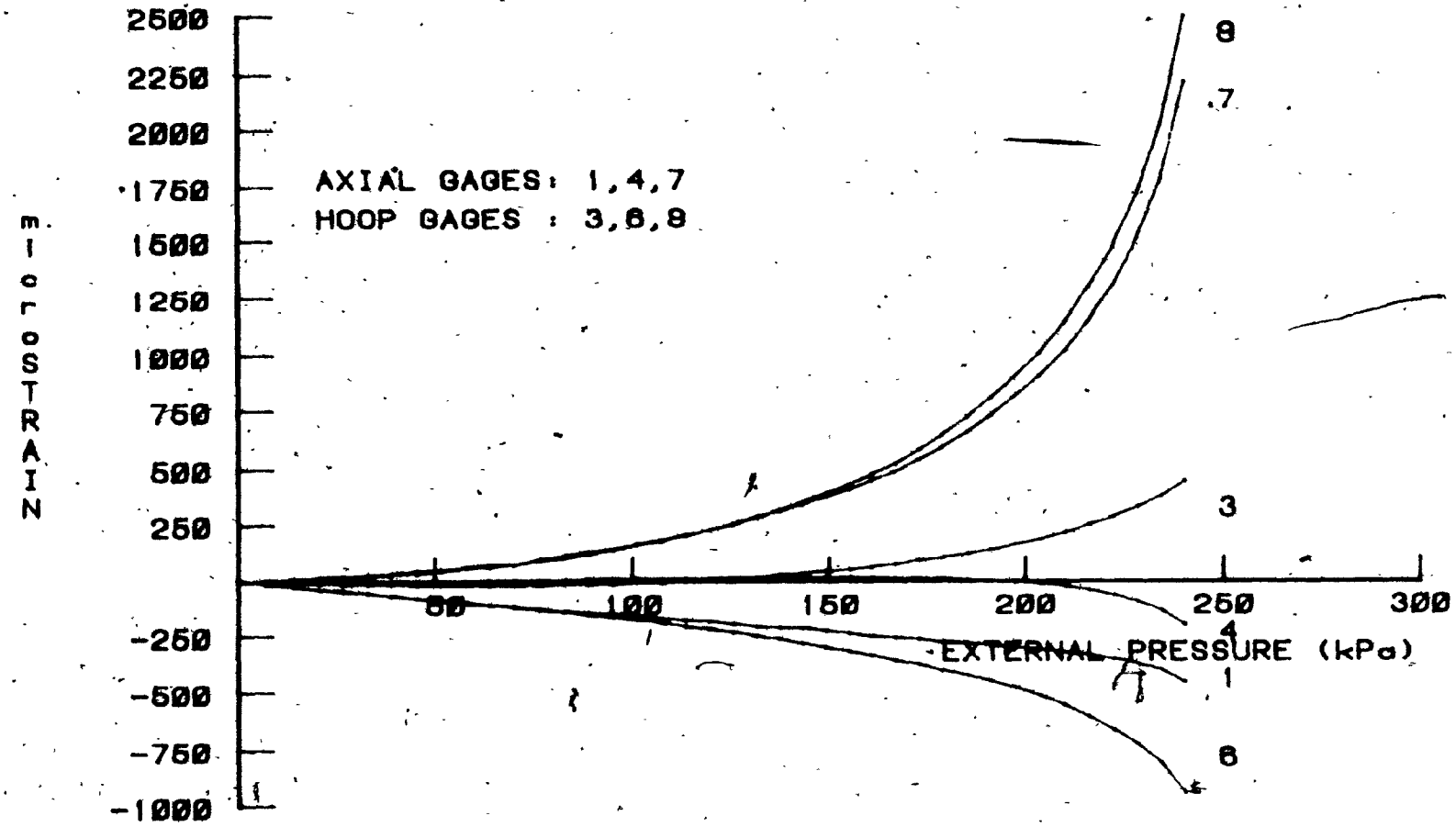

Figure 23. Test of tube 4 to failure.

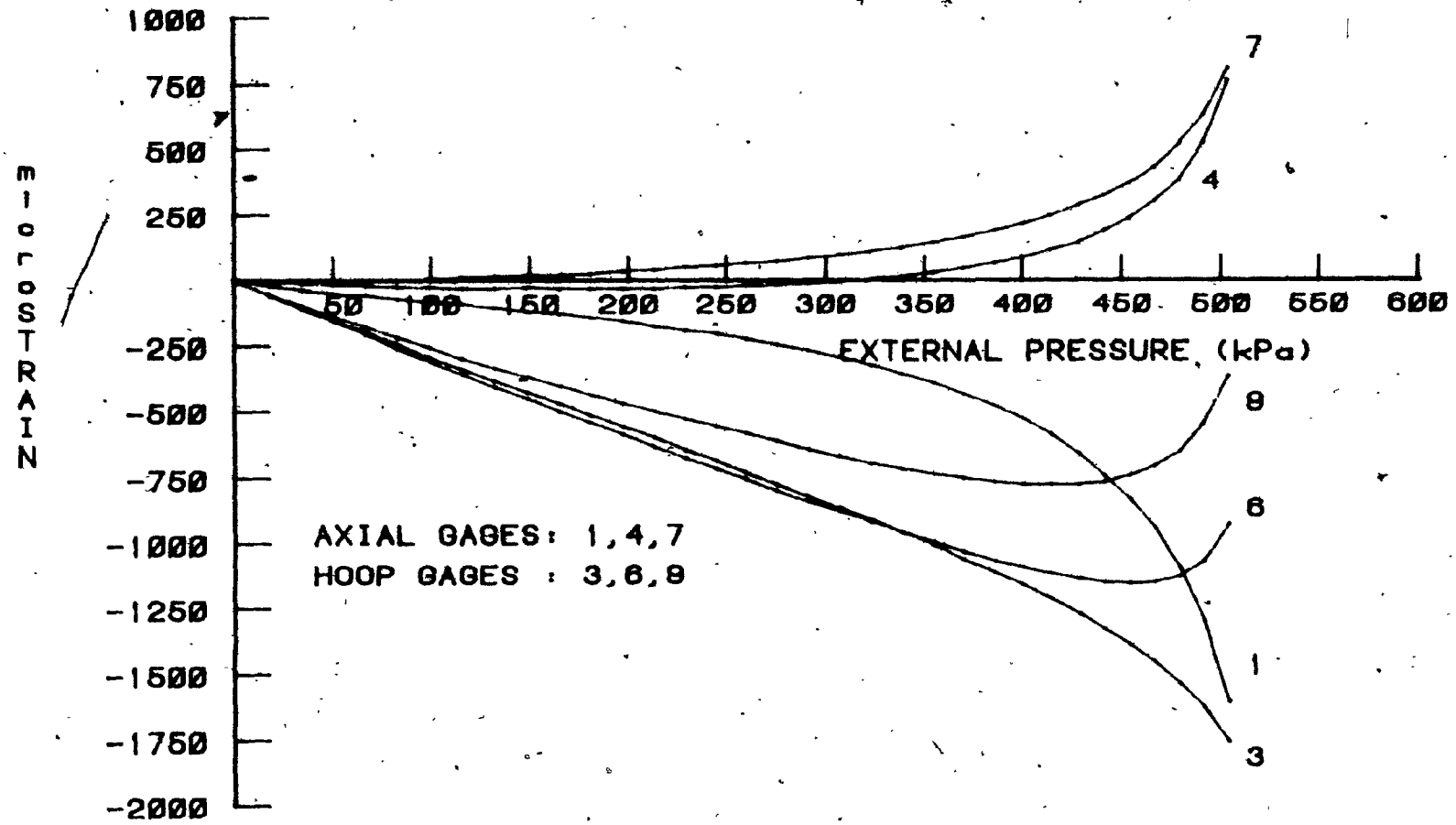

Figure 24. Test of tube 1 to failure.

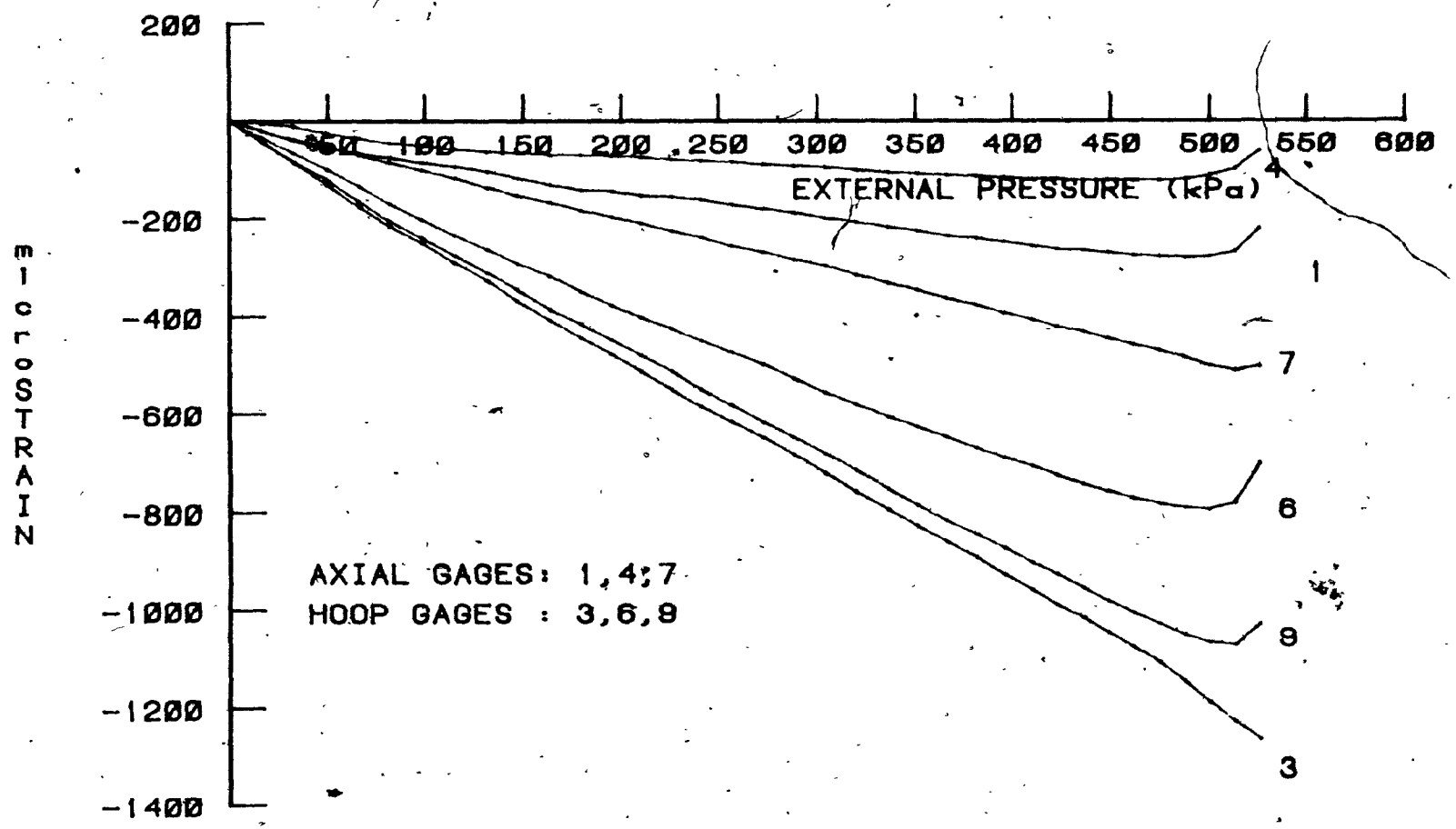

Figure 25. Test of tube 2 to failure.

relative humidity. The printout of the reduced data for all buckling tests is given in Appendix 6.

Figures 26 to 30 are reproductions showing the effect of pressurizing the four tubes to destruction. Each tube is shown from the 'front' and from the 'back', in Figures 27 to 30. Figure 26 shows tube 1 after failure. Most of the PVC liner has shattered, and both flange-and-cover sets have been blown from the shell. The close-up shows that the force of the implosion was sufficient to tear the strain gage rosettes from the tubes.

Figures 27 and 28 show tubes 1 and 2, respectively. The dark patches are due to islands of PVC liner which are still adherent inside the tubes. The cracking and delamination are extensive around the whole tube. Note that there is little or no cracking in the areas where the PVC liner is still present. (It is from these areas that samples of the tubes were cut out to determine the weight-fraction of glass in the wall, and where thickness was checked using a micrometer.) The flange-and-cover sets are not completely separated from tube 2.

Unlined tubes 3 and 4 are shown in Figures 29 and 30. In both cases, the most serious damage occured on diametrically opposed generators of the nominally cylindrical form. In tube 3 these two principal lines are

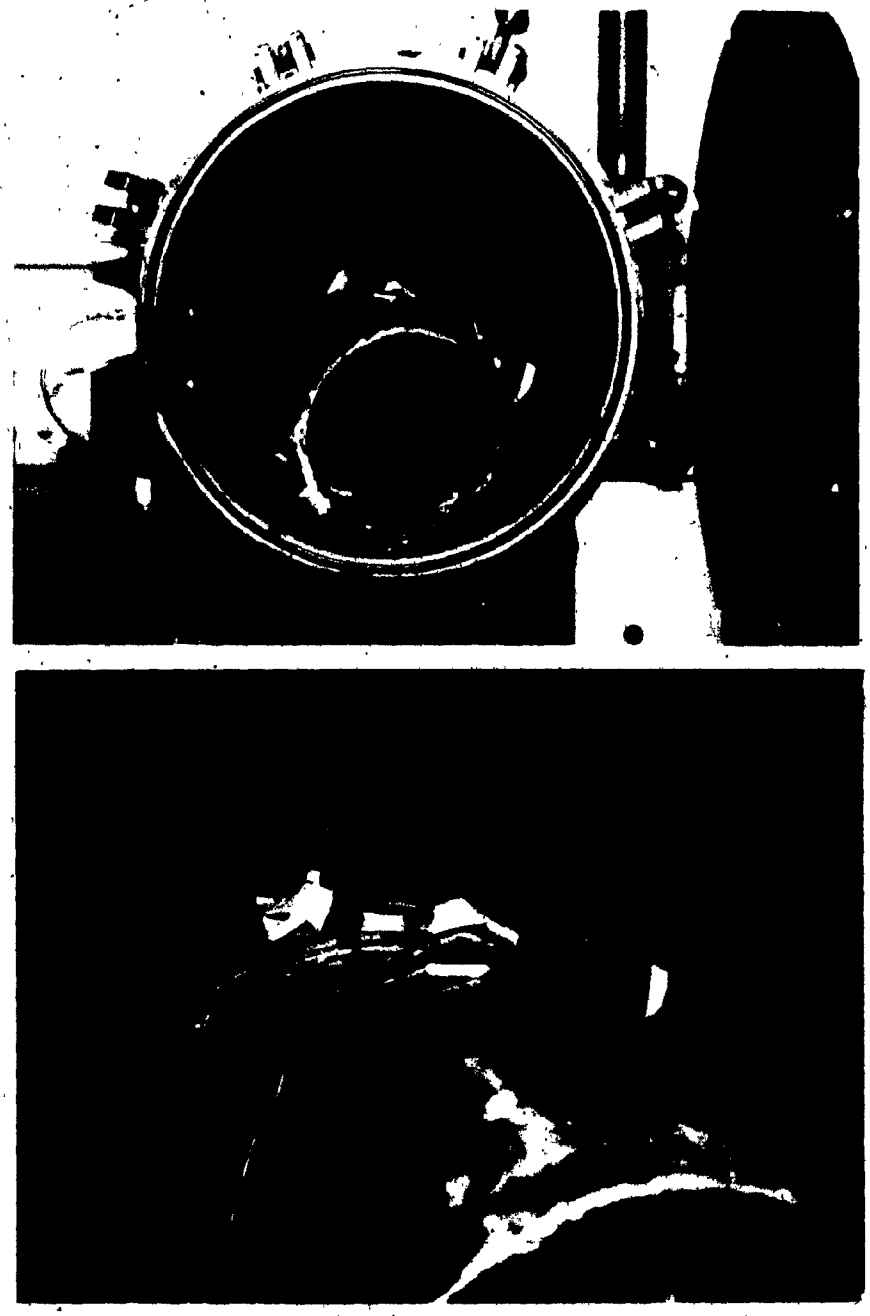

Figure 26. Top: tube 1 after failure; note shattered PVC.
Bottom: tube 1 showing gages torn off.

Figure 27. Tube 1 after failure at 504 kPa; the flanges have been blown off in testing.

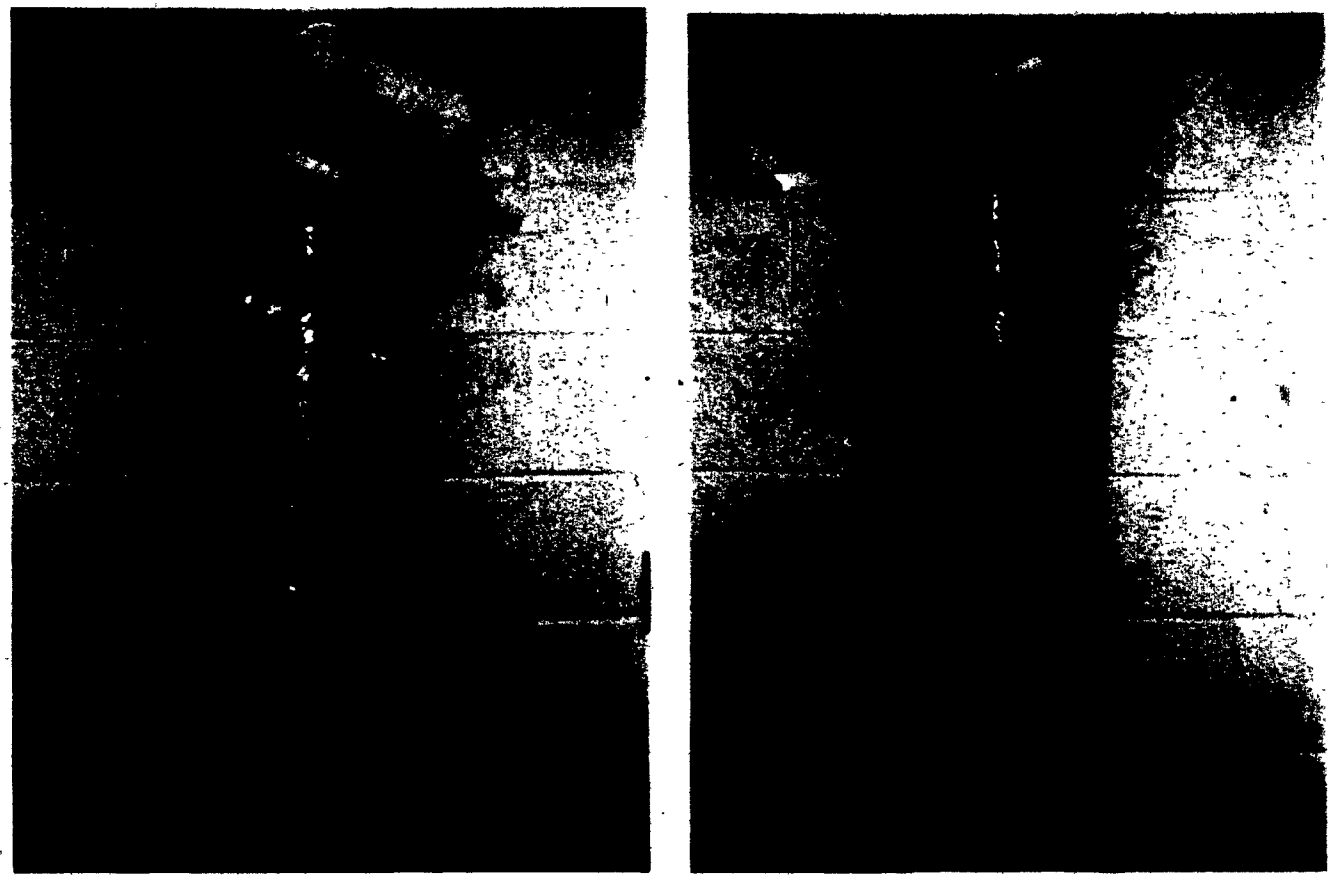

Figure 28. Tube 2 after failure at 526 kPa, showing tacky-tape sealing covers.

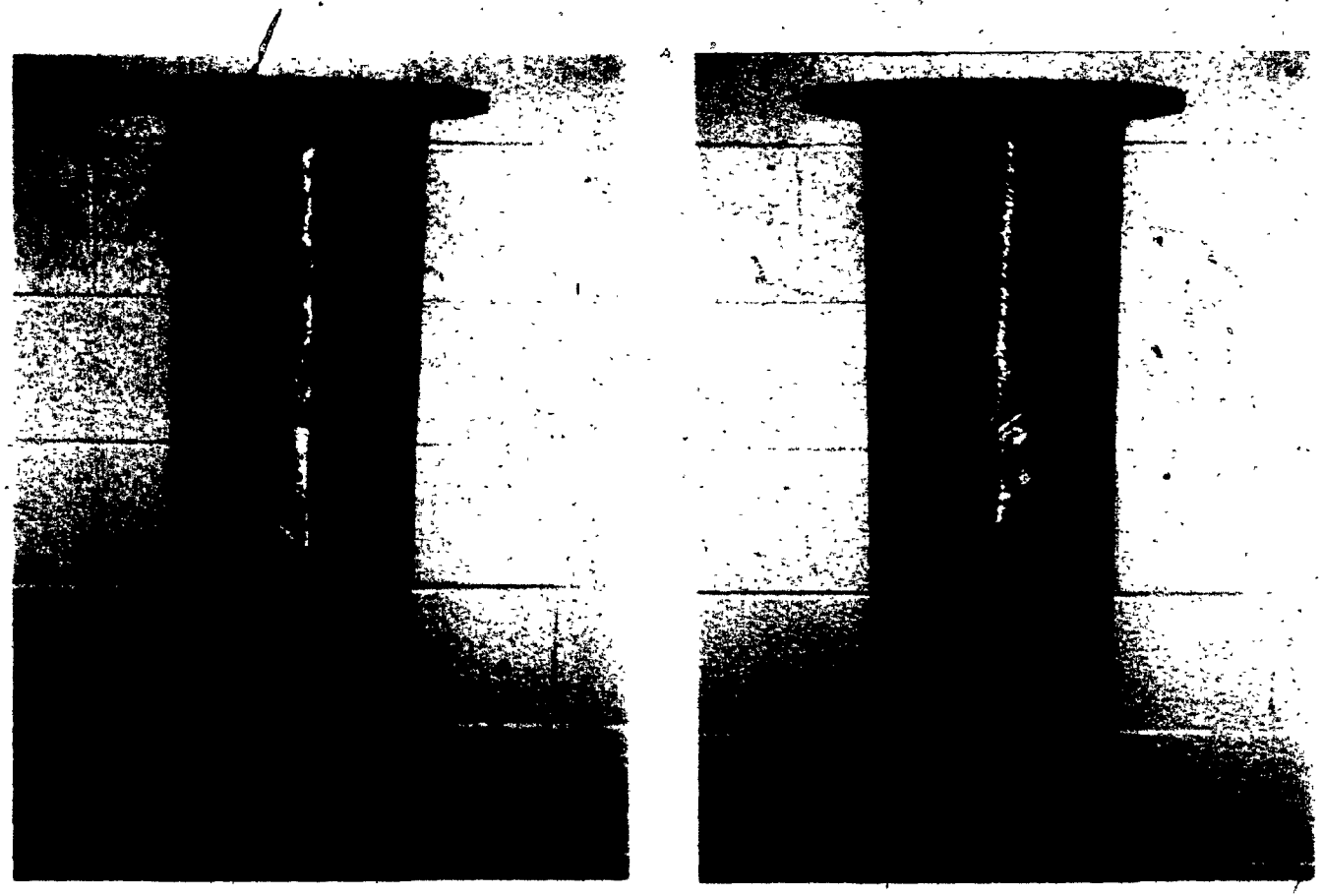

Figure 29. Tube 3 after failure at 243 kPa; note principal damage at 90° and 270° positions corresponding to the major axis of the initial elliptical form.

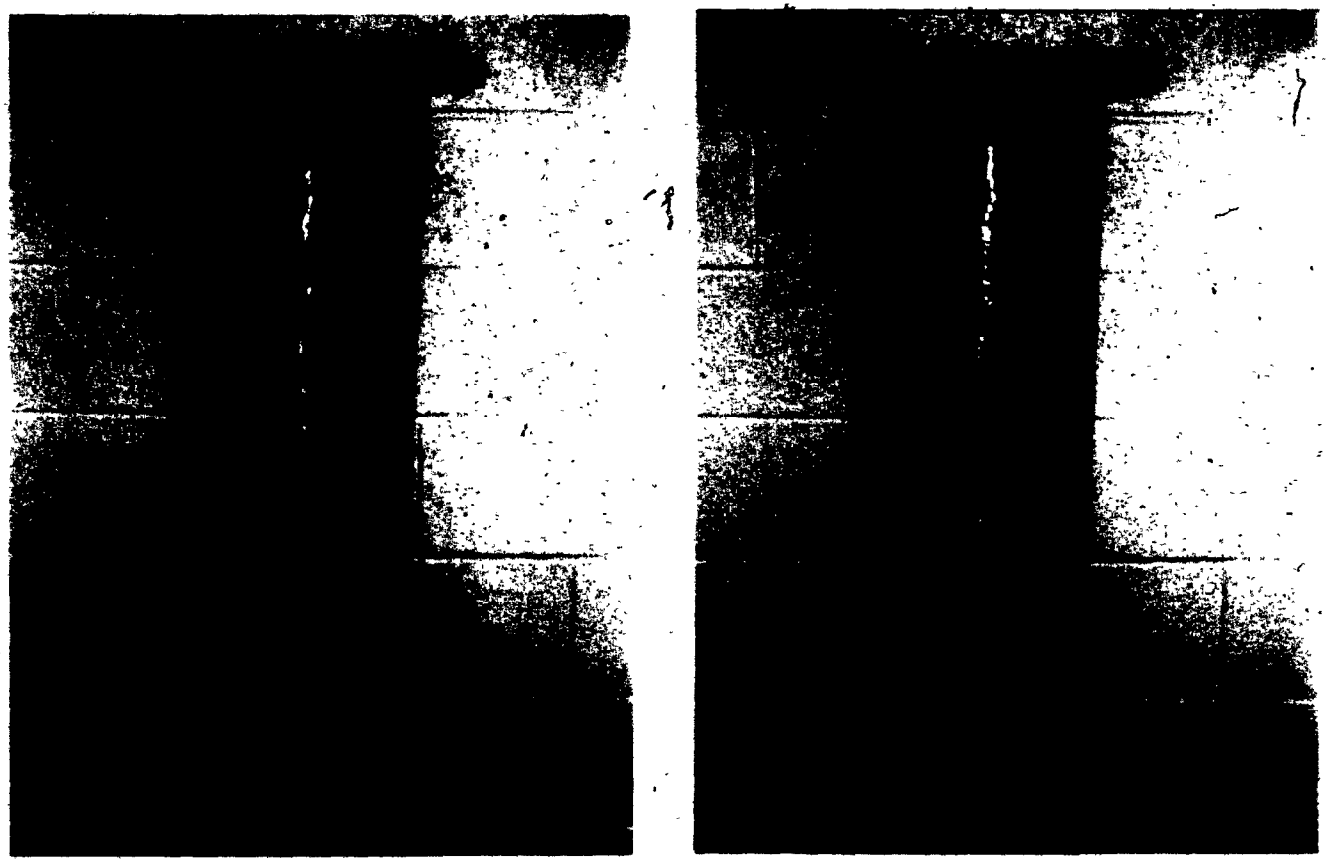

Figure 30. Tube 4 after failure at 240 kPa; note principal damage at 135° and 315° positions corresponding to the major axis of the elliptical form.

at about the 90° and 270° positions. In tube 4 they are approximately at the 135° and 315° positions. These locations closely match the ends of the major axes of the initial elliptical form as can be seen from Figures 8 and 10.

II.1.4 Testing of Tube Samples

After the four tubes were tested, one rectangular sample was cut from each of the tube walls. The samples were taken from areas showing the least amount of cracking and delamination. Thickness measurements were taken on the samples with a micrometer. The results are close to those determined with the thickness sensor and given in Table 4. Note however that there is considerable variation in thickness compared to a metallic vessel made from plate. At present, more uniformity is not feasible for commercial structures, and the values of Table 4 will be used in all calculations.

Each tube sample was cut into smaller pieces, the aim being to determine the amount of reinforcement present, and the lay-up sequence in the laminated wall. Both factors have an important effect on stiffness and deformation behaviour of the shell wall, and both can be found by using a "burn off" test. (See Appendix 7 for details.) This consists of weighing a piece of the laminate, heating to

600° C., maintaining the temperature for about 30 minutes, and weighing the material left behind. The heat is sufficient to decompose and drive off the resin, leaving only the glass. Knowing the densities of the resin and the reinforcement (Tables 1 to 3), the volume fraction of glass can be calculated. Three samples from each tube were tested, and the average fractions are shown in Table 6.

Table 6. Amount of Reinforcement in Tubes

	Tube 1	Tube 2	Tube 3	Tube 4
Wt. of laminate (g)	8.1678 5.1298 4.9379	6.1432 5.3059 4.6039	3.3138 4.6765 4.3142	3.5883 3.2674 3.5837
Wt. of PVC (g)	6.1774 4.0005 3.7665	4.4925 4.0808 3.5372	N.A. N.A. N.A.	N.A. N.A. N.A.
Wt. of glass (g)	1.2400 0.7298 0.7068	1.1465 0.8577 0.7635	2.1337 2.9945 2.7827	2.5389 2.3205 2.5678
No. of glass layers	2 2 2	2 2 2	6 6 6	6 6 6
Wt.-fraction	0.62 0.65 0.60	0.69 0.70 0.72	0.64 0.64 0.65	0.71 0.71 0.72
Vol.-fraction	0.40 0.44 0.38	0.48 0.49 0.52	0.42 0.42 0.44	0.50 0.50 0.52
Average vol.-frac.	0.41	0.50	0.43	0.51

Note.: The weight of PVC was determined by measuring the volume of the PVC layer, and using a specific gravity value of 1.4.

II.2.0 DESIGN PROCEDURES

In this sub-section several methods of determining the critical pressure for thin cylindrical shells will be examined. The aim is to assess which is most appropriate in view of the experimental results obtained. This judgement, however, will be postponed until the final section.

The first procedure is the most complex and complete of these methods. It will be considered before the others because this will present an opportunity to sketch the analysis of generally anisotropic laminated cylindrical thin shells subjected to buckling loads. Also, some of the details in the analysis will be required in using the other methods.

II.2.1 Present Design Procedure

Thus, we now consider the analysis presented in 1963 by Cheng and Ho. [20] These workers considered cylindrical shells made of laminated anisotropic materials, subject to axial compression, lateral pressure, and torsional loads, or combinations thereof. Their analysis is based on second-order shell theory assumptions, viz., i) the shell wall is thin compared to the shell mid-surface radius, ii) displacements are small compared to the shell thickness, iii) transverse or thickness shear strains and thickness

normal strains are negligibly small compared to in-plane strains.

The procedure is identical to that required for isotropic shell analysis except that the stress-strain relations are in a more general form. (Details on these relations can be found in a number of texts, for example [29].) Since Cheng and Ho concisely give the requisite equations, only some points will be detailed here.

The most general form of the stress-strain relations is given by generalized Hooke's Law (assuming linear elastic behaviour):

$$\begin{Bmatrix} \sigma_1 \\ \sigma_2 \\ \sigma_3 \\ \sigma_4 \\ \sigma_5 \\ \sigma_6 \end{Bmatrix} = \begin{bmatrix} C_{11} & C_{12} & C_{13} & C_{14} & C_{15} & C_{16} \\ C_{21} & C_{22} & C_{23} & C_{24} & C_{25} & C_{26} \\ C_{31} & C_{32} & C_{33} & C_{34} & C_{35} & C_{36} \\ C_{41} & C_{42} & C_{43} & C_{44} & C_{45} & C_{46} \\ C_{51} & C_{52} & C_{53} & C_{54} & C_{55} & C_{56} \\ C_{61} & C_{62} & C_{63} & C_{64} & C_{65} & C_{66} \end{bmatrix} \begin{Bmatrix} \varepsilon_1 \\ \varepsilon_2 \\ \varepsilon_3 \\ \varepsilon_4 \\ \varepsilon_5 \\ \varepsilon_6 \end{Bmatrix} \qquad (1)$$

where [C] is the elastic stiffness matrix,

σ_i are engineering stress components, and

ε_i are engineering strain components.

Consideration of the strain energy in a conservative material system has shown that the elastic stiffness matrix

must be symmetric, i.e., $C_{ij} = C_{ji}$. Thus, the 36 constants in (1) are reduced to 21. Material layers of technological importance do not have the general anisotropy described by (1). Some are orthotropic, some are isotropic in their plane of lamination, while others are conventional isotropic materials. In our case, all the materials have properties which can be given by a subset of the constants in (1):

$$\begin{Bmatrix} \sigma_1 \\ \sigma_2 \\ \sigma_3 \\ \sigma_4 \\ \sigma_5 \\ \sigma_6 \end{Bmatrix} = \begin{bmatrix} C_{11} & C_{12} & C_{13} & 0 & 0 & 0 \\ C_{12} & C_{22} & C_{23} & 0 & 0 & 0 \\ C_{13} & C_{23} & C_{33} & 0 & 0 & 0 \\ 0 & 0 & 0 & C_{44} & 0 & 0 \\ 0 & 0 & 0 & 0 & C_{55} & 0 \\ 0 & 0 & 0 & 0 & 0 & C_{66} \end{bmatrix} \begin{Bmatrix} \varepsilon_1 \\ \varepsilon_2 \\ \varepsilon_3 \\ \varepsilon_4 \\ \varepsilon_5 \\ \varepsilon_6 \end{Bmatrix} \qquad (2)$$

where we have applied $C_{ij} = C_{ji}$ in the notation.

Using the first assumption (i.e., $\sigma_3 = 0$) and the third assumption (i.e., $\varepsilon_4 = \varepsilon_5 = 0$), the system is reduced to the two-dimensional form used for the thin shell analysis:

$$\begin{Bmatrix} \sigma_1 \\ \sigma_2 \\ \sigma_6 \end{Bmatrix} = \begin{bmatrix} Q_{11} & Q_{12} & 0 \\ Q_{12} & Q_{22} & 0 \\ 0 & 0 & Q_{66} \end{bmatrix} \begin{Bmatrix} \varepsilon_1 \\ \varepsilon_2 \\ \varepsilon_6 \end{Bmatrix} \qquad (3)$$

where the Q matrix is the modulus matrix or reduced

stiffness matrix for our specially orthotropic layers. A material is said to be specially orthotropic when its principal material directions coincide with the natural directions of the structure in which it is incorporated. For example, the unidirectional fibers may be aligned with the hoop direction or the axial direction in a shell. For filament-wound shells, however, this is not usually the case since the fibers make an angle θ with the shell axis. Because the equilibrium equations will be expressed in the natural coordinate system of the shell (where x is the axial direction, y is the circumferential direction, and z is the direction normal to the mid-surface and positive outward), (3) must be transformed from the material directions '1-2' to the shell 'x-y' system (Figure 17). Transformation gives

$$\begin{Bmatrix} \sigma_x \\ \sigma_y \\ \sigma_{xy} \end{Bmatrix} = \begin{bmatrix} \overline{Q_{11}} & \overline{Q_{12}} & \overline{Q_{16}} \\ \overline{Q_{12}} & \overline{Q_{22}} & \overline{Q_{26}} \\ \overline{Q_{16}} & \overline{Q_{26}} & \overline{Q_{66}} \end{bmatrix} \begin{Bmatrix} \varepsilon_x \\ \varepsilon_y \\ \varepsilon_{xy} \end{Bmatrix} \qquad (4)$$

where the $\overline{Q}$ matrix is the transformed modulus matrix.

Note that strains can be given in terms of stress as

$$\begin{Bmatrix} \varepsilon_x \\ \varepsilon_y \\ \varepsilon_{xy} \end{Bmatrix} = \begin{bmatrix} \overline{S_{11}} & \overline{S_{12}} & \overline{S_{16}} \\ \overline{S_{12}} & \overline{S_{22}} & \overline{S_{26}} \\ \overline{S_{16}} & \overline{S_{26}} & \overline{S_{66}} \end{bmatrix} \begin{Bmatrix} \sigma_x \\ \sigma_y \\ \sigma_{xy} \end{Bmatrix} \qquad (5)$$

where $[\bar{S}] = [\bar{Q}]^{-1}$.

We can see that (5) may be used to relate these transformed reduced compliance coefficients $\bar{S}_{ij}$ to the familiar engineering constants, viz.,

$$\varepsilon_x = \bar{S}_{11}\sigma_x + \bar{S}_{12}\sigma_y + \bar{S}_{16}\sigma_{xy} . \qquad (6)$$

In a uniaxial tensile test in the x-direction,

$$\sigma_y = \sigma_{xy} = 0 \qquad (7)$$

Thus, $\varepsilon_x = \bar{S}_{11}\sigma_x$. (8)

But, $\varepsilon_x = \sigma_x / E_x$. (9)

Therefore, $E_x = \bar{S}_{11}^{-1}$. (10)

Other such relations can be found for different engineering constants.

By definition, the stress resultants for the shell theory being used are:

$$N_x = \int_{-h/2}^{h/2} \sigma_x[1+(z/a)]dz \quad , \quad M_x = \int_{-h/2}^{h/2} \sigma_x[1+(z/a)]z dz$$

$$N_y = \int_{-h/2}^{h/2} \sigma_y\, dz \quad , \quad M_y = \int_{-h/2}^{h/2} \sigma_y\, z\, dz \qquad (11)$$

$$N_{xy} = \int_{-h/2}^{h/2} \sigma_{xy}[1+(z/a)]dz \quad , \quad M_{xy} = \int_{-h/2}^{h/2} \sigma_{xy}[1+(z/a)]z dz$$

$$N_{yx} = \int_{-h/2}^{h/2} \sigma_{yx}\, dz \quad , \quad M_{yx} = \int_{-h/2}^{h/2} \sigma_{yx}\, z\, dz$$

where a is the radius to the mid-surface,

and h is the shell thickness.

As given in (11), these quantities result from integration over the full thickness of the shell wall. For homogeneous shells, this presents no problem since, when (4) is substituted into (11), the $\overline{Q}$ matrix is not a function of the z-coordinate. In the case of a heterogeneous laminated structure with either varying winding angles, or varying materials, or both, the procedure is modified. First, the integration is carried out over the thickness of each layer separately, then the results are summed over the whole thickness. I.e.,

$$N_x = \sum_{k=1}^{n} \int_{\text{lower } z}^{\text{upper } z} \sigma_x[1+(z/a)]dz, \text{ and so on,} \qquad (12)$$

where k refers to a particular layer,

n refers to the total number of layers,

and the limits of integration are from the bottom to the top of layer k.

The strain-displacement relations are those developed by Flügge [17] in terms of mid-surface displacements. The stress resultants may then be expressed in terms of the material properties, the lamination structure (i.e., position, thickness, and orientation of the various layers), mid-surface displacements, and shell geometry. The equilibrium of a differential element may be expressed in terms of the stress resultants, and the external loads. Finally then, the equilibrium equations are given in terms

of material properties, lamination structure, mid-surface displacements u, v, w, shell geometry, and external loads. (We note in passing that Cheng and Ho use a different set of sign conventions from Flügge, and this results in differences in signs of certain terms in their equilibrium equations.)

Since the displacements are in terms of differentials of the space coordinates, we have a system of three differential equations of fourth order. Cheng and Ho assume a displacement field

$$u = U \sin[(\lambda x/a) + ny]$$
$$v = V \sin[(\lambda x/a) + ny] \qquad (13)$$
$$w = W \cos[(\lambda x/a) + ny]$$

where y is the circumferential coordinate (denoted by θ in Cheng and Ho)

$\lambda = m \pi a/L$

L is the shell length,

m is an integral number of axial half-waves,

n is an integral number of hoop waves,

and U, V, W are unknown constants.

Upon substituting the displacements into the equilibrium equations, the trigonometric terms can be eliminated and there remains a set of three homogeneous algebraic equations in U, V, W. These equations are:

$$\begin{bmatrix} (F_{11}-\lambda^2 q_2-2n\lambda q_3-n^2 q_1) & (F_{12}) & (F_{13}+\lambda q_1) \\ (F_{12}) & (F_{22}-\lambda^2 q_2-2n\lambda q_3-n^2 q_1) & (F_{23}-2\lambda q_3-nq_1) \\ (F_{13}+\lambda q_1) & (F_{23}-2\lambda q_3-nq_1) & (F_{33}-\lambda^2 q_2-2n\lambda q_3-n^2 q_1) \end{bmatrix} \begin{Bmatrix} U \\ V \\ W \end{Bmatrix} = 0 \qquad (14)$$

where the F's are functions of material properties lamination structure, shell geometry, λ, and n,

q_1 is the external radial pressure loading factor,

q_2 is the axial loading factor,

q_3 is the torsional loading factor.

Non-trivial solutions exist if and only if the determinant of the coefficient matrix equals zero.

Thus far we have followed the analysis of Cheng and Ho. Now we particularize it to our specific problem. Of the three external loadings considered by these authors, we drop the torsion factor q_3 in (14). Since we are concerned with hydrostatic external pressure, the loading factors q_1 and q_2 are uniquely related. Viz., by definition,

$$q_1 = pa/A_{22} \quad , \qquad (15)$$

and $$q_2 = P/A_{22} \quad . \qquad (16)$$

Also, $$\sigma_y = pa/h \quad , \qquad (17)$$

$$\sigma_x = 2\pi aP/2\pi ah = P/h \quad . \qquad (18)$$

But, $\sigma_y = 2\,\sigma_x$. (19)

Therefore, $P = pa/2$. (20)

Substituting (20) into (16),

$$q_2 = pa/2A_{22} \quad . \quad (21)$$

Thus, comparing (15) and (21),

$$q_1 = 2q_2 \quad . \quad (22)$$

In the above, p is external lateral pressure,
P is axial load,

and $$A_{22} = \sum_{k=1}^{n} \int_{\text{lower } z}^{\text{upper } z} \overline{Q_{22}}\, dz \quad .$$

If we now expand the determinant, the characteristic equation is in terms of the F's, n, λ, and q_1. The object then is to determine the root q_1 which is the least positive real root that satisfies the characteristic equation. This can be done by performing iterations on m, n, and q_1. First, we set m = 1 (i.e., assume one half-wave in the axial direction --- this is always the actual deformation for external hydrostatic pressure), and n = 2 (i.e., assume two waves in the circumferential direction --- this is the least physically meaningful value for n). With these parameters set, we iterate on q_1 starting at zero and continuing until the value of the characteristic equation changes sign (i.e., a "root" has been bracketed). If the difference between the last trial value of q_1 and the current trial value of q_1 is less than or equal to 1% of the current value, these last two values of q_1 are averaged, and the result is taken as a

root of the characteristic equation, and recorded as a possible solution for the critical value of q_1. The procedure continues with higher integral values of n up to a user-defined upper limit. Of all the possible solutions found, the least value of q_1 is chosen as the critical loading factor, and the critical pressure is calculated as

$$p_{cr} = q_{1(min.)}A_{22}/a \qquad (23)$$

Since manual computations are not practical, a program was coded in subset FORTRAN 77 for use on personal computers. The program requires about 72 kbytes in executable form and can be run on 16-bit machines running MS-DOS 2.0 or higher without modification. The program works in interogative mode, the user supplying data on material properties, shell geometry, and lamination structure as required; it can produce output on the terminal, and in report form for later printout. The listing of the program appears as Appendix 8, and the reports for the four tubes tested are shown in Appendix 9.

The calculated critical external pressures are:

	Tube 1	Tube 2	Tube 3	Tube 4
Computer-Program: Critical External Hydrostatic Pressure (kPa)	317	305	134	173

Before we consider other methods of finding the critical pressure, some remarks on the analysis and our specific implementation are in order. The simplifications due to the effective assumption of the Love-Kirchhoff hypotheses and small deformations have already been mentioned. Furthermore, the assumed displacement field will not completely satisfy any of the traditional shell boundary conditions. Thus, the solution having been determined from the characteristic equation without imposing boundary conditions can only be approximate unless the shell is infinitely long. Within the body of the program, the user can choose to calculate laminate properties from the basic properties of the constituents of the composite layers. This will introduce approximations into the material properties used in the solution. (See [29], chapter 9, on micromechanics of composite materials. It is perhaps not superfluous to mention the variability in mechanical properties which can occur as a result of differences in workmanship and curing methods in these structures.)

Since the minimum root is found by iteration, its accuracy is limited by the criterion of 1% difference imposed in the computer algorithm. This resolution is considered consistent with general requirements and speed of execution. Some extreme cases were run to determine approximate solution times:

Case 1) a short, thin , stiff tube: time = 18 s .

Case 2) a short, thick, stiff tube: time = 16 s .

Case 3) a short, thin , flexible tube: time = 13 s .

Case 4) a short, thick, flexible tube: time = 18 s .

Case 5) a long , thin , stiff tube: time = 14 s .

Case 6) a long , thick, stiff tube: time = 13 s .

Case 7) a long , thin , flexible tube: time = 12 s .

Case 8) a long , thick, flexible tube: time = 17 s .

A short tube is one with $L/a = 0.5$.

A long tube is one with $L/a = 10$.

A thin tube is one with $h/a = 0.01$.

A thick tube is one with $h/a = 0.1$.

A stiff tube is made of graphite/resin with $\theta = +/- 80$.

A flexible tube is made of glass/resin with $\theta = +/- 20$.

The times given above were obtained using an 8087 arithmetic co-processor. Without this optional chip, the same solutions required 7 to 10 minutes each.

As already mentioned, no boundary conditions were imposed when solving for critical pressure. In order to get an idea of the effect of this neglect, results from the computer solution were compared with curves published in [21]. The latter paper shows that the effect depends on lamination structure, boundary conditions, and length-to-radius ratio. The effect is most serious for

generally anisotropic layups, for hinged boundary conditions, and small (L/a) ratios. For these cases, they report the ratid of critical pressure without B.C. to that with B.C. is about 1.7 at (L/a)=1, about 1.3 at (L/a)=10, and 1 at (L/a)=100. Results from the present computer program were compared to results for B.C. SS1 plotted in [21]. This comparison gives ratios of our computed results without B.C. to plotted values with B.C. of about 1.7 at (L/a)=1, to about 1.2 at (L/a)=30. Thus, the present program implemented gives solutions comparable to those in [21]. For isotropic and orthotropic cases, the agreement is within about 5%. Similar agreement was obtained in comparisons made with [25] for orthotropic shells, and with [30] for isotropic shells.

II.2.2 Two Code Procedures

In the Introduction, we mentioned a draft proposal circulated by the RTP Committee of the ASME and a French Standard. These are applicable to containers which may experience up to full vacuum. The procedures will be outlined in the following two subsections using our four tubes as test cases.

II.2.2.1 RTP Draft Proposal No. 5

This document [personal communication] is not a standard, but has been submitted for consideration to Subcommittee X of the ASME on fiber reinforced plastic vessels. The proposal gives two options for designing: A) design by rules, and B) design by stress analysis. Since buckling is not mentioned in Mandatory Appendix M-9 which describes the method by stress analysis, we will only consider design by rules as given in subpart 3A, article -310. There, cylindrical shells subjected to external pressure are dealt with. The procedure is as follows.

Compute the values L/D_o

and $1.73(D_o/t)^{1/2}$

If the latter is less than the former, calculate

$$p_a = 2.6(E/F)(D_o/L)(t/D_o)^{2.5}$$

If not, calculate

$$p_a = [2.6(E/F)(t/D_o)^{2.5}]/[(L/D_o)-0.45(t/D_o)^{1/2}]$$

The symbols have the following meanings:

D_o = outside diameter (in.)

E = the lower of hoop tensile modulus and axial tensile modulus (psi)

F = safety factor = 5

L = length of cylinder (in.)

t = wall thickness (in.)

p_a = allowable external pressure (psi)

For our structures, the axial modulus is the lower. Therefore, $E = E_x^{lam}$. The method of calculating E_x^{lam} is shown in Appendix 10. The values for the four tubes tested are presented below in Table 7.

TABLE 7. Critical Pressures Using RTP Draft Proposal No.5

	Tube 1	Tube 2	Tube 3	Tube 4
D_o (in.)	10.929	10.921	11.008	10.921
L (in.)	34.016	34.016	34.488	34.173
t (in.)	0.228	0.224	0.110	0.106
E (psi)	530 700	568 400	1 183 200	1 450 000
p_a (psi)	5.692	5.838	1.989	2.269
$5p_a$ (psi)	28.46	29.19	9.945	11.34
$5p_a$ (kPa)	196	201	68.6	78.2

We can see that the procedure is relatively simple and does not require long calculations. The equation for critical pressure is a specialization of an equation which was developed at the U.S. Experimental Model Basin, which is itself a simplified form of a relation published by von Mises.[31] This equation in its original context refers to isotropic shells. The draft proposal merely chooses the lesser of the axial and hoop moduli in place of the isotropic modulus, and maintains the assumption of a Poisson's ratio of 0.3. Figure 31 shows the comparison of experimental data and the prediction for isotropic shells. The authors of [31] point out that "...experimental points lie above the theoretical line..." for the thinner vessels.

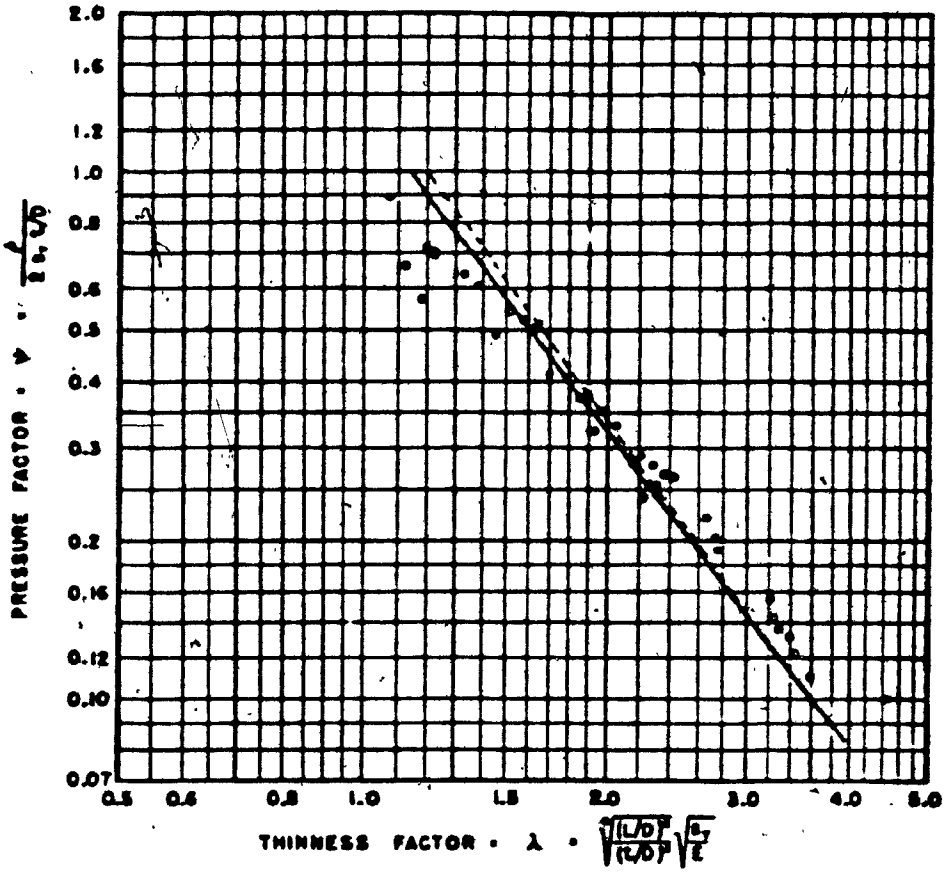

Figure 31. Comparison of Experimental and Predicted Hydrostatic Buckling Pressure for Isotropic Cylindrical Shells [31]

This is said to be due to the fact that the data represent ultimate collapsing pressure while the curve represents "...the pressure at which deflections increase rapidly..."

The determination of the hoop and axial laminate moduli is to be made experimentally using ASTM D 1599, as per Part 7 of the proposal. This involves testing sample tubes to destruction under internal pressure. In the present case, these moduli were calculated as shown in Appendix 10. This part of the procedure is perhaps the most tedious and error-prone, but it can easily be coded so that a computer or even some programmable calculators can be used.

II.2.2.2 French Standard [6]

This standard was published in December 1976 by the Commission Chaudronnerie Génie Chimique du Syndicat Général de l'Industrie du Plastique Armé. It deals with thermoset resins reinforced with glass, including containers made by filament winding. The problem of cylinders buckling under external pressure or vacuum is addressed in article 3.11. The procedure is similar to the previous one, and it is outlined below.

First, calculate L/R ,

and $2.5(E_x/E_y)^{1/4}\ (R/t)^{1/2}$.

If the former is greater than or equal to the latter,

then calculate $p_{cr} = 3E_y i/R^3$

Otherwise, $p_{cr} = 0.83E_s(t/R)^{5/2}(R/L)$

The symbols have the following meaning:

L = cylinder length

R = cylinder radius

t = wall thickness

i = 2nd moment of area of shell wall

E_x = axial modulus

E_y = hoop modulus

p_{cr} = critical pressure

and E_s is given as

$$E_s = n^{3/4}E_y(E_x/E_y)^{1/4}/[1-0.1(E_x/E_y)]$$

with $n = \frac{\text{flexural modulus in hoop direction}}{\text{tensile modulus in hoop direction}}$

We have no experimental data for the flexural modulus of the tube walls. However, previous testing of similar materials [32] indicates that a value of 80% of the tensile modulus is not unreasonable. We will use this value in the calculations. The results for the four tubes are given below in Table 8.

TABLE 8. Critical Pressures Using French Standard

	Tube 1	Tube 2	Tube 3	Tube 4
R * (mm)	136	136	138	137
L (mm)	864	864	876	868
t (mm)	5.8	5.7	2.8	2.7
E_x (kPa)	3.66 E6	3.92 E6	8.16 E6	10.0 E6
E_y (kPa)	3.99 E6	4.81 E6	10.1 E6	15.6 E6
ν	0.80	0.80	0.80	0.80
E_s (kPa)	3.72 E6	4.38 E6	9.29 E6	12.6 E6
p_{cr} (kPa)	183	206	71.2	90.0

* We take R to be the mid-surface radius.

We point out that, unlike the American proposal, a safety factor of 3 is recommended for buckling in article 3.12.C.

II.2.3 Miscellaneous Design Methods

In this subsection, three methods are cited for determining the critical pressure for thin isotropic shells and we briefly discuss methods for orthotropic shells. (More than 190 design methods/equations are given in [33] for isotropic and orthotropic circular cylindrical shells under various loadings and with different boundary conditions. Most of the orthotropic cases deal with shells that have ring and/or longitudinal stiffeners. In some cases, the predictions are compared with experimental results.)

Since we have already used the design equation from the U.S. Experimental Model Basin in Section II.2.2.1, and since it is considered to give acceptable results for

isotropic shells, we cite the following three cases for reference only. One method gives the critical pressure explicitly but requires iteration on the number of circumferential lobes formed to find the minimum pressure [34]. Another gives a critical pressure formula which requires graphical evaluation of one of the equation's constants.[35] The third gives the critical design pressure in a simple equation.[36] Before proceeding to orthotropic cases, we want to point out that there are sources which suggest the use of methods developed for isotropic materials in the design of reinforced plastic structures. In particular, such a design curves for hydrostatic external pressure is shown in Figure 32. For purposes of comparison, the predicted critical pressures for our tubes were calculated using the axial modulus in the design equation as we did above. The following results were obtained:

Tube 1 : critical pressure = 234 kPa .

Tube 2 : critical pressure = 251 kPa .

Tube 3 : critical pressure = 98.7 kPa .

Tube 4 : critical pressure = 121 kPa .

Note that these curves were developed for isotropic materials, though they are recommended for composite shells in reference [37] cited for Figure 32.

One of the earliest analysis of orthotropic cylindrical

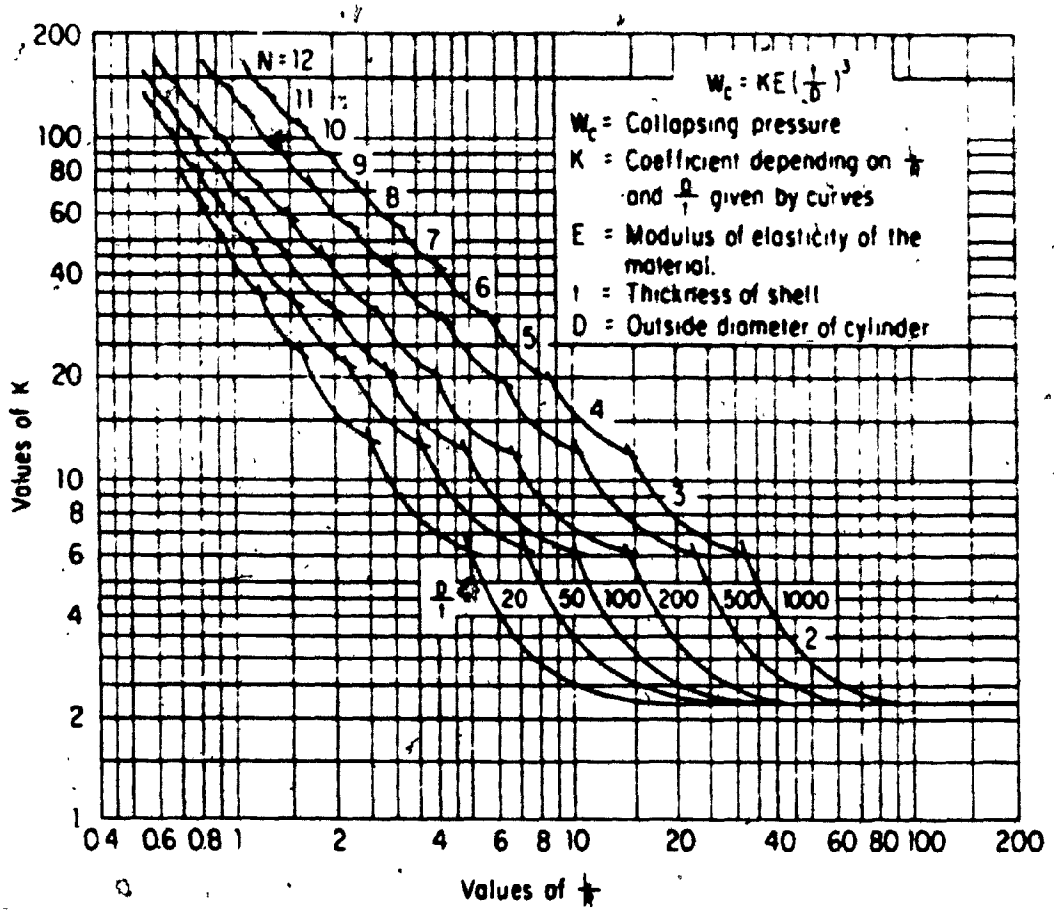

Figure 32. Suggested Design Curves for Reinforced Plastic Vessels Under Hydrostatic External Pressure
See text on p. 77 for details. [37]

shells subjected to buckling loads was done by Hess.[19] In his paper, Flügge's differential equations are used and assumed displacement functions corresponding to simply supported ends are borrowed from Timoshenko. The equilibrium equations are formulated and the characteristic determinant solved to find the minimum load parameters by varying the wave numbers in the axial and circumferential directions. Thus, the method is similar to the one we implemented except that the shell is neither heterogeneous (laminated) nor generally anisotropic. Hess goes on to simplify the equations, and produces families of curves for a few material properties and shell geometries. Using these curves, critical loading parameters in the axial and lateral directions can be calculated, and a linear interaction plot made. If the actual load values are below the interaction curve (which is considered conservative), then the structure is deemed safe. Hess' method requires the production of design curves which necessitates the solution of numerous and long equations. For this reason, and because of the restriction to orthotropic shells it was not thought useful to implement the procedure. Hess claims very good agreement with experimental results on isotropic shells (no data being available on orthotropic shells), but the procedure described above also gives good agreement for the isotropic case (page 35 above).

We have already briefly mentioned the work of Lei and

Cheng.[25] The method is that of Cheng and Ho [20] except that the developement is for orthotropic shells. The present analytical results are very close to those of Lei and Cheng for the orthotropic cases compared (page 35 above).

Since the computational effort is almost the same, and shell buckling is sensitive to generally anisotropic constructions, it was decided that the more general formulation taken from Cheng and Ho [20] should be implemented.

III.1.0 DISCUSSION AND CONCLUSION

In this final section, the experimental results are examined and compared to the three specific methods of calculating critical pressure detailed in Section II. The conclusion is developed on the basis of this comparison, and some comments are made on the problems encountered in the testing and the interpretation of the data.

III.1.1 Data Interpretation

The data is shown in Appendix 6 and consist of strain-pressure values collected during the test runs on the four tubes. All tubes were taken to collapse in a single run except tube 3 on which three runs were made before destruction. The data is plotted in Figures 19 and 21 to 25. In these plots the curves are numbered to correspond to the scheme described in Figure 16.

When strain gages are used in buckling tests it is usual to take the load value where strain reversal occurs as the critical load. This is done because buckling causes a large change in the shape of the shell which can cause more-or-less sudden reversal in the strain. It is thought, however, that in the present case where the absolute strains attained are less than 0.3% another criterion should also be considered, viz. large deviations from linearity. Because

we are operating in the linear elastic region of these materials [38], such deviations are considered to result from instability. There are at least six strain gages bonded to each tube (9 in the case of the first test run on tube 3). Since the shell may become unstable at one location before others, we must take the lowest pressure where evidence of instability appears to be the buckling pressure. Since we do not have full-field monitoring of the tubes (which would be best), there is a possibility that instability may occur at an uninstrumented location at a pressure lower than that identified as the buckling pressure.

There is a slight further complication in that some strains show some minor fluctuations at low pressures. The "strain reversals" which appear in this low-pressure region are not considered to be due to instability for our purposes, but rather drift in the gages. For verification of the negligible character of these "reversals", enlarged plots are shown in Figures 33 to 36. The fact that these low-pressure "reversals" are followed by single major reversals before collapse is an indication that the former features are not pertinent.

With these considerations in mind, the following values are established as the experimental buckling pressures for the four tubes tested:

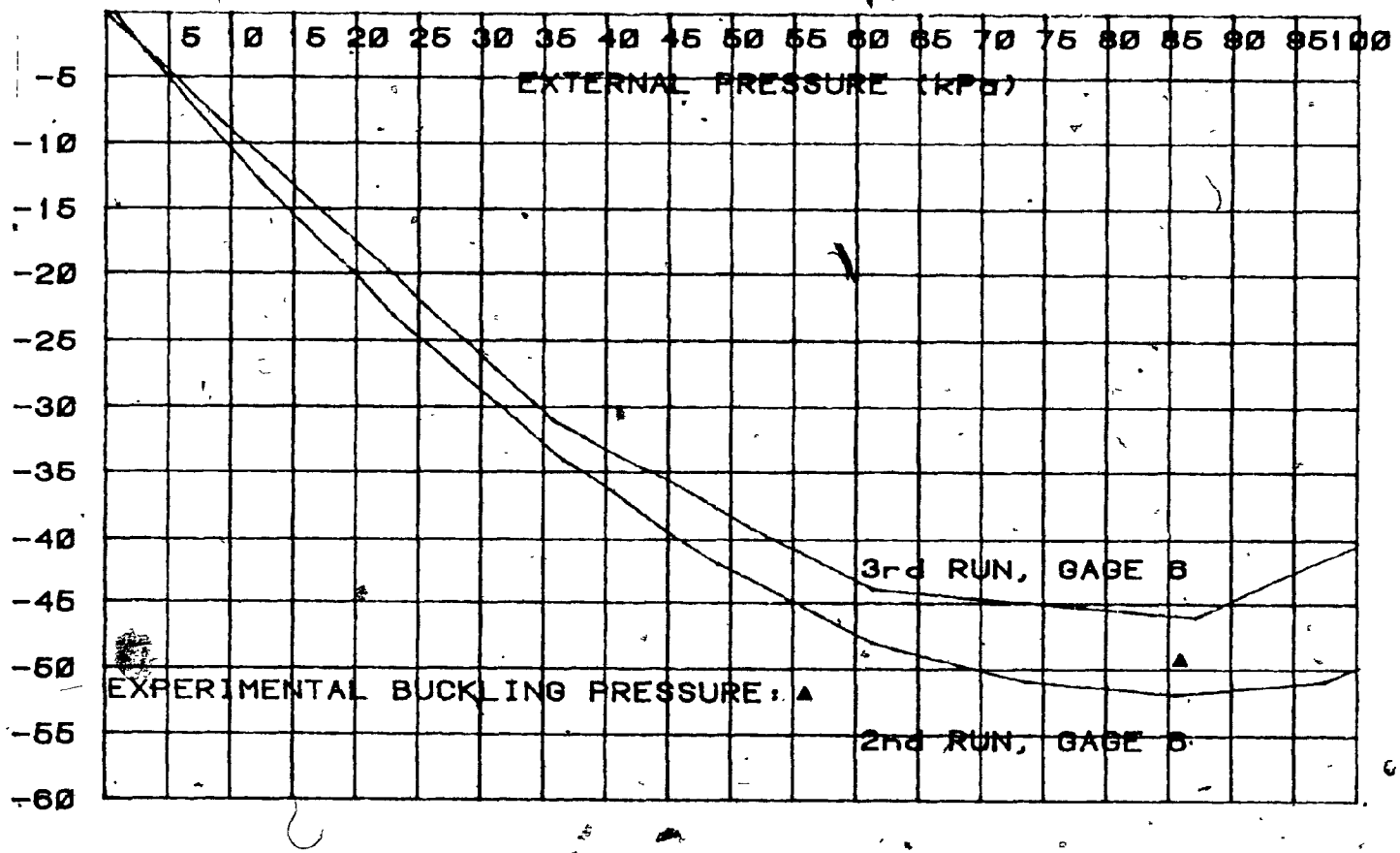

Figure 33. Enlarged plot for Tube 3.

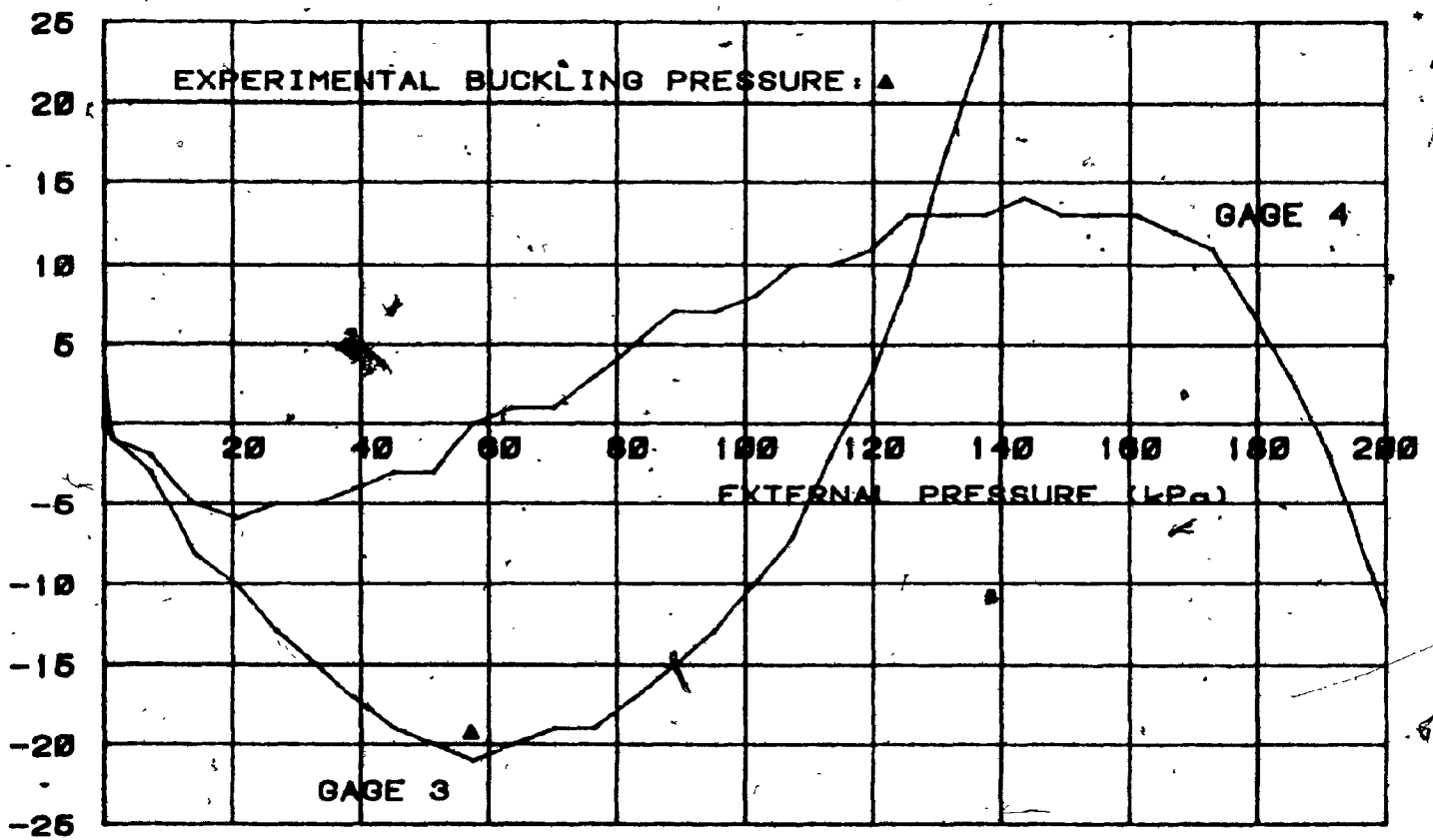

Figure 34. Enlarged plot for tube 4.

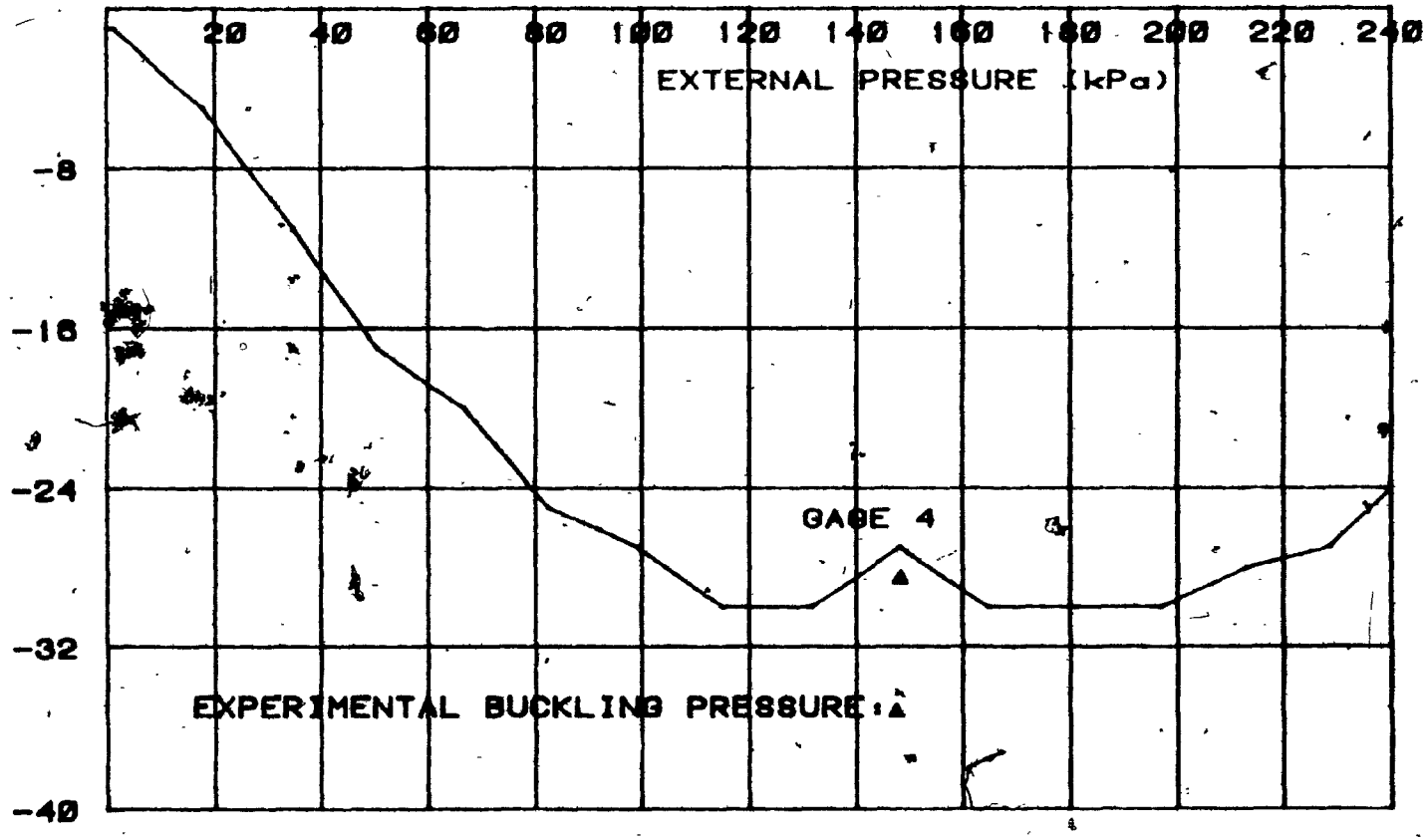

Figure 35. Enlarged plot for tube 1.

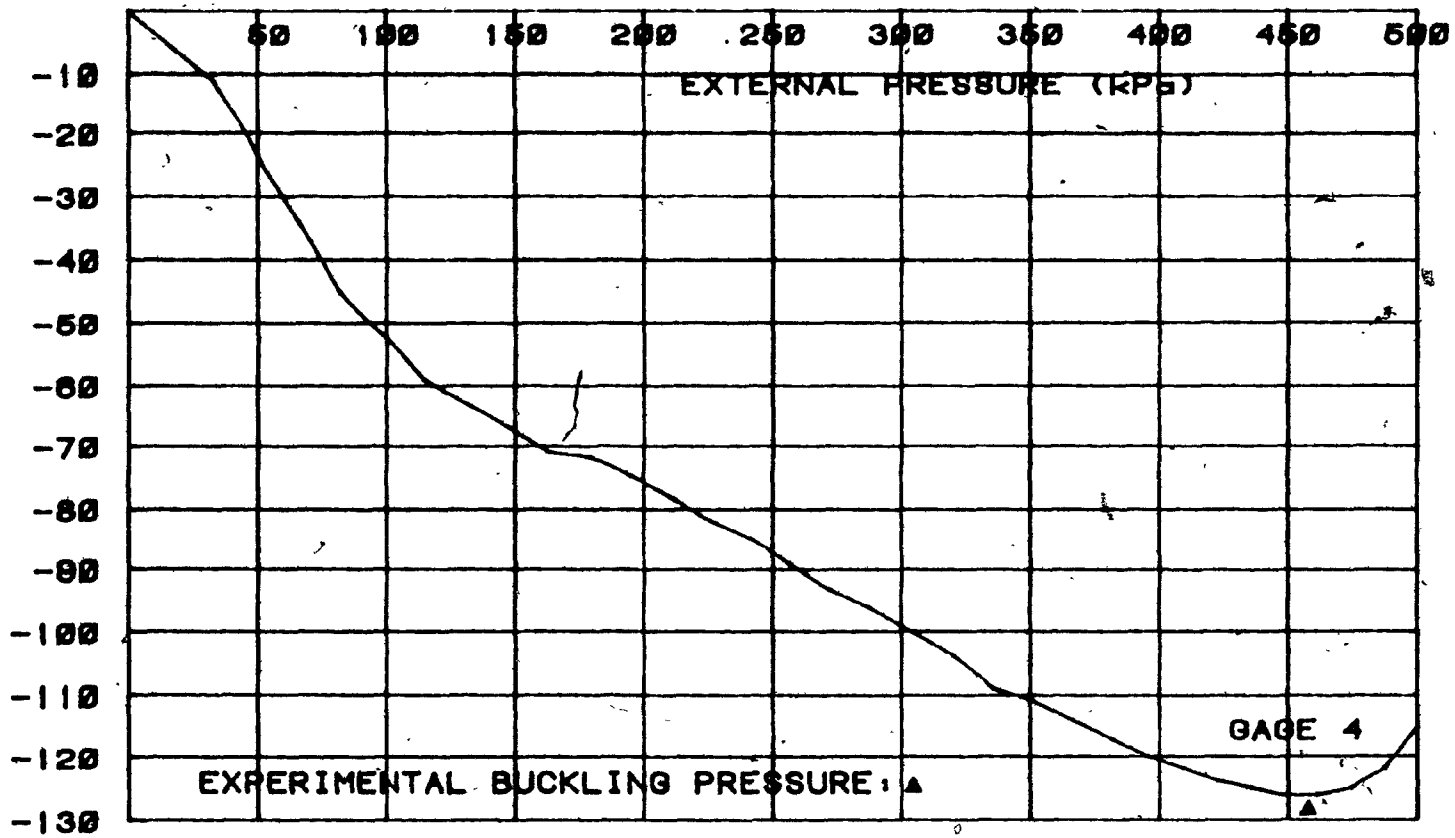

Figure 36. Enlarged plot for tube 2.

Tube 1: Experimental buckling pressure = 148 kPa.

Tube 2: " " " = 460 kPa

Tube 3: " " " = 86 kPa

Tube 4: " " " = 58 kPa

The buckling pressures are marked on Figures 33 to 36.

A perfectly cylindrical tube would be expected to give compressive strains in both axial and circumferential directions during pressurization. Looking at the results from tube 2 in Figure 25, we see this is the case for the tube showing the least imperfection amplitudes combined with the most cylindrical form. In the case of the other three tubes, which had a clearly elliptical form, the signs of the strains depend on a combination of position of the gages on the imperfect surface, on bending of the tube during pressurization, along with the expected compressive strains.

As mentioned previously, three runs were made on tube 3 before it collapsed on the third run. We should point out that despite the non-linear strain-pressure behaviour, the strains on the second run returned almost to zero (see inset in Figure 21), and after a longer time at zero pressure the values would no doubt have been even closer to zero. Thus, the elastic regime seems not to have been exceeded. Furthermore, the final collapse pressure is 2.8 times higher than the buckling pressure established above,

giving a margin of safety to this tube. It should be cautioned, however, that the final collapse pressure is slightly lower than the maximum pressure attained in the second run, and damage, invisible to the unaided eye, may have been incurred during the penultimate pressurization.

III.1.2 Comparison of Results

The comparison of the predicted and experimental buckling pressures are tabulated below in Table 9.

TABLE 9. Experimental vs Calculated Pressures (kPa)

	EXPERIMENTAL RESULT	PRESENT METHOD	RTP DRAFT PROPOSAL	FRENCH STANDARD
Tube 1	148	317 (0.47)*	196 (0.76)	183 (0.81)
Tube 2	460	305 (1.51)	201 (2.29)	206 (2.23)
Tube 3	86	134 (0.64)	68.6 (1.25)	71.2 (1.21)
Tube 4	58	173 (0.34)	78.2 (0.74)	90.0 (0.64)

* Number in parentheses is ratio (Experiment/Prediction)

The experimentally determined buckling pressure for tube 2 is 1.51 to 2.29 times greater than the prediction. Recall that this tube did not have an elliptical shape. Furthermore, it has relatively small imperfections compared to tubes 3 and 4 (see Table 5). Since the critical pressure also corresponds to an elliptical shape according to analysis by the present method (see Appendix 9), tube 2 may be said to be the least imperfect of the structures tested.

Thus, that the ratio of experimental to calculated pressure is highest might have been expected. However, that the ratio is greater than 1.0 is unexpected. Re-examining the data shows no great difference between tubes 1 and 2, except in the shape and winding angle. The large ratios of pressures must therefore be attributed to the small number of locations gaged. In other words, it is thought that, had many more gages been used, a much lower instability pressure might have been detected. Note that the present method of calculation gives the closest prediction. Pressure ratios larger than 1.0 for tube 3 also are given by the Proposal and the Standard, but not by the present method.

Tubes 3 and 4, with winding angles of 54^{o} and 63^{o} respectively, have unexpected buckling pressures with respect to each other; i.e,, tube 4 should exhibit a higher buckling pressure than tube 3, but the reverse is observed. The major contributing factor is considered to be the larger relative circumferential imperfections of tube 4 as shown in Table 5.

From Table 9 we see that the RTP Draft Proposal No. 5 and the French Standard are more conservative than the present method, and the former two give similar results for the structures tested. If we incorporate the recommended safety factors of 5 for the Proposal and 3 for the Standard, and a reduction factor of 5 for the present method (based on

a factor of 1.7 due to neglect of boundary conditions --- as discussed on page 69 above---, and a factor of 3 based on the lowest ratio of 0.34 shown in Table 9), the following table results.

TABLE 10. Experimental vs Design Pressures (kPa)

	EXPERIMENTAL RESULT	PRESENT METHOD	RTP DRAFT PROPOSAL	FRENCH STANDARD
Tube 1	148	63 (2.3)*	39 (3.8)	61 (2.4)
Tube 2	460	61 (7.5)	40 (11.5)	69 (6.7)
Tube 3	86	27 (3.2)	14 (6.1)	24 (3.6)
Tube 4	58	35 (1.7)	16 (3.6)	30 (1.9)

* Number in parentheses is the ratio (Experiment/Design)

The RTP Draft Proposal No. 5 gives the most conservative design pressures. The French Standard and the present method give very similar results and both provide some safety margin.

III.1.3 Conclusion

It was the purpose of this thesis to determine which analysis or set of rules was most appropriate to predict the buckling pressure of composite tubes made by the process of filament winding. The procedure adopted must be easy to use for designers of glass-fiber reinforced equipment working in small and medium-size companies. It must also provide designers and users with confidence in the structures fabricated. These considerations led to the selection of

three specific procedures which were compared to one another and to the results of tests on structures typical of those used in the chemical processing industry, though smaller in size. The tests included imperfection survey as well as determination of buckling pressures.

All three procedures give design pressures which are lower than the experimental buckling pressures. The ASME RTP Draft Proposal No. 5 gives the most conservative design pressure with values ranging from 3.6 to 11.5 times less than the observed buckling pressures. The present method, which is an implementation of an analysis by Cheng and Ho [20], and the French Standard give very similar results, the comparable factors ranging from 1.7 to 7.5.

(The reader is cautioned that the factor of 5 used to calculate the design pressure from the predicted pressure using the present method does not necessarily mean that a structure can withstand a buckling pressure five times greater than the design pressure, as the present data shows!)

As can be seen in Figures 8 and 10, and Figures 29 and 30, the principal areas of damage occur at the lines of maximum curvature of the elliptically shaped tubes 3 and 4. Tubes 1 and 2 which did not have such pronounced imperfections show more widespread damage in Figures 27 and 28. Imperfections are larger than those reported for steel shells. It is encouraging to note then that acceptable design pressures can still be arrived at, and that the ultimate collapse pressure is higher than the buckling

pressure in each case.

In general then, the French Standard can be said to meet the criteria of "ease of application" and "good agreement with experiment" to a greater extent than the other two procedures investigated. The analytical procedure implemented here is more complex to formulate and solve, but once coded, it gives results comparable to the French Standard, and it offers the advantage that it can be improved to account for boundary conditions, as well as shape imperfections. The ASME Draft Proposal No. 5 is practically as complicated as the French Standard and gives more conservative design pressures. It must be cautioned that fatigue and creep are not included in the present work, although the designer of reinforced plastic structures must always consider these complications in practice.

It must be remembered that only four tubes were tested in this study, and each tube was different in some respect from the others. Clearly, the results must be used with prudence in the absence of a larger data base. More extensive testing might uncover typical shapes and imperfection amplitudes for the filament winding process. This statistical information would then be used to impose more appropriate knock-down factors in designing.

REFERENCES

1. Attributed to Eugene E. Lundquist, NASA, by Paul, Seide, Small Elastic Deformations of Thin Shells, Noordhoff International Publishing, Leyden, The Netherlands, 1975, p. XVI.

2. Leonard, R.W., Anderson, M.S., Heard, W.L. Jr., "Design of a Mars Entry 'Aeroshell'", in Buckling of Structures, Symposium of IUTAM, Budiansky, B., ed., Cambridge/USA, June 17-21, 1974, Springer-Verlag, Berlin, 1976, p. 363.

3. Lubin, George, ed., Handbook of Composites, Van Nostrand Reinhold Co., New York, N.Y., 1982.

4. _____, Boiler and Pressure Vessel Code, Section X, Fiberglass Reinforced Plastic Pressure Vessels, ASME, New York, 1980 edition.

5. _____, Vessels and Tanks in Reinforced Plastics, British Standards Institution, London, 1973.

6. _____, Code de construction des appareils chaudronnes en plastique armé, AFNOR, Paris, 1976.

7. Bushnell, D., "Buckling of Shells --- Pitfall for Designers", AIAA Journal, Vol.19, No.9, 1981.

8. Todhunter, I., Pearson, K., A History of the Theory of Elasticity and of the Strength of Materials from Galilei to Lord Kelvin, Dover Pub. Inc., New York, 1960, Vol. II, Part I, pp.662-666.

9. Love, A.E.H., A Treatise on the Mathematical Theory of Elasticity, 4th edition, Dover Pub. Inc., New York, 1944.

10. Hoff, N.J., "The Perplexing Behaviour of Thin Circular Cylindrical Shells in Axial Compression", Israel Journal of Technology, Vol. 4, No. 1, 1966, pp. 1-28.

11. Timoshenko, S., Theory of Elastic Stability, 2nd ed., McGraw-Hill Book Co., Inc., New York, 1961.

12. Citerley, R.L., "Imperfection Sensistivity and Post-buckling Behavior of Shells", in Pressure Vessel and Piping : Design Technology - 1982 - A Decade of Progress, Zamrik, S.Y., and Dietrich, D., eds., ASME, New York, 1982.

13. Donnell, L.H., "Effect of imperfections on buckling of thin cylinders under external pressure", Journal of Applied Mechanics, Vol. 23, 1956, pp. 569-575.

14. Budiansky, B., Amazigo, J.C., "Initial Post-Buckling Behavior of Cylindrical Shells Under External Pressure", Journal of Mathematics and Physics, Vol. 47, 1968, pp. 223-235.

15. Vinson, J.R., Chou, T.-W., Composite Materials and Their Use in Structures, Wiley, New York, 1975, chapter 7.

16. Ambartsumian, S., "Contributions to the Theory of Anisotropic Layered Shells", Applied Mechanics Reviews, Vol. 15, No. 4, 1962, p. 245.

17. Flügge, W., Stresses in Shells, Springer-Verlag, Berlin, 1960.

18. Tennyson, R.C., "Buckling of laminated composite cylinders: a review", Composites, Jan. 1975, pp. 17-24.

19. Hess, T.E., "Stability of Orthotropic Cylindrical Shells Under Combined Loading", American Rocket Society Journal, Vol. 31, No. 2, April 1961, pp.237-246.

20. Cheng, S., Ho, B.P.C., "Stability of Heterogeneous Aeolotropic Cylindrical Shells Under Combined Loading", AIAA Journal, Vol. 1, No. 4., April 1963, pp. 892-898.

21. Ho, B.P.C., Cheng, S., "Some Problems in Stability of Heterogeneous Aeolotropic Cylindrical Shells under Combined Loading", AIAA Journal, Vol. 1, No. 7, July 1963, pp. 1603-1607.

22. Tasi, J., Feldman, A., Stang, D.A., "The buckling strength of filament-wound cylinders under axial compression", NASA, CR-266, July 1965.

23. Tasi, J., "Effect of heterogeneity on the stability of composite cylindrical shells under axial compression", AIAA Journal, Vol. 4, No. 6., June 1966, pp. 1058-1062.

24. Martin, R.E., Drew, D.D., "A Batdorf Type Modified Equation for the Stability Analysis of Anisotropic Cylindrical Shells", Technical Report No. 10, Project Themis, Texas A&M Univ., March 1969.

25. Lei, M.M., Cheng, S., "Buckling of Composite and Homogeneous Isotropic Cylindrical Shells Under Axial and Radial Loading", Journal of Applied Mechanics, Dec. 1969, pp. 791-798.

26. Herring, H.W., Baucom, R.M., Pride, R.A., "Mechanical Behavior of Boron-Epoxy and Glass-Epoxy Filament-Wound Cylinders Under Various Loads", NASA, TN D-5050, Dec. 1968.

27. Almroth, B.O., "Design of Composite Material Structues for Buckling --- An Evaluation of the State-of-the-Art", Technical Report, AFWAL-TR-81-3102, Wright-Patterson Air Force Base, Ohio 45433, 1981.

28. Donnell, L.H., Beams Plates and Shells, McGraw-Hill Book Co., New York, 1976.

29. Tsai, S.W., Hahn, H.T., Introduction to Composite Materials, Technomic Pub. Co., Inc., Westport, CT 06880, 1980.

30. Yamaki, N., Otomo, K., "Experiments in the Postbuckling Behavior of Circular Cylindrical Shells Under Hydrostatic Pressure", Experimental Mechanics (SESA), Vol. 13, No. 7, 1973, pp. 299-304.

31. Windenburg, D.F., Trilling, C., "Collapse by Instability of Thin Cylindrical Shells Under External Pressure", ASME Trans., Vol. 56, 1934, pp. 819-825.

32. Hoa, S.V., Sankar, T.S., Bargiora, R., "Tension, compression and bending behavior of hand layup laminates for fiber reinforced plastic vessels", Report 1, PRAI Project "Stress Analysis for Optimum Design of Fiber Reinforced Plastic Vessels", October 1983.

33. _____, Handbook of Structural Stability, edited by Column Research Committee of Japan, Corona Pub. Co. Ltd., Tokyo, 1971.

34. Fried, N., "Survey of Methods of Test for Parallel Filament Reinforced Plastics", in Symposium on on Standards for Filament-Wound Reinforced Plastics, ASTM STP 327, ASTM, Philadelphia, 1963.

35. Baker, E.H., et al., "Shell Analysis Manual", NASA, CR-912, April 1968.

36. Weingarten, V.I., Seide, P., "Elastic Stability of Thin-Walled Cylindrical and Conical Shells under Combined External Pressure and Axial Compression", AIAA Journal, Vol. 3, No. 5, May 1965, pp. 913-920.

37. Mallinson, J.H., Chemical Plant Design with Reinforced Plastics, McGraw-Hill Book Co., N.Y., 1969, Figure 14.8.

38. Hoa, S.V., et al., "Tensile and Compressive Properties of Laminates made by Filament Winding with Glass Fiber Reinforced Polyester Materials", Report 2, PRAI Project "Stress Analysis for Optimum Design of Fiber Reinforced Plastic Vessels", December 1983.

Appendix 1. Calibration of Thickness Sensor

Instrument: Polygauge Model "C" Thickness Sensor (ser. no. 290) R.C. Maybee Ltd., P.O. Box 40, Oakville, Ontario, L6J 4Z5.

Standard: Mitutoyo Combimike 0-1 inch micrometer, resolution 0.01mm.

Specimen: Cut-out from burst cylindrical pressure vessel (radius of 900mm); construction: PVC liner/glass mat/filament winding in Derakane 411.

Procedure: Thickness measurements with the two systems were compared. The results are tabulated below.

Polygauge readout	Corresponding thick. * (mm)	Micrometer reading(mm)	Ratio (gauge/ micrometer)
1390	13.7	13.67	1.002
1296	11.4	11.56	0.986
1347	12.7	12.47	1.018
1365	13.2	13.09	1.008

* From Table No. 1 supplied with instrument.

Notes: 1. The instrument had to be recalibrated often because considerable drift was noticed.
2. The thickness correction for a tube of radius 900mm is negligible.

Conclusion: Corrected measurements taken with the gauge are considered sufficiently accurate for the present study.

Appendix 2. Calibration of Rotary Potentiometer

Instrument: Ten-turn potentiometer (manufacturer unknown)

Standard: Hardinge dividing head (ser. no. D216) with resolution of one degree.

Accessories: Fluke 8010A D.M.M. (ser. no. 2945016)
Dynascan 1650 power source set to "B tracks A 100%".

Procedure: The dividing head was used to input a known angular displacement to the pot. The output of the pot. was recorded as a function of the input. Three tests were conducted with the pot. powered by voltages of 50, 25, and 10 volts, respectively. All measurements were started with the pot. at approximate mid-range. Results are tabulated below.

Input (degree)	Test 1 (50 v in) Pot. output (volts)	Test 2 (25 v in) Pot. output (v)	Test 3 (10 v in) Pot. output (v)
0	-1.744	-1.278	-0.558
1	-1.732		
2	-1.713		
3	-1.699		
4	-1.690		
5	-1.673		
6	-1.663		
7	-1.648		
8	-1.634		
9	-1.620		
10	-1.606		
15	-1.535		
20	-1.466		
30	-1.330		
40	-1.190		
50	-1.054		
75	-0.712		
90	-0.501	-0.653	-0.308
91	-0.486		
92	-0.473		
93	-0.458		
94	-0.445		
95	-0.431		
96	-0.418		
97	-0.406		
98	-0.390		
99	-0.379		
100	-0.362		
120	-0.093		
150	0.323		
180	0.744	-0.035	-0.061

220	1.300		
221	1.316		
222	1.328		
223	1.344		
224	1.357		
225	1.372		
226	1.386		
227	1.398		
228	1.415		
229	1.427		
230	1.442		
260	1.855		
300	2.41		
310	2.54		
320	2.68		
330	2.82		
340	2.96		
350	3.10		
351	3.12		
352	3.13		
353	3.14		
354	3.16		
355	3.17		
356	3.19		
357	3.20		
358	3.21		
359	3.23		
360	3.24	1.213	0.439
270		0.593	0.190

The results were analyzed using a linear least-squares fit giving the following sensitivities for the three tests, respectively: 0.01385, 0.00692, 0.00277 volts/degree; all linear correlation coefficients were better than 0.99999.

The Potentiometer characteristic was determined by dividing the sensitivity in a test by the voltage input to the pot. for that test, and then taking the arithmetic average. The three characteristics obtained were, in order, 0.00028, 0.00028, 0.00028 volt output per degree per volt input.

Conclusion: The characteristic of the rotary potentiometer is 0.00028 volt output per degree rotation per volt input to the pot.

Appendix 3. Calibration of Linear Potentiometer

Instrument: Penny & Giles type LCP Conductive plastic potentiometer (ser. no. 822SA4K)

Standard: Starrett micrometer gage, resolution = 0.001 inch.

Accessories: Fluke 8010A D.M.M. (ser. no. 2945016)
Dynascan 1650 power source set at "B tracks A 100%".

Procedure: The same procedure was used as described in the previous appendix, except that input was linear displacement generated by the micrometer gage. Again, three different input voltages to the pot. were used in the tests; they were 25, 10, and 5 volts, respectively. All measurements were started with the pot. at mid-range approximately. Results are tabulated below.

Input (inch x 1000)	Test 1 (25 v in) Pot. output (v)	Test 2 (10 v in) Pot. output (v)	Test 3 (5 v in) Pot. output (v)
0	-0.699	-0.319	-0.195
10	-0.633	-0.296	-0.184
25	-0.538	-0.257	-0.165
50	-0.382	-0.194	-0.133
75	-0.234	-0.133	-0.103
100	-0.076	-0.070	-0.072
150	0.232	0.052	-0.010
200	0.549	0.181	0.056
250	0.876	0.312	0.121
300	1.214	0.444	0.189

The sensitivities were, in order, 6.32416, 2.53419, and 1.27552 volts per inch; the linear correlation coefficients were better than 0.9997.

The characteristics were determined as, in order, 0.253, 0.253, and 0.255 volts per inch per volt input, the average being 0.254.

Conclusion: The characteristic of the linear potentiometer is 0.254 volt output per inch displacement per volt input to the pot.

Appendix 4. Calibration of the Pressure Transducer

Instrument: Pace differential pressure transducer, model KP 15 (ser. no. 150338) with 25 psi and 100 psi membranes; Dynasciences Transducer Indicator, model CD25 (ser. no. 150565) with span set to 2.80 and 2.51, respectively, in the two tests conducted.

Standard: Merriam U-Tube Mercury manometer 36" range, model 10 AA 25 WM. USG 0-100 psi standard pressure gage.

Accessories: Fluke data logger, model 2280A (ser. no. 3220035) with High Performance A/D converter, model -161 and Voltage input connector, model -176.
Vacuum pump.

Procedure: Calibration for vacuum testing --- The pressure transducer with the 25 psi membrane installed and the U-Tube manometer were subjected to the same vacuum. The manometer readings and corresponding voltage readings from the data logger were used to determine the sensitivity as 10.24 cm Hg per volt for the transducer. Once established, the sensitivity was used to program the data logger, and the data logger values were then compared to the manometer readings. Typical comparative results are:

Manometer (cm Hg);	74.3,60.4,49.6,40.0,30.8,19.8,10.0
Data logger(cm Hg);	74.3,60.2,49.4,39.5,30.4,19.5, 9.9

Thus the largest % difference was -1.5%.
The final programmed expression was scaled to give output in kPa, and it is:

Vacuum(kPa) = -10.24[(current voltage)-(initial voltage)]
x[101.4 kPa/atm./(76 cm Hg/atm.)]

Calibration for pressure chamber testing --- The same procedure was used, except that the stiffer 100 psi membrane was installed in the transducer and a standard USG pressure gage replaced the manometer. The pressure source was a utility line at 8.8 atm. After regulating, the pressure was lead to the gage and the transducer, and the readings were related, giving a sensitivity of 12.13 psi per volt.
The final programmed expression with conversion to kPa was:

pressure(kPa)= 83.66[(current voltage)-(initial voltage)]*

Conclusion: Pressures were accurately given by the data logger.
* Errors were of the magnitude given above.

Appendix 5. Data logger strain recording verification

Instrument: Fluke data logger, model 2280A (ser. no. 3220035) with High Performance A/D converter, model -161, and Transducer Excitation module, model -164/AA.

Standard: The strain gage used was an MM type CEA-06-250UW-120 bonded with M-200 adhesive. A three-wire quarter-bridge configuration was used in the calibration as well as in the tests. The gage was bonded to an aluminium cantilever beam which could be given known end-deflections in a Photolastic Calibrator, model 010-B. The gage was connected to a Vishay Strain Indicator, model P-350 AK (ser. no. Q23051).

Procedure: The data logger was programmed for strain gage recording, and its readings compared to the Vishay readings for various deflections of the beam. Several comparison runs were made, and typical results are given below.

Calibrator position	: 25, 50, 75,100,,50,200,250,300,350
Strain Indicator (με)	: 104,183,258,334,486,636,784,934,1084
Data logger (με)	: 106,183,259,336,489,641,794,945,1096

Conclusion: The data logger strain readings were acceptable.

Appendix 6. Reduced strain-pressure data for four tubes.

DATA FOR TEST ON TUBE 3 UNDER VACUUM ONLY (RUN 1)

NUMBER OF GABES = 9
NUMBER OF DATA POINTS = 117

THE PRESSURE VALUES, IN kPa, FOLLOW:

22.09	23.86	24.72	26.86	29.56	32.04	34.30	36.41
38.40	40.32	42.17	43.95	45.67	47.34	48.96	50.53
52.05	53.50	54.92	56.32	57.68	59.03	60.31	61.56
62.76	63.93	65.06	66.12	67.16	68.16	69.13	70.06
70.94	71.79	72.61	73.41	74.17	74.91	75.63	76.32
77.02	77.67	78.29	78.87	79.38	79.95	80.47	81.00
81.49	81.98	82.43	82.87	83.29	83.72	84.13	84.50
84.88	85.23	85.58	85.91	86.22	86.49	86.78	87.08
87.34	87.61	87.88	88.12	88.35	88.59	88.82	89.02
89.29	89.50	89.70	89.87	90.04	90.22	90.38	90.55
90.70	90.87	91.01	91.15	91.30	91.43	91.59	91.74
91.87	92.00	92.11	92.18	92.29	92.40	92.50	92.60
92.70	92.79	92.89	92.98	93.07	93.17	93.25	93.33
93.42	93.50	93.57	93.65	93.72	93.80	93.86	93.94
94.00	94.07	94.72	94.74	94.79			

GAGE # 1 (MICROSTRAIN):

-6.	-9.	-10.	-13.	-18.	-21.	-25.	-29.
-31.	-34.	-35.	-39.	-40.	-43.	-46.	-48.
-51.	-52.	-55.	-56.	-59.	-60.	-61.	-63.
-65.	-67.	-68.	-69.	-72.	-72.	-75.	-76.
-76.	-77.	-79.	-80.	-81.	-81.	-82.	-85.
-85.	-85.	-88.	-89.	-89.	-90.	-89.	-90.
-91.	-92.	-92.	-93.	-95.	-95.	-95.	-95.
-95.	-98.	-96.	-100.	-97.	-98.	-98.	-99.
-100.	-98.	-99.	-100.	-101.	-100.	-101.	-101.
-101.	-102.	-102.	-102.	-102.	-102.	-101.	-102.
-101.	-103.	-101.	-103.	-103.	-101.	-102.	-103.
-104.	-102.	-103.	-103.	-104.	-104.	-103.	-103.
-103.	-104.	-104.	-103.	-103.	-103.	-102.	-103.
-104.	-103.	-104.	-105.	-105.	-104.	-103.	-104.
-105.	-105.	-103.	-103.	-103.			

GAGE # 2 (MICROSTRAIN):

-6.	-10.	-11.	-15.	-20.	-23.	-27.	-30.
-32.	-35.	-39.	-41.	-44.	-47.	-48.	-52.
-53.	-56.	-58.	-60.	-62.	-64.	-64.	-66.
-69.	-70.	-71.	-74.	-76.	-76.	-78.	-80.
-82.	-81.	-82.	-84.	-86.	-86.	-85.	-88.
-89.	-90.	-91.	-92.	-91.	-93.	-92.	-94.
-93.	-94.	-96.	-97.	-99.	-97.	-100.	-101.

-100.	-101.	-100.	-101.	-101.	-101.	-102.	-102.
-102.	-102.	-103.	-103.	-103.	-103.	-105.	-105.
-104.	-105.	-106.	-106.	-106.	-105.	-106.	-106.
-105.	-107.	-106.	-106.	-107.	-105.	-107.	-108.
-107.	-106.	-107.	-106.	-108.	-109.	-107.	-108.
-107.	-108.	-108.	-108.	-107.	-108.	-106.	-109.
-109.	-108.	-108.	-109.	-107.	-110.	-107.	-109.
-109.	-108.	-108.	-107.	-109.			

GAGE # 3 (MICROSTRAIN):

-6.	-11.	-13.	-18.	-22.	-27.	-30.	-33.
-36.	-40.	-43.	-45.	-50.	-52.	-52.	-56.
-58.	-61.	-64.	-66.	-68.	-70.	-71.	-72.
-75.	-76.	-77.	-80.	-81.	-81.	-83.	-84.
-86.	-86.	-88.	-90.	-91.	-91.	-92.	-92.
-93.	-96.	-96.	-97.	-96.	-96.	-97.	-99.
-98.	-98.	-101.	-102.	-102.	-101.	-102.	-102.
-103.	-103.	-103.	-105.	-105.	-104.	-105.	-104.
-105.	-106.	-106.	-106.	-106.	-107.	-106.	-108.
-107.	-107.	-106.	-107.	-107.	-108.	-109.	-107.
-108.	-107.	-107.	-108.	-108.	-110.	-110.	-111.
-110.	-112.	-108.	-109.	-109.	-110.	-108.	-110.
-110.	-110.	-110.	-111.	-108.	-110.	-110.	-110.
-110.	-111.	-110.	-110.	-110.	-110.	-111.	-111.
-109.	-109.	-110.	-109.	-109.			

GAGE # 4 (MICROSTRAIN):

8.	11.	14.	18.	23.	27.	32.	36.
41.	43.	49.	53.	55.	60.	64.	66.
70.	73.	77.	80.	83.	86.	89.	94.
97.	99.	102.	104.	107.	109.	113.	116.
118.	120.	123.	124.	127.	129.	131.	133.
135.	136.	138.	139.	142.	146.	146.	148.
149.	152.	153.	154.	155.	156.	158.	159.
160.	161.	163.	164.	165.	167.	168.	169.
169.	171.	171.	172.	173.	174.	174.	176.
177.	178.	179.	180.	180.	180.	179.	183.
184.	184.	184.	184.	186.	185.	187.	185.
187.	188.	190.	189.	191.	189.	191.	192.
192.	191.	192.	192.	195.	193.	192.	195.
196.	198.	196.	197.	197.	198.	197.	199.
199.	199.	204.	205.	204.			

GAGE # 5 (MICROSTRAIN):

2.	3.	3.	5.	6.	6.	7.	9.
9.	10.	12.	15.	15.	16.	18.	19.
19.	21.	23.	23.	24.	26.	27.	29.
31.	32.	33.	35.	35.	36.	39.	40.
41.	42.	43.	44.	45.	45.	47.	49.
50.	50.	51.	51.	53.	53.	54.	56.
57.	59.	59.	60.	60.	60.	61.	62.

62.	64.	63.	65.	67.	65.	68.	68.
68.	69.	70.	70.	70.	71.	70.	72.
72.	72.	74.	72.	75.	74.	75.	75.
76.	76.	76.	77.	76.	77.	78.	78.
79.	79.	80.	80.	79.	80.	79.	81.
82.	80.	82.	82.	82.	82.	81.	82.
80.	83.	85.	84.	85.	84.	85.	87.
81.	84.	89.	90.	88.			

GAGE # 6 (MICROSTRAIN):

-5.	-6.	-9.	-11.	-13.	-18.	-19.	-20.
-22.	-23.	-26.	-24.	-27.	-28.	-30.	-30.
-31.	-32.	-32.	-35.	-35.	-35.	-36.	-38.
-37.	-37.	-39.	-39.	-39.	-39.	-38.	-40.
-40.	-41.	-40.	-41.	-41.	-43.	-42.	-42.
-42.	-41.	-42.	-42.	-42.	-43.	-43.	-44.
-43.	-42.	-42.	-42.	-42.	-43.	-43.	-44.
-44.	-42.	-43.	-43.	-42.	-43.	-42.	-42.
-42.	-42.	-42.	-42.	-41.	-43.	-42.	-41.
-43.	-41.	-41.	-43.	-41.	-42.	-41.	-42.
-42.	-41.	-43.	-41.	-43.	-44.	-42.	-41.
-40.	-41.	-41.	-41.	-40.	-39.	-41.	-41.
-41.	-40.	-41.	-41.	-41.	-41.	-42.	-41.
-40.	-41.	-39.	-41.	-39.	-39.	-39.	-39.
-40.	-40.	-39.	-36.	-37.			

GAGE # 7 (MICROSTRAIN):

5.	9.	10.	14.	18.	22.	23.	29.
31.	35.	39.	41.	45.	48.	50.	55.
57.	59.	61.	64.	68.	70.	72.	74.
78.	80.	81.	85.	87.	90.	92.	95.
96.	98.	101.	102.	105.	105.	107.	108.
110.	112.	115.	115.	117.	118.	120.	121.
121.	123.	126.	127.	128.	129.	130.	130.
132.	133.	135.	135.	136.	137.	138.	139.
139.	141.	141.	143.	143.	144.	146.	146.
146.	147.	148.	147.	149.	150.	151.	151.
151.	152.	154.	154.	154.	153.	154.	155.
158.	157.	158.	156.	158.	160.	160.	158.
159.	162.	155.	159.	162.	161.	158.	162.
164.	163.	165.	164.	165.	166.	166.	167.
166.	166.	170.	170.	171.			

GAGE # 8 (MICROSTRAIN):

5.	9.	11.	15.	18.	22.	25.	28.
31.	36.	40.	42.	46.	49.	51.	56.
59.	62.	65.	69.	71.	75.	77.	81.
84.	86.	88.	93.	94.	97.	99.	103.
106.	108.	111.	112.	116.	117.	119.	120.
123.	125.	127.	128.	129.	132.	135.	135.
137.	138.	142.	143.	143.	143.	146.	148.

151.	149.	152.	153.	154.	154.	156.	156.
158.	159.	160.	160.	161.	163.	164.	165.
165.	166.	166.	167.	168.	168.	172.	171.
171.	172.	173.	174.	174.	175.	176.	177.
177.	177.	177.	179.	178.	181.	180.	181.
181.	181.	182.	181.	181.	184.	181.	184.
186.	185.	187.	186.	187.	188.	189.	190.
188.	188.	194.	194.	194.			

GAGE # 9 (MICROSTRAIN):

3.	5.	8.	11.	12.	17.	19.	22.
24.	28.	31.	34.	38.	39.	43.	45.
51.	52.	55.	58.	61.	64.	67.	71.
73.	76.	78.	82.	84.	86.	88.	90.
94.	98.	98.	101.	104.	106.	109.	111.
111.	115.	117.	118.	119.	122.	124.	126.
127.	129.	131.	132.	134.	135.	135.	138.
139.	140.	142.	143.	144.	144.	146.	147.
149.	149.	151.	152.	153.	154.	154.	156.
157.	158.	158.	158.	160.	161.	162.	163.
163.	164.	164.	166.	164.	167.	168.	169.
169.	170.	169.	171.	169.	171.	171.	172.
173.	173.	174.	174.	172.	176.	175.	176.
177.	177.	177.	178.	178.	178.	180.	179.
178.	180.	185.	186.	185.			

DATA FOR TEST ON TUBE 3, LOADING AND UNLOADING (RUN 2)

NUMBER OF GAGES = 6
NUMBER OF DATA POINTS = 67

THE PRESSURE VALUES, IN kPa, FOLLOW:

0.02	3.14	12.41	24.13	36.59	49.05	61.34	73.49
85.51	97.34	109.04	120.61	132.14	143.70	155.31	166.94
178.62	185.75	191.16	194.94	198.28	201.63	205.84	209.96
214.11	220.06	225.81	231.50	237.16	242.81	248.48	249.99
247.06	242.07	228.33	207.41	185.72	166.51	148.20	131.95
117.21	103.74	91.43	80.18	69.88	60.51	52.02	44.33
37.45	31.29	25.79	20.98	16.75	13.11	10.01	7.44
5.36	3.71	2.47	1.58	1.02	0.70	0.53	0.46
0.42	0.37	0.32					

GAGE # 1 (MICROSTRAIN):

0.	-2.	-12.	-24.	-36.	-47.	-59.	-70.
-81.	-91.	-102.	-112.	-121.	-130.	-137.	-143.
-147.	-146.	-145.	-143.	-141.	-139.	-136.	-133.
-128.	-118.	-106.	-91.	-70.	-40.	2.	20.
-10.	-46.	-100.	-128.	-129.	-118.	-102.	-87.
-72.	-57.	-44.	-32.	-22.	-13.	-5.	3.
10.	15.	20.	24.	25.	28.	29.	30.

32.	32.	32.	31.	31.	30.	29.	29.
27.	27.	27.					

GAGE # 3 (MICROSTRAIN):

0.	-4.	-19.	-36.	-55.	-71.	-86.	-100.
-111.	-122.	-129.	-136.	-139.	-138.	-133.	-121.
-101.	-83.	-66.	-52.	-40.	-27.	-8.	13.
36.	78.	127.	188.	264.	361.	492.	548.
454.	336.	145.	0.	-66.	-88.	-89.	-82.
-71.	-58.	-43.	-29.	-17.	-4.	7.	18.
27.	35.	41.	47.	51.	54.	57.	58.
60.	60.	60.	59.	58.	57.	55.	53.
52.	50.	49.					

GAGE # 4 (MICROSTRAIN):

-1.	4.	16.	35.	56.	79.	105.	132.
163.	195.	232.	270.	314.	363.	419.	484.
559.	613.	655.	686.	713.	741.	779.	819.
862.	935.	1016.	1111.	1222.	1358.	1535.	1615.
1500.	1348.	1067.	793.	598.	471.	374.	303.
247.	202.	164.	131.	103.	81.	61.	46.
33.	21.	11.	3.	-4.	-9.	-14.	-17.
-20.	-22.	-23.	-23.	-24.	-24.	-23.	-23.
-22.	-22.	-21.					

GAGE # 6 (MICROSTRAIN):

1.	-3.	-13.	-24.	-34.	-42.	-48.	-51.
-52.	-51.	-46.	-38.	-26.	-9.	16.	49.
93.	127.	155.	176.	196.	215.	244.	273.
307.	365.	431.	509.	602.	718.	866.	918.
808.	665.	421.	212.	95.	37.	6.	-7.
-12.	-11.	-8.	-3.	3.	10.	16.	23.
29.	33.	38.	42.	44.	47.	49.	49.
50.	51.	50.	50.	49.	48.	47.	46.
44.	43.	42.					

GAGE # 7 (MICROSTRAIN):

0.	5.	13.	24.	39.	57.	77.	101.
126.	153.	184.	217.	256.	298.	347.	404.
470.	518.	557.	584.	609.	634.	669.	704.
744.	808.	879.	963.	1062.	1184.	1342.	1411.
1308.	1170.	920.	680.	512.	403.	322.	261.
213.	174.	143.	115.	91.	71.	55.	42.
30.	20.	12.	5.	-1.	-6.	-10.	-13.
-15.	-17.	-19.	-20.	-20.	-21.	-21.	-21.
-21.	-21.	-21.					

GAGE # 9 (MICROSTRAIN):

0.	2.	9.	18.	33.	50.	71.	97.

127.	163.	205.	253.	310.	378.	459.	557.
675.	758.	826.	873.	916.	960.	1023.	1088.
1160.	1280.	1415.	1570.	1752.	1974.	2256.	2359.
2154.	1885.	1404.	951.	654.	474.	350.	267.
207.	162.	130.	104.	84.	69.	57.	48.
41.	36.	31.	28.	24.	22.	20.	18.
17.	16.	14.	13.	13.	12.	12.	12.
11.	11.	11.					

DATA FOR TEST ON TUBE 3 TO FAILURE (RUN 3)

NUMBER OF GAGES = 6
NUMBER OF DATA POINTS = 12

THE PRESSURE VALUES, IN kPa, FOLLOW:

0.01	8.92	35.77	61.37	87.09	112.96	138.53	163.15
186.81	209.86	228.59	242.65				

GAGE # 1 (MICROSTRAIN):

0.	-7.	-31.	-55.	-79.	-103.	-123.	-138.
-140.	-116.	-50.	70.				

GAGE # 3 (MICROSTRAIN):

0.	-13.	-51.	-82.	-108.	-124.	-126.	-106.
-49.	82.	314.	689.				

GAGE # 4 (MICROSTRAIN):

0.	13.	56.	108.	172.	254.	358.	490.
667.	927.	1282.	1776.				

GAGE # 6 (MICROSTRAIN):

0.	-8.	-31.	-44.	-46.	-35.	-2.	60.
168.	360.	653.	1072.				

GAGE # 7 (MICROSTRAIN):

0.	10.	42.	83.	137.	207.	297.	413.
570.	801.	1119.	1570.				

GAGE # 9 (MICROSTRAIN):

1.	8.	37.	80.	145.	242.	380.	574.
850.	1276.	1859.	2662.				

DATA FOR TEST ON TUBE 1 TO FAILURE

NUMBER OF GAGES = 6

NUMBER OF DATA POINTS = 35

THE PRESSURE VALUES, IN kPa, FOLLOW:

0.00	1.28	14.73	34.39	50.50	66.49	82.61	98.85
115.21	131.69	148.30	164.78	181.03	197.10	212.95	228.63
244.16	259.58	275.17	290.87	306.73	322.64	338.47	354.38
370.02	385.13	399.83	414.22	427.89	441.01	453.65	466.23
478.89	491.60	504.28					

GAGE # 1 (MICROSTRAIN):

0.	-1.	-19.	-35.	-49.	-57.	-69.	-80.
-92.	-106.	-118.	-130.	-144.	-161.	-178.	-193.
-206.	-225.	-247.	-267.	-292.	-321.	-353.	-390.
-433.	-479.	-531.	-592.	-660.	-739.	-830.	-945.
-1092.	-1295.	-1608.					

GAGE # 3 (MICROSTRAIN):

-1.	-5.	-56.	-108.	-156.	-200.	-246.	-290.
-335.	-380.	-426.	-470.	-515.	-560.	-602.	-643.
-685.	-729.	-774.	-818.	-864.	-910.	-958.	-1007.
-1058.	-1110.	-1162.	-1216.	-1272.	-1330.	-1388.	-1455.
-1534.	-1629.	-1755.					

GAGE # 4 (MICROSTRAIN):

-1.	-1.	-5.	-11.	-17.	-20.	-25.	-27.
-30.	-30.	-27.	-30.	-30.	-30.	-28.	-27.
-23.	-18.	-15.	-9.	-3.	6.	15.	29.
44.	64.	87.	114.	147.	188.	235.	300.
392.	527.	763.					

GAGE # 6 (MICROSTRAIN):

-1.	-5.	-56.	-110.	-160.	-209.	-259.	-307.
-355.	-403.	-451.	-498.	-543.	-590.	-634.	-676.
-717.	-757.	-798.	-839.	-879.	-919.	-959.	-996.
-1031.	-1063.	-1091.	-1116.	-1136.	-1148.	-1155.	-1149.
-1125.	-1067.	-928.					

GAGE # 7 (MICROSTRAIN):

0.	0.	-3.	0.	-2.	1.	1.	5.
9.	13.	18.	22.	27.	34.	40.	48.
55.	63.	72.	83.	95.	110.	125.	143.
164.	188.	215.	247.	283.	326.	375.	437.
520.	634.	812.					

GAGE # 9 (MICROSTRAIN):

-1.	-5.	-51.	-96.	-140.	-179.	-220.	-255.
-293.	-329.	-365.	-400.	-436.	-468.	-499.	-529.

-560. -587. -616. -643. -669. -693. -716. -736.
-752. -765. -773. -777. -773. -763. -742. -707.
-649. -552. -366.

DATA FOR TEST ON TUBE 2 TO FAILURE

NUMBER OF GAGES = 6
NUMBER OF DATA POINTS = 36

THE PRESSURE VALUES, IN kPa, FOLLOW:

0.28 16.41 33.11 49.39 65.63 81.86 98.21 114.62
131.08 147.34 163.38 179.19 194.83 210.26 225.52 240.84
256.35 271.98 287.79 303.71 319.75 335.69 351.23 366.37
381.04 395.58 409.31 422.54 435.50 448.43 461.42 474.38
487.33 500.22 513.08 525.59

GAGE # 1 (MICROSTRAIN):

1. -18. -39. -57. -68. -78. -87. -97.
-107. -120. -134. -143. -147. -154. -158. -163.
-173. -181. -190. -201. -209. -218. -227. -237.
-244. -251. -259. -266. -269. -275. -280. -283.
-286. -283. -271. -222.

GAGE # 3 (MICROSTRAIN):

0. -42. -89. -133. -175. -215. -252. -293.
-330. -370. -409. -446. -482. -517. -552. -586.
-619. -652. -687. -725. -760. -795. -830. -865.
-897. -930. -961. -991. -1020. -1051. -1082. -1115.
-1150. -1189. -1232. -1271.

GAGE # 4 (MICROSTRAIN):

0. -6. -11. -23. -34. -45. -52. -59.
-63. -67. -71. -72. -75. -78. -82. -85.
-89. -93. -96. -100. -104. -109. -111. -114.
-117. -120. -122. -124. -125. -126. -126. -125.
-122. -115. -101. -64.

GAGE # 6 (MICROSTRAIN):

1. -32. -66. -102. -136. -170. -204. -235.
-265. -295. -324. -351. -378. -404. -428. -454.
-480. -505. -532. -557. -582. -607. -630. -652.
-674. -695. -712. -730. -746. -760. -773. -785.
-793. -796. -781. -707.

GAGE # 7 (MICROSTRAIN):

1. -19. -38. -52. -71. -89. -105. -121.
-139. -155. -169. -185. -197. -212. -226. -241.

-258. -273. -288. -302. -321. -335. -350. -366.
-379. -395. -409. -423. -436. -450. -463. -478.
-492. -506. -515. -506.

GAGE # 9 (MICROSTRAIN):

0. -41. -85. -124. -165. -205. -241. -278.
-316. -350. -386. -417. -451. -486. -518. -552.
-585. -619. -652. -686. -720. -754. -786. -818.
-848. -878. -906. -932. -958. -984. -1008. -1033.
-1055. -1072. -1078. -1032.

DATA FOR TEST ON TUBE 4 TO FAILURE

NUMBER OF GAGES = 6
NUMBER OF DATA POINTS = 41

THE PRESSURE VALUES, IN kPa, FOLLOW:

0.01 1.15 7.22 14.09 20.51 26.76 32.92 39.06
45.21 51.40 57.62 63.86 70.14 76.43 82.75 89.02
95.24 101.40 107.50 113.56 119.63 125.60 131.57 137.51
143.38 149.24 155.09 161.01 166.96 172.96 179.04 185.09
191.21 197.39 203.62 209.86 216.06 222.20 228.27 234.28
240.23

GAGE # 1 (MICROSTRAIN):

0. 5. -13. -25. -38. -47. -57. -67.
-77. -86. -96. -105. -114. -123. -134. -143.
-151. -161. -169. -179. -185. -196. -204. -212.
-212. -227. -236. -245. -253. -262. -269. -279.
-288. -297. -308. -318. -332. -349. -370. -400.
-456.

GAGE # 3 (MICROSTRAIN):

3. -1. -3. -8. -10. -13. -15. -17.
-19. -20. -21. -20. -19. -19. -17. -15.
-13. -10. -7. -2. 3. 9. 17. 24.
32. 42. 51. 62. 74. 88. 105. 120.
139. 161. 187. 214. 246. 281. 324. 373.
439.

GAGE # 4 (MICROSTRAIN):

0. -1. -2. -5. -6. -5. -5. -4.
-3. -3. 0. 1. 1. 3. 5. 7.
7. 8. 10. 10. 11. 13. 13. 13.
14. 13. 13. 13. 12. 11. 7. 3.
-2. -9. -16. -28. -44. -65. -93. -135.
-202.

GAGE # 6 (MICROSTRAIN):

1.	-2.	-11.	-24.	-36.	-46.	-57.	-68.
-78.	-89.	-99.	-110.	-121.	-131.	-143.	-154.
-167.	-180.	-192.	-205.	-217.	-230.	-247.	-261.
-277.	-292.	-310.	-330.	-350.	-371.	-398.	-421.
-450.	-482.	-518.	-557.	-605.	-661.	-727.	-814.
-948.							

GAGE # 7 (MICROSTRAIN):

0.	0.	3.	9.	14.	20.	26.	34.
42.	52.	62.	72.	76.	98.	113.	130.
146.	164.	184.	205.	227.	251.	277.	305.
337.	370.	407.	446.	490.	540.	595.	655.
727.	808.	902.	1014.	1145.	1305.	1506.	1776.
2213.							

GAGE # 9 (MICROSTRAIN):

1.	0.	3.	7.	11.	15.	20.	26.
34.	44.	54.	64.	76.	90.	105.	122.
139.	158.	179.	201.	227.	253.	283.	315.
349.	386.	428.	474.	523.	582.	646.	719.
804.	896.	1008.	1139.	1294.	1480.	1713.	2021.
2494.							

Appendix 7. Procedure for Fiber Percent Determination

Object: to determine the amount of glass reinforcement in the resin matrix composite.

Equipment: glass containers (Pyrex)
precision scale---Sauter, model/11 (ser. no. 12105), calibrated with Ohaus standard weights.
furnace---Thermolyne, type 1400, model F-A1415M (ser. no. 124530)

Procedure: The glass containers are heated to about 250° C., removed from the furnace and placed in a desiccator to cool to room temperature. The containers are then weighed. The specimens are weighed at room temperature. The volume of PVC liner is measured, and its weight is calculated using a specific gravity value of 1.4. The specimens are put in separate containers and the containers are placed in the furnace. The temperature is then raised to 600° C. and maintained for about 30 minutes, or until no ash residue is evident.

CAUTION: If material is placed in a hot furnace, it may ignite; if the temperature goes much above 600° C. the containers and/or reinforcing glass may distort or melt.

The containers are allowed to cool in the desiccator. The weight of reinforcement is found by weighing the container plus its contents, and subtracting the previously measured weight of the container.

The weight-fraction of reinforcement is then

(weight of reinforcement)/ {(weight of spec.)-(weight of PVC)}

The volume-fraction may then be determined from

$$v_f = w_f / \{w_f + p_f(1-w_f)/p_m + p_f(v_v)\}$$

where, v_f = volume-fraction of fiber

w_f = weight-fraction of fiber

p_f = density of fiber

p_m = density of matrix

v_v = volume-fraction of voids, if available.

The void volume-fraction was taken as zero in all calculations.

Note: The PVC layer could not be burned off completely. It left ash which was removed using 70% nitric acid and water.

Appendix B. Listing of Computer Program

```
C
C
C                        BUCKLING OF
C                  COMPOSITE PRESSURE VESSELS
C
C
C     ORIGIN: CONCORDIA UNIVERSITY
C             MECHANICAL ENGINEERING DEPT.
C             COMPOSITE MATERIALS RESEARCH GROUP
C             1455 de MAISONNEUVE O.
C             MONTREAL, QUEBEC H3G 1M8
C
C     DATE WRITTEN: 84.09.17
C
C     DATE OF LAST REVISION: 85.03.31
C
C
C
C
C
C     THIS PROGRAM CALCULATES THE CRITICAL EXTERNAL PRESSURE FOR
C     RIGHT CIRCULAR CYLINDRICAL SHELLS SUBJECTED TO BUCKLING LOADS.
C
C     TWO LOADING CASES ARE CONSIDERED:
C          1. HYDROSTATIC EXTERNAL PRESSURE
C          2. UNIFORM LATERAL ( OR RADIAL ) EXTERNAL PRESSURE.
C
C     THE SHELL WALL CONSTRUCTION MAY VARY FROM SINGLE-LAYER
C     HOMOGENEOUS ISOTROPIC TO ANISOTROPIC LAMINATED, OR ANY
C     COMBINATION OF SUCH LAYERS (A MAXIMUM OF 101 LAYERS IS ALLOWED).
C
C     ALL CALCULATIONS REFER TO THE GEOMETRIC MIDDLE SURFACE OF THE
C     SHELL.
C
C     THE PROCEDURE USED FOLLOWS THAT OF CHENG, S., AND HO, B.P.C.,
C     "STABILITY OF HETEROGENEOUS AEOLOTROPIC CYLINDRICAL SHELLS
C     UNDER COMBINED LOADING", AIAA J., VOL. 1, NO. 4, 1963,
C     PP. 892-898, WHERE THE RELATION BETWEEN THE LOADING PARAMETERS
C     Q1 AND Q2 IS TAKEN AS:
C          1. HYDROSTATIC CASE    : Q2=Q1/2
C          2. LAT. PRESSURE CASE  : Q2=0
C     WITH NO TORSIONAL LOADING PRESENT.
C
C     NO BOUNDARY CONDITIONS ARE IMPOSED ON THE SHELL.
C
C     THE CHARACTERISTIC POLYNOMIAL IN Q1 IS SOLVED FOR
C     THE MINIMUM POSITIVE REAL ROOT. (SEE EQ. 16 OF REF.)
C
C     TWO SOLUTION PATHS ARE AVAILABLE. THE FIRST PATH WILL
```

```
C     FIND THE SINGLE CRITICAL PRESSURE FOR A KNOWN VESSEL
C     WALL CONSTRUCTION.
C     THE SECOND PATH WILL FIND THE "N" CRITICAL PRESSURES
C     FOR A VESSEL WITH A SINGLE INTERNAL CORROSION BARRIER
C     LAYER AND "N" PAIRS OF FILAMENT WINDING LAYERS ("N"
C     CAN BE AS MANY AS 50). ALL THE F.W. LAYERS WILL HAVE
C     THE SAME +/- WINDING ANGLE.
C     THE FORMER IS CALLED A "SINGLE SOLUTION" RUN.
C     THE LATTER IS CALLED A "MULTI-SOLUTION" RUN.
C
C     THE PROGRAM RUNS IN INTEROGATIVE MODE, THE USER
C     ANSWERING QUESTIONS FROM THE TERMINAL.
C
C     RESULTS OF ANY RUN CAN BE OUTPUT IN REPORT FORM TO
C     FILE "BUCKREP.DAT" WHICH THE USER CAN PRINT OUT.
C
C*****************************************************************
C
C   THE MAIN PROGRAM PERMITS CHOOSING A SOLUTION PATH
C   AND THE NUMBER OF LAYER PAIRS IN THE CASE OF A
C   "MULTI-SOLUTION" RUN.
C
      PROGRAM BUCKLING
C
      REAL CRP(50)
      REAL NUMLAY(50)
      INTEGER REPEAT
      CHARACTER*1 ANSWER,MORE,RANS
C
      WRITE(*,4400)
      WRITE(*,4410)
      WRITE(*,4420)
      WRITE(*,4421)
      WRITE(*,4422)
      WRITE(*,4423)
      WRITE(*,4424)
      WRITE(*,4440)
      WRITE(*,4450)
      WRITE(*,*) ' '
      WRITE(*,*) ' '
      WRITE(*,'(1x,A\)') 'PROGRAM INFO.?(Y=YES/N=NO) '
      READ (*,'(A)') ANSWER
      IF((ANSWER .EQ. 'Y') .OR. (ANSWER .EQ. 'y'))
     $      CALL INFO1
      WRITE(*,*) ' '
      WRITE(*,*) ' '
   10 MORE = 'N'
      DO 20, K=1,50
         CRP(K)    = 0.0
         NUMLAY(K) = 0.0
   20 CONTINUE
      WRITE(*,'(1x,A\)') 'A "MULTI-SOLUTION RUN"? (Y/N) '
      READ (*,'(A)') ANSWER
      IF((ANSWER .EQ. 'N') .OR. (ANSWER .EQ. 'n')) THEN
```

```
        NLAY = 1
        GO TO 100
      ENDIF
      WRITE(*,'(1x,A\)') 'NO. OF F.W. LAYER PAIRS (50 AT MOST)?'
      READ (*,*) NLAY
  100 CALL ONE(MORE,REPEAT,NLAY,CRP,NUMLAY)
      IF((MORE .EQ. 'Y') .OR. (MORE .EQ. 'y')) THEN
        REPEAT = 1
        GO TO 10
      ENDIF
 4400 FORMAT(/////,30X,'BUCKLING OF')
 4410 FORMAT(22X,'COMPOSITE PRESSURE VESSELS')
 4420 FORMAT(///,5X,'ORIGIN: CONCORDIA UNIVERSITY')
 4421 FORMAT(13X,'MECHANICAL ENGINEERING DEPT.')
 4422 FORMAT(13X,'COMPOSITE MATERIALS RESEARCH GROUP')
 4423 FORMAT(13X,'1455 de MAISONNEUVE O.')
 4424 FORMAT(13X,'MONTREAL, QUEBEC H3G 1M8')
 4440 FORMAT(//,5X,'DATE WRITTEN: 84.09.17')
 4450 FORMAT(//,5X,'DATE OF LAST REVISION: 85.04.16')
      END
C
C*********************************************************************
C
C   THIS SUBROUTINE ACCEPTS USER INPUT OF MATERIAL PROPERTIES
C   AND GEOMETRIC DATA.
C   IT PERFORMS SOME CALCULATIONS, AND CALLS SUBROUTINES.
C   IT ALSO GENERATES OUTPUT.
C
      SUBROUTINE ONE(MORE,REPEAT,NLAY,CRP,NUMLAY)
C
      REAL CRP(NLAY)
      REAL NUMLAY(NLAY)
      INTEGER REPEAT,CRCWN,CRAHWN
      REAL VF(101)
      INTEGER IM(101)
      REAL Z(102),EM(101),EF(101),C(101),GM(101),GF(101)
      REAL ALL(101),TT(101),EE1(101),EE2(101),GG(101),CCP(101)
      REAL QN(3,3),A(3,3),B(3,3),D(3,3),Q(3,3),F(3,3),QN1(3,3)
      CHARACTER*60 UNITS,TITLE
      CHARACTER*1 MORE,ANSWER,RANS
      DATA PI/3.141592654/
C
   10 CONTINUE
C
C
      DO 5400, LAYPR=1, NLAY

        IF((NLAY.GT.1).AND.(LAYPR.GT.1))THEN
          IL   = LAYPR*2 + 1
          IN   = 2
          IM(1)= 1
          IM(2)= IL - 1
          GO TO 350
        ELSE IF( (NLAY.GT.1) .AND. (LAYPR.EQ.1) ) THEN
```

```
          IL    = 3
          IN    = 2
          IM(1)= 1
          IM(2)= 2
          WRITE(*,*)'      ****   NOW   ****'
          WRITE(*,*)'PROCEED AS FOR A CASE WITH ONE CORROSION BARRIER'
          WRITE(*,*)'INSIDE, AND ONE PAIR OF F.W. LAYERS OUTSIDE.'
          GO TO 50
        ELSE
              CONTINUE
        ENDIF

        WRITE(*,*) ' '
        WRITE(*,'(1X,A\)') 'HOW MANY LAMINA IN THE WALL (101 MAX.)?'
        READ (*,*) IL
        WRITE(*,'(1X,A\)') 'HOW MANY DIFFERENT LAMINA MATERIALS ?'
        READ (*,*) IN
        WRITE(*,*) ' '
        WRITE(*,*)'LIST NO. OF LAYERS IN EACH MATERIAL GROUP IN ORDER'
        WRITE(*,*)'STARTING FROM THE INSIDE.'
        WRITE(*,*)'FOR EXAMPLE, IF THERE ARE 9 LAYERS AND 3 MATERIALS'
        WRITE(*,*)'IN 4 MATERIAL GROUPS AS FOLLOWS (STARTING INSIDE),'
        WRITE(*,*)'1-HLU/2-F.W./2-W.R./4-F.W., THEN INPUT'
        WRITE(*,*)'WILL BE: 1,2,2,4.'
        WRITE(*,*) ' '
        READ (*,*) (IM(I),I=1,IN)
     50 WRITE(*,*) ' '
        WRITE(*,*) 'CALCULATE LAMINA PROPERTIES FROM FIBER'
        WRITE(*,'(1X,A\)') 'AND MATRIX PROPERTIES? (Y/N)'
        READ (*,'(A)') ANSWER
        IF((ANSWER .EQ. 'N') .OR. (ANSWER .EQ. 'n')) GO TO 200
C
C   THE LAMINAE PROPERTIES ARE CALCULATED FROM FIBER AND MATRIX DATA
C   FOR LAMINAE WITH CONTINUOUS, UNIDIRECTIONAL REINFORCEMENT.
C   *** NOTE THAT FIBERS ARE ASSUMED TO BE ISTROPIC. ***
C
C   THE FIBER VOLUME-FRACTION MAY BE OPTIONALLY CALCULATED.
        WRITE(*,*)'DO YOU WANT FIBER VOL.-FRAC. CALCULATED FROM'
        WRITE(*,*)'RESULTS OF A FIBER WT.-FRAC. DETERMINATION'
        WRITE(*,'(1x,A\)')'TEST? (Y/N)'
        READ (*,'(A)') ANSWER
        IF((ANSWER .EQ. 'Y') .OR. (ANSWER .EQ. 'y')) CALL VOLFRA
C
        WRITE(*,*)'CONSTITUENTS'' PROPERTIES MUST BE INPUT FOR EACH'
        WRITE(*,*)'MATERIAL STARTING INSIDE. USING THE EXAMPLE ABOVE,'
        WRITE(*,*)'THE ORDER WOULD BE: HLU, F.W., W.R., F.W.'
        WRITE(*,*)' '
     90 WRITE(*,*)'ENTER VOLUME FRACTION OF FIBRES'
        WRITE(*,*)' '
        READ (*,*) (VF(I),I=1,IN)
     92 WRITE(*,*)' '
        WRITE(*,*) 'ENTER NORMAL ELASTIC MODULUS OF FIBRES'
        WRITE(*,*)' '
        READ (*,*) (EF(I),I=1,IN)
```

```
      WRITE(*,*)' '
      WRITE(*,*)'ENTER NORMAL ELASTIC MODULUS OF MATRIX'
      WRITE(*,*)' '
      READ (*,*) (EM(I),I=1,IN)
      WRITE(*,*)' '
      WRITE(*,*) 'ENTER SHEAR MODULUS OF FIBRES'
      WRITE(*,*)' '
      READ (*,*) (GF(I),I=1,IN)
      WRITE(*,*)' '
      WRITE(*,*)'ENTER SHEAR MODULUS OF MATRIX'
      WRITE(*,*)' '
      READ (*,*) (GM(I),I=1,IN)
      DO 100, I=1,IN
         CALL CE1(EE1,EF,VF,EM,IN)
         CALL MODE2(EE2,EF,VF,EM,IN)
         CALL MODG(GG,GF,GM,VF,IN)
         CALL CCCPF(EF,EM,VF,GF,GM,CCP,IN)
  100 CONTINUE
      GO TO 300
  200 CONTINUE
C
C   LAMINA PROPERTIES ARE INPUT.
      WRITE(*,*)'ENTER  MODULUS E1 FOR EVERY TYPE OF LAYER'
      WRITE(*,*)'(STARTING FROM INSIDE)?'
      READ (*,*) (EE1(I),I=1,IN)
      WRITE(*,*)' '
      WRITE(*,*)'ENTER MODULUS E2 FOR EVERY TYPE OF LAYER'
      WRITE(*,*)'(STARTING FROM INSIDE) ?'
      READ (*,*) (EE2(I),I=1,IN)
      WRITE(*,*)' '
      WRITE(*,*)'ENTER SHEAR MODULUS G  FOR EVERY TYPE OF LAYER '
      WRITE(*,*)'(STARTING FROM INSIDE) ?'
      READ (*,*) (GG(I),I=1,IN)
      WRITE(*,*)' '
      WRITE(*,*)'ENTER MAJOR POISSON RATIOS FOR EVERY TYPE OF LAYER'
      WRITE(*,*)'(STARTING FROM INSIDE)?'
      READ (*,*) (CCP(I),I=1,IN)
  300 CONTINUE
C
C   LAMINA THICKNESSES ARE INPUT.
      WRITE(*,*)' '
      WRITE(*,*)'ENTER THICKNESSES OF EACH MATERIAL LAYER TYPE'
      WRITE(*,*)'(STARTING FROM INSIDE).'
      READ (*,*) (TT(I),I=1,IN)
  350 CONTINUE
C
C   THE MATERIAL PROPERTIES ARE ASSIGNED TO EACH LAYER.
         CALL PUT(CCP,C,IM,IL,IN)
         CALL PUT(TT,C,IM,IL,IN)
         CALL PUT(EE1,C,IM,IL,IN)
         CALL PUT(EE2,C,IM,IL,IN)
         CALL PUT(GG,C,IM,IL,IN)
C
C   THE THICKNESS OF THE LAMINATE IS CALCULATED.
```

```
  400 T =.0
      DO 500, I=1,IL
        T = T + TT(I)
  500 CONTINUE
C
C   THE INTEGRATION LIMITS FOR EACH LAYER ARE CALCULATED WITH
C   RESPECT TO THE MIDDLE SURFACE OF THE SHELL.
C   Z IS POSITIVE IN THE "OUTWARD" DIRECTION.
C
      Z(1) = -T/2
      DO 600, I=2,IL+1
         Z(I) = Z(I-1) + TT(I-1)
  600 CONTINUE

      IF(LAYPR .GT. 1) THEN
      R = RAD + T/2
         CALL MDPUT1(ALL,IL,LAYPR)
      GO TO 800
      ENDIF

  790 WRITE(*,*)' '
      WRITE(*,'(1X,A\)')'MAX. NO. OF CIRCUM. WAVES ? (TRY 10)'
      READ (*,*) NC
      IF(NC .LT. 2) THEN
         WRITE(*,*)'!!! THIS VALUE MUST BE AT LEAST 2 !!!'
         GO TO 790
      ENDIF
      WRITE(*,*)' '
      WRITE(*,'(1X,A\)')'MAX. NO. OF AX. HALF-WAVES ? (TRY 1)!'
      READ (*,*) MC
      WRITE(*,'(1X,A\)')'INSIDE RADIUS OF THE VESSEL?'
      READ (*,*) RAD
      R = RAD + T/2
      WRITE(*,*)' '
      WRITE(*,'(1X,A\)')'VESSEL LENGTH?'
      READ (*,*) DL
C
      WRITE(*,*)' '
      WRITE(*,*)' '
      WRITE(*,*)'TYPE IN THE ANGLE FOR EACH LAYER WITH RESPECT'
      WRITE(*,*)'TO THE VESSEL AXIS (STARTING INSIDE).'
      WRITE(*,*)'NOTE: ASSIGN ZERO TO ISOTROPIC LAYERS.'
      READ (*,*) (ALL(I),I=1,IL)
  800 CONTINUE
C
      DO 900, KK=1,IL
         E1   = EE1(KK)
         E2   = EE2(KK)
         G    = GG(KK)
         CP   = CCP(KK)
         ALFA = ALL(KK)
         ALFA = PI * (ALFA/180)
         CP2  = CP*E2/E1
         CP   = 1 - CP*CP2
```

```
C
C.   MATRIX [Q] IS CALCULATED.
          QN1(1,1) = E1/CP
          QN1(1,2) = E1*CP2/CP
          QN1(2,2) = E2/CP
          QN1(3,3) = G
C
C    MATRIX [Q] IS TRANSFORMED TO MATRIX [QN].
          CALL MODQ(QN1,ALFA,QN)
          ZLL  = Z(KK)
          ZLU  = Z(KK+1)
          ZLL2 = (ZLU**2 - ZLL**2)
          ZLL3 = (ZLU**3 - ZLL**3)
C
C    MATRICES [A],[B],AND [D] ARE CALCULATED.
          DO 850, I=1,3
          DO 850, J=1,3
             A(I,J) = A(I,J) + QN(I,J)*TT(KK)
             B(I,J) = B(I,J) + QN(I,J)*ZLL2/2
             D(I,J) = D(I,J) + QN(I,J)*ZLL3/3
  850     CONTINUE
          PP = A(2,2)
  900     CONTINUE
C
C    THE A-BAR, B-BAR, AND D-BAR MATRICES ARE CALCULATED (SEE CHEN8 & HO)
        DO 1000, I=1,3
          DO 1000, J=1,3
             A(I,J) = A(I,J)/PP
             B(I,J) = B(I,J)/(PP*R)
             D(I,J) = D(I,J)/(PP*R**2)
 1000 CONTINUE
C
C    A LARGE VALUE IS INITIALLY ASSIGNED TO THE VARIABLE
C    WHICH WILL CONTAIN THE LOWEST REAL POSITIVE ROOT OF
C    THE CHARACTERISTIC EQUATION.
        QMIN = 1.E9
C
        IF(LAYPR .GT. 1) GO TO 1025
        WRITE(*,*)'SPECIFY THE LOADING CASE:'
        WRITE(*,*)' *****   FOR HYDROSTATIC PRESSURE, TYPE 1.'
        WRITE(*,'(1X,A\)')' *****   FOR LATERAL PRESSURE, TYPE 2.'
        READ (*,*) LCASE
 1025   WRITE(*,*)' '

        IF(NLAY .GT. 1).THEN
        WRITE(*,*)'___ PASS No. ',LAYPR,' OF ',NLAY,' (1 PER LAYER PAIR)'
        WRITE(*,*)' '
        ENDIF

        DO 1100, M=1,MC
          P = M*PI*R/DL
          WRITE(*,*)' '
          WRITE(*,*)'***** EXECUTING AXIAL HALF-WAVE NO. ',M,' *****'
          WRITE(*,*)' '
```

```
            DO 1050, N=2,NC
               CALL FUNE1(A,B,D,F,N,P,R,PP)
               CALL FINDMIN(F,N,P,Q1,LCASE)

               IF(Q1  .LT. QMIN) THEN
                  QMIN   = Q1
                  CRCWN  = N
                  CRAHWN = M
                  ENDIF

 1050    CONTINUE
 1100 CONTINUE
      CRP(LAYPR) = QMIN*PP/R
      WRITE(*,*)'*************************************************'
      WRITE(*,*)'*                                               *'
      WRITE(*,*)'*    CRITICAL PRESSURE     =  ',CRP(LAYPR)
      WRITE(*,*)'*                                               *'
      WRITE(*,*)'*    CRIT. CIRCUM. WAVE #  = ',CRCWN
      WRITE(*,*)'*    CRIT. AX. HALF-WAVE # = ',CRAHWN
      WRITE(*,*)'*                                               *'
      WRITE(*,*)'*************************************************'
      WRITE(*,*)' '
      WRITE(*,*)' '
      WRITE(*,*)' '
      IF(LAYPR .GT. 1) GO TO 3990
      WRITE(*,'(1X,A\)')'DO YOU WANT A REPORT LISTING? (Y/N)' '
      READ (*,'(A)') RANS
      IF((RANS .EQ. 'N') .OR.(RANS .EQ. 'n')) GO TO 5400
 3990 IF((RANS .EQ. 'Y') .OR.(RANS .EQ. 'y')) THEN
C    A REPORT OF THE COMPUTER RUN IS OUTPUT
C    TO A FILE NAMED "BUCKREP.DAT".
      IF(LAYPR .GT. 1) THEN
        WRITE (7,4000) CHAR(12)
 4000   FORMAT(A,///)
        GO TO 5015
      ENDIF
        WRITE(*,*)' '
        WRITE(*,*)'*** REPORT AVAILABLE ON FILE "BUCKREP.DAT".'
        WRITE(*,*)' '
      IF(REPEAT .EQ. 1.) GO TO 4500
        OPEN(7,FILE='BUCKREP.DAT',STATUS='NEW')
        WRITE (7,4400)
 4400   FORMAT(/////,35X,'BUCKLING OF')
        WRITE (7,4410)
 4410   FORMAT(27X,'COMPOSITE PRESSURE VESSELS')
        WRITE (7,4420)
 4420   FORMAT(///,15X,'ORIGIN: CONCORDIA UNIVERSITY')
        WRITE (7,4421)
 4421   FORMAT(23X,'MECHANICAL ENGINEERING DEPT.')
        WRITE (7,4422)
 4422   FORMAT(23X,'COMPOSITE MATERIALS RESEARCH GROUP')
        WRITE (7,4423)
 4423   FORMAT(23X,'1455 de MAISONNEUVE O.')
        WRITE (7,4424)
```

```
 4424   FORMAT(23X,'MONTREAL, QUEBEC H3G 1M8')
        WRITE (7,4440)
 4440   FORMAT(//,15X,'DATE WRITTEN: 84.09.17')
        WRITE (7,4450)
 4450   FORMAT(//,15X,'DATE OF LAST REVISION: 85.04.16')
 4500   WRITE(*,*)' '
        WRITE(*,*)'INPUT A TITLE FOR THIS REPORT (60 CHAR. MAX.).'
        READ (*,'(A)') TITLE
        WRITE (7,5000) CHAR(12), TITLE
 5000   FORMAT(A,///,10X,A60)
        WRITE (7,5002)
 5002   FORMAT(10X,65('='))

          IF(LCASE .EQ. 1) THEN
            WRITE (7,5005)
 5005       FORMAT(//,10X,'HYDROSTATIC PRESSURE LOADING')
          ELSE
            WRITE (7,5007)
 5007       FORMAT(//,10X,'LATERAL PRESSURE LOADING')
          ENDIF

        WRITE(*,*)'WHAT UNITS WERE USED (60 CHAR. MAX.)?'
        READ (*,'(A)') UNITS
        WRITE (7,5010) UNITS
 5010   FORMAT(//,10X,'*** NOTE UNITS: ',A60)
 5015   WRITE(7,5020)
 5020   FORMAT(//,16X,'VESSEL WALL CONSTRUCTION :')
        WRITE (7,5040)
 5040   FORMAT(/,10X,'Layer #',6X,'E11',7X,'E22',7X,'G12',
     $          4X,'NU 12',2X,'THETA',2X,'THICKNESS')
        WRITE (7,5050)
 5050   FORMAT(10X,65('-'))
        DO 5060, I=1,IL
           WRITE (7,5055) I,EE1(I),EE2(I),GG(I),CCP(I),ALL(I),TT(I)
 5055      FORMAT(/,14X,I2,3X,E8.3,2X,E8.3,1X,E8.3,4X,F5.3,
     $             1X,F6.1,3X,F7.5)
 5060   CONTINUE
        WRITE (7,5050)
        WRITE (7,5070) T
 5070   FORMAT(///,10X,'WALL THICKNESS = ',F10.5)
        WRITE (7,5080) R
 5080   FORMAT(//,10X,'RADIUS TO MIDDLE SURFACE = ',F10.5)
        WRITE (7,5090) DL
 5090   FORMAT(//,10X,'VESSEL LENGTH = ',F10.3)
        WRITE (7,5100)
 5100   FORMAT(//,10X,60('*'),/,10X,'*',58X,'*')
        WRITE (7,5110) CRP(LAYPR)
 5110   FORMAT(10X,'*',5X,'CRITICAL PRESSURE           = ',
     $      G15.5,7X,'*')
        WRITE (7,5112) CRCWN
 5112   FORMAT(10X,'*',5X,'CRITICAL CIRCUM. WAVE NO.   =
     $      I3,16X,'*')
        WRITE (7,5114) CRAHWN
 5114   FORMAT(10X,'*',5X,'CRITICAL AXIAL HALF WAVE NO. =     ',
```

```
     *     I3,16X,'*')
           WRITE (7,5120)
 5120      FORMAT(10X,'*',58X,'*',/,10X,60('*'))
           ENDIF

 5400 CONTINUE

      WRITE(*,*)' '
      WRITE(*,'(1X,A\)')'DO YOU WANT ANOTHER JOB RUN? (Y/N)'
      READ (*,'(A)') MORE
      IF((MORE .EQ. 'Y') .OR. (MORE .EQ. 'y')) RETURN
      WRITE(*,5500)
      IF((RANS .EQ. 'N') .OR. (RANS .EQ. 'n')) GO TO 9000
      WRITE (7,5500)
 5500 FORMAT(///,10X,'*****   THE END   *****')
 9000 END
C
C*************************************************************************
C
C   THIS SUBROUTINE CALCULATES THE TRANSFORMED STIFFNESS MATRIX [QN].
C   IT WAS CHECKED AND FOUND CORRECT.
C
      SUBROUTINE MODQ(QN1,ALFA,QN)
C
      REAL QN(3,3),QN1(3,3)
C
      DO 100, I=1,3
         DO 100, J=1,3
            QN(I,J) = 0
  100 CONTINUE
      S       = SIN(ALFA)
      S2      = S**2
      S3      = S2*S
      S4      = S2*S2
      C       = COS(ALFA)
      C2      = C**2
      C3      = C2*C
      C4      = C2*C2
      SC      = C2*S2
      QA      = QN1(1,1)
      QB      = QN1(1,2)
      QC      = QN1(2,2)
      QD      = QN1(3,3)
      QN(1,1) = QA*C4 + QC*S4 + 2*(2*QD+QB)*SC
      QN(1,2) = (QA + QC - 4*QD)*SC + QB*(C4 + S4)
      QN(1,3) = (QA - QB - 2*QD)*C3*S + (QB + 2*QD - QC)*C*S3
      QN(2,2) = QA*S4 + QC*C4 + 2*(2*QD + QB)*SC
      QN(2,3) = (QA - QB - 2*QD)*C*S3 + (QB -QC + 2*QD)*C3*S
      QN(3,3) = (QA + QC - 2*QB - 2*QD)*SC + QD*(C4 + S4)
      QN(2,1) = QN(1,2)
      QN(3,1) = QN(1,3)
      QN(3,2) = QN(2,3)
      RETURN
      END
```

```
C
C*************************************************************************
C
C   THIS SUBROUTINE USES ITERATION TO FIND THE LOWEST POSITIVE
C   REAL ROOT OF THE CHARACTERISTIC EQUATION.
C   THE EQUATION IS EXPRESSED AS A FUNCTION OF Q1 ONLY.
C   IT WAS CHECKED AND FOUND SATISFACTORY.
C
      SUBROUTINE FINDMIN(F,N,P,Q1,LCASE)
C
      REAL F(3,3)
      REAL SUM,SUMOLD,LLIM,ULIM,DELTA
      REAL DIFF,Q1,OLDQ1
C
      P2    = P**2
      N2    = N**2
      LLIM = 0.0
      ULIM = 1.0
   20 CONTINUE
      DELTA = (ULIM - LLIM)/1000.0
      IPOS = 0
      INEG = 0
      DO 200, I=0,1000
         Q1 = LLIM + I*DELTA
         IF(LCASE .EQ. 1) Q2 = 0.5*Q1
         IF(LCASE .EQ. 2) Q2 = 0.0

         SUM = (F(1,1) - N2*Q1 - Q2*P2)*(F(2,2) - N2*Q1
     $         - Q2*P2)*(F(3,3) - N2*Q1 - Q2*P2)
     $         - (F(1,1) - N2*Q1 - Q2*P2)*(F(2,3) - N*Q1)**2
     $         - (F(1,2)**2*(F(3,3) - N2*Q1 - Q2*P2))
     $         + (F(1,2))*(F(1,3) + P*Q1)*(F(2,3) - N*Q1)
     $         + (F(1,3) + P*Q1)*(F(1,2))*(F(2,3) - N*Q1)
     $         - (F(1,3) + P*Q1)**2*(F(2,2) - N2*Q1 - Q2*P2)

         IF(SUM .GE. 0.) IPOS = 1
         IF(SUM .LT. 0.) INEG = 1
         IF(IPOS .EQ. INEG) THEN
            DIFF = ABS((Q1 - OLDQ1)/Q1)
            IF(DIFF .LE. 0.01) THEN
               Q1 = (Q1 + OLDQ1)/2
               RETURN
            ELSE
               ULIM = Q1
               LLIM = OLDQ1
               GO TO 20
            ENDIF
         ENDIF
      SUMOLD = SUM
      OLDQ1  = Q1
  200 CONTINUE
      LLIM = LLIM + 1.0
      ULIM = ULIM + 1.0
      GO TO 20
```

```
      END
C
C*********************************************************************
C
C   THIS SUBROUTINE CALCULATES LAMINA TRANSVERSE MODULUS E2
C   USING EQUATIONS (9.49) AND (9.62) IN REFERENCE
C   TSAI, S.W., AND HAHN, H.T., "INTRODUCTION TO COMPOSITE
C   MATERIALS", TECHNOMIC PUB. CO., INC., WESTPORT, CT
C   06880, 1980. THE VALUE OF "eta" IS TAKEN AS 0.5.
C   IT WAS CHECKED AND FOUND CORRECT.
C
      SUBROUTINE MODE2(EE2,EF,VF,EM,IN)
C
      REAL EE2(101),EF(101),EM(101),VF(101),ETA
C
      ETA = 0.5
      DO 100, I=1,IN
         EE2INV = (1./(VF(I) + ETA*(1 - VF(I)))) *
     $            (VF(I)/EF(I) + ETA*(1 - VF(I))/EM(I))
         EE2(I) = 1./EE2INV
  100 CONTINUE
      END
C
C*********************************************************************
C
C   THIS SUBROUTINE CALCULATES THE LAMINA IN-PLANE SHEAR
C   MODULUS USING THE HALPIN-TSAI RELATION ASSUMING
C   "XI" TO BE 1.0. (SEE REFERENCE JONES, R.M., "MECHANICS
C   OF COMPOSITE MATERIALS", SCRIPTA BOOK CO., WASHINGTON, D.C.,1975,
C   SECTION 3.3.5.) THE RESULT IS COMPARABLE TO THAT OBTAINED
C   USING EQUATIONS (9.49) AND (9.62) IN REFERENCE TSAI AND HAHN,
C   WITH "eta" TAKEN AS 0.5.
C   IT WAS CHECKED AND FOUND CORRECT.
C
      SUBROUTINE MODG(GG,GF,GM,VF,IN)
C
      REAL GG(101),GF(101),GM(101),VF(101),ETA
C
      DO 100, I=1,IN
         ETA  = (GF(I)/GM(I) - 1)/(GF(I)/GM(I) + 1)
         GG(I) = GM(I)*(1 + ETA*VF(I))/(1 - ETA*VF(I))
  100 CONTINUE
      RETURN
      END
C
C*********************************************************************
C
C   THIS SUBROUTINE CALCULATES THE [F] MATRIX (SEE REF. CHENG & HO).
C   IT WAS CHECKED AND FOUND CORRECT.
C
      SUBROUTINE FUNE1(A,B,D,F,N,P,R,PP)
C
      REAL A(3,3),B(3,3),D(3,3),F(3,3)
C
```

```
      P2     = P**2
      N2     = N**2
      F(1,1) = (A(1,1) + B(1,1))*P2 + (A(3,3) - B(3,3) + D(3,3))*N2
     $         + 2*N*A(1,3)*P
      F(1,2) = (A(1,2) + A(3,3) + B(1,2) + B(3,3))*P*N
     $         + N2*A(2,3) + P2*(A(1,3) + 2*B(1,3) + D(1,3))
      F(1,3) = (B(1,1) + D(1,1))*P**3 + ((B(1,2) + 2*B(3,3) -D(3,3))*N2
     $         + A(1,2))*P + N*P2*(3*B(1,3) + D(1,3))
     $         + N**3*(B(2,3) - D(2,3)) + N*(A(2,3) - B(2,3) + D(2,3))
      F(2,2) = (A(3,3) + 3*B(3,3) + 3*D(3,3))*P2 + (1 + B(2,2))*N2
     $         + 2*N*(A(2,3) + 2*B(2,3) + D(2,3))*P
      F(2,3) = (B(1,2) + 2*B(3,3) + D(1,2) + 3*D(3,3))*P2*N
     $         + B(2,2)*N**3 + N + (B(1,3) + 2*D(1,3))*P**3
     $         + (N2*(3*B(2,3) + 2*D(2,3)) + A(2,3) + B(2,3))*P
      POM    = D(2,2)*(N2 - 1)**2 + (2*N2 - 1)*B(2,2) + 1
      F(3,3) = D(1,1)*P2**2 + 2*(N2*(D(1,2) + 2*D(3,3))
     $         + B(1,2))*P2 + POM + 4*N*D(1,3)*P**3
     $         + 2*N*(2*N2*D(2,3) + 2*B(2,3) - D(2,3))*P
      F(2,1) = F(1,2)
      F(3,1) = F(1,3)
      F(3,2) = F(2,3)
      RETURN
      END
C
C*************************************************************************
C
C   THIS SUBROUTINE CALCULATES THE FIBER VOLUME-FRACTION FROM THE RESULTS
C   OF FIBER WEIGHT-FRACTION DETERMINATION TESTS AND FIBER AND MATRIX
C   DENSITIES, AS WELL AS VOID VOLUME WHEN IT IS AVAILABLE.
C   IT WAS CHECKED AND FOUND CORRECT.
C
      SUBROUTINE VOLFRA
C
    5 DO 10, I=1,8
        WRITE(*,*)' '
   10 CONTINUE
      WRITE(*,*)'*** VOLUME-FRACTION CALCULATION ***'
      WRITE(*,*)' '
      WRITE(*,*)'SUPPLY THE FOLLOWING DATA:'
      WRITE(*,*)'FIBER WT-FRAC.,VOID VOL.,FIBER DEN.,MATRIX DEN.'
      READ (*,*) WTFRAC,VVOID,FIBDEN,RESDEN
      VFRAC = WTFRAC/(WTFRAC + FIBDEN*(1-WTFRAC)/RESDEN
     $        + FIBDEN*VVOID)
      WRITE(*,*)' '
      WRITE(*,*)'*** VOLUME FRACTION OF FIBER = ',VFRAC
      WRITE(*,*)'*** PLEASE NOTE THIS VALUE NOW !!!!! ***'
      WRITE(*,*)'*** IT WILL NOT BE RETAINED !!!!!!!! ***'
      WRITE(*,*)'FOR ANOTHER CALCULATION, PRESS 1; OTHERWISE, PRESS 0.'
      READ (*,*) IREPET
      IF(IREPET .EQ. 1) GO TO 5
      RETURN
      END
C
C*************************************************************************
```

```
C
C   THIS SUBROUTINE EXPANDS THE VECTORS OF MATERIAL PROPERTIES
C   TO ALL THE LAYERS IN THE WALL THICKNESS.
C   IT WAS CHECKED AND FOUND CORRECT.
C
      SUBROUTINE PUT(A,B,IM,IL,IN)
C
      REAL A(101),B(101)
      INTEGER IM(101)
C
      JJ = 0
      DO 300, I=1,IN
         IP = IM(I) - 1
         IF(IP .EQ. 0) GO TO 200
         K = JJ + IP + 1
         DO 100, KK=JJ+1,K
            JJ    = JJ + 1
            B(KK) = A(I)
  100    CONTINUE
         GO TO 300
  200    JJ = JJ + 1
         B(JJ) = A(I)
  300 CONTINUE
      DO 400, I=1,IL
         A(I) = B(I)
  400 CONTINUE
      RETURN
      END
C
C*****************************************************************
C
C   THIS SUBROUTINE GENERATES ANGLES IN A "MULTI-SOLUTION" RUN.
C   IT WAS CHECKED AND FOUND CORRECT.
C
      SUBROUTINE MDPUT1(A,IL,LAYPR)
C
      REAL A(101)
C
      DO 100, K=LAYPR*2,LAYPR*2+1
         A(K) = - A(K-1)
  100 CONTINUE
      RETURN
      END
C
C*****************************************************************
C
C   THIS SUBROUTINE GENERATES ANGLES IN A SINGLE-SOLUTION RUN.
C   IT WAS CHECKED AND FOUND CORRECT.
C
      SUBROUTINE MDPUT2(A,IL,LAYPR)
C
      REAL A(101)
C
      DO 100, I=2,IL
```

```
         A(I) = - A(I-1)
  100 CONTINUE
      RETURN
      END
C
C*****************************************************************
C
C   THIS SUBROUTINE CALCULATES THE ELASTIC MODULUS PARALLEL TO
C   THE FIBER DIRECTION USING THE RULE OF MIXTURES.
C   IT WAS CHECKED AND FOUND CORRECT.
C
        SUBROUTINE CE1(EE1,EF,VF,EM,IN)
C
        REAL EE1(101),EF(101),EM(101),VF(101)
C
      DO 100, I=1,IN
         EE1(I) = EF(I)*VF(I) + EM(I)*(1 - VF(I))
  100 CONTINUE
      RETURN
      END
C
C*****************************************************************
C
C   THIS SUBROUTINE CALCULATES THE MAJOR POISSON'S RATIO USING
C   THE RULE OF MIXTURES.
C   IT WAS CHECKED AND FOUND CORRECT.
C
      SUBROUTINE CCCPF(EF,EM,VF,GF,GM,CCP,IN)
C
      REAL EM(101),EF(101),GF(101),GM(101),VF(101),CCP(101)
      REAL CPF(101),CPM(101)
C
      DO 100, I=1,IN
         CPF(I) = EF(I)/(2*GF(I)) - 1
         CPM(I) = EM(I)/(2*GM(I)) - 1
         CCP(I) = CPF(I)*VF(I) + CPM(I)*(1 - VF(I))
  100 CONTINUE
      RETURN
      END
C
C*****************************************************************
C
C   THIS SUBROUTINE SUPPLIES INFORMATION ON THE PROGRAM WHEN
C   REQUIRED BY THE USER.
C
      SUBROUTINE INFO1
C
      WRITE(*,*)' '
      WRITE(*,*)' '
      WRITE(*,*)'      *****  PROGRAM INFORMATION  *****'
      WRITE(*,*)' '
      WRITE(*,*)' '
      WRITE(*,*)'THIS PROGRAM CALCULATES  CRITICAL EXT. PRESSURE FOR'
      WRITE(*,*)'CIRCULAR CYL. SHELLS SUBJECTED TO BUCKLING LOADS.'
```

```
      WRITE(*,*)'TWO LOADING CASES ARE CONSIDERED:'
      WRITE(*,*)'     1. HYDROSTATIC EXTERNAL PRESSURE'
      WRITE(*,*)'     2. UNIFORM LATERAL EXTERNAL PRESSURE.'
      WRITE(*,*)' '
      WRITE(*,*)'THE WALL CONSTRUCTION MAY VARY FROM SINGLE-LAYER'
      WRITE(*,*)'HOMOGENEOUS ISOTROPIC TO ANISOTROPIC LAMINATED,OR ANY'
      WRITE(*,*)'COMBINATIONS OF SUCH SUCH LAYERS (MAX. OF 101 LAYERS).'
      WRITE(*,*)' '
      WRITE(*,*)'ALL CALCULATIONS REFER TO THE SHELL MIDDLE SURFACE.'
      WRITE(*,*)' '
      WRITE(*,*)' '
      WRITE(*,*)' '
      PAUSE
      WRITE(*,*)' '
      WRITE(*,*)'TWO SOLUTION PATHS ARE AVAILABLE. THE FIRST'
      WRITE(*,*)'WILL FIND THE SINGLE CRITICAL PRESSURE FOR A KNOWN'
      WRITE(*,*)'VESSEL WALL CONSTRUCTION.'
      WRITE(*,*)'THE SECOND PATH WILL FIND THE "N" CRITICAL PRESSURES'
      WRITE(*,*)'FOR A VESSEL WITH A SINGLE CORROSION BARRIER LAYER'
      WRITE(*,*)'INSIDE, AND "N" PAIRS OF FILAMENT WINDING LAYERS'
      WRITE(*,*)'(WHERE "N" CAN BE AS MANY AS 50). ALL F.W. LAYERS'
      WRITE(*,*)'WILL HAVE THE SAME +/- WINDING ANGLE.'
      WRITE(*,*)'THE FORMER IS CALLED A "SINGLE-SOLUTION" RUN.'
      WRITE(*,*)'THE LATTER IS CALLED A "MULTI-SOLUTION" RUN.'
      WRITE(*,*)' '
      WRITE(*,*)'THE PROGRAM RUNS IN INTEROGATIVE MODE, THE USER'
      WRITE(*,*)'ANSWERING QUESTIONS FROM THE TERMINAL.'
      WRITE(*,*)' '
      WRITE(*,*)'RESULTS OF ANY RUN CAN BE OUTPUT IN REPORT FORM TO'
      WRITE(*,*)'FILE "BUCKREP.DAT" WHICH THE USER CAN PRINT OUT.'
      WRITE(*,*)' '
      PAUSE
      RETURN
      END
C
C*********************************************************************
```

Appendix 9. Program Output on Four Tubes

BUCKLING OF
COMPOSITE PRESSURE VESSELS

ORIGIN: CONCORDIA UNIVERSITY
MECHANICAL ENGINEERING DEPT.
COMPOSITE MATERIALS RESEARCH GROUP
1455 de MAISONNEUVE O.
MONTREAL, QUEBEC H3G 1M8

DATE WRITTEN: 84.09.17

DATE OF LAST REVISION: 85.04.16

REPORT ON TUBE #1

HYDROSTATIC PRESSURE LOADING

*** NOTE UNITS: kPa, m, degrees

VESSEL WALL CONSTRUCTION :

Layer #	E11	E22	G12	NU 12	THETA	THICKNESS
1	.276E+07	.276E+07	.100E+07	.380	.0	.00476
2	.337E+08	.776E+07	.283E+07	.307	54.0	.00052
3	.337E+08	.776E+07	.283E+07	.307	-54.0	.00052

WALL THICKNESS = .00580

RADIUS TO MIDDLE SURFACE = .13590

VESSEL LENGTH = .864

```
**********************************************************************
*                                                                    *
*     CRITICAL PRESSURE              =      317.19                   *
*     CRITICAL CIRCUM. WAVE NO.      =      2                        *
*     CRITICAL AXIAL HALF WAVE NO.   =      1                        *
*                                                                    *
**********************************************************************
```

REPORT ON TUBE #2

HYDROSTATIC PRESSURE LOADING

*** NOTE UNITS: kPa, m, degrees

VESSEL WALL CONSTRUCTION :

Layer #	E11	E22	G12	NU 12	THETA	THICKNESS
1	.276E+07	.276E+07	.100E+07	.380	.0	.00476
2	.403E+08	.950E+07	.346E+07	.298	63.0	.00047
3	.403E+08	.950E+07	.346E+07	.298	-63.0	.00047

WALL THICKNESS = .00570

RADIUS TO MIDDLE SURFACE = .13585

VESSEL LENGTH = .864

```
**********************************************************************
*                                                                    *
*     CRITICAL PRESSURE              =      304.88                   *
*     CRITICAL CIRCUM. WAVE NO.      =      2                        *
*     CRITICAL AXIAL HALF WAVE NO.   =      1                        *
*                                                                    *
**********************************************************************
```

REPORT ON TUBE #3

HYDROSTATIC PRESSURE LOADING

*** NOTE UNITS: kPa, m, degrees

VESSEL WALL CONSTRUCTION :

Layer #	E11	E22	G12	NU 12	THETA	THICKNESS
1	.352E+08	.811E+07	.296E+07	.305	54.0	.00047
2	.352E+08	.811E+07	.296E+07	.305	-54.0	.00047
3	.352E+08	.811E+07	.296E+07	.305	54.0	.00047
4	.352E+08	.811E+07	.296E+07	.305	-54.0	.00047
5	.352E+08	.811E+07	.296E+07	.305	54.0	.00047
6	.352E+08	.811E+07	.296E+07	.305	-54.0	.00047

WALL THICKNESS = .00282

RADIUS TO MIDDLE SURFACE = .13841

VESSEL LENGTH = .876

```
**************************************************************
*                                                            *
*     CRITICAL PRESSURE              =      134.39           *
*     CRITICAL CIRCUM. WAVE NO.      =      3                *
*     CRITICAL AXIAL HALF WAVE NO.   =      1                *
*                                                            *
**************************************************************
```

REPORT ON TUBE #4

HYDROSTATIC PRESSURE LOADING

*** NOTE UNITS: kPa, m, degrees

VESSEL WALL CONSTRUCTION :

Layer #	E11	E22	G12	NU 12	THETA	THICKNESS
1	.411E+08	.973E+07	.354E+07	.297	63.0	.00045
2	.411E+08	.973E+07	.354E+07	.297	-63.0	.00045
3	.411E+08	.973E+07	.354E+07	.297	63.0	.00045
4	.411E+08	.973E+07	.354E+07	.297	-63.0	.00045
5	.411E+08	.973E+07	.354E+07	.297	63.0	.00045
6	.411E+08	.973E+07	.354E+07	.297	-63.0	.00045

WALL THICKNESS = .00270

RADIUS TO MIDDLE SURFACE = .13735

VESSEL LENGTH = .868

```
**************************************************************
*                                                            *
*     CRITICAL PRESSURE              =      172.73           *
*     CRITICAL CIRCUM. WAVE NO.      =      3                *
*     CRITICAL AXIAL HALF WAVE NO.   =      1                *
*                                                            *
**************************************************************
```

***** THE END *****

Appendix 10. Determination of Laminate Modulus

Consider an element of the shell wall as shown in the sketch below. For equilibrium in the axial direction,

$$F = A_1 \sigma_1 + A_2 \sigma_2 + \ldots + A_n \sigma_n \quad , \qquad \text{(A10.1)}$$

where A_i is the area of layer i

σ_i is the stress in layer i

F is the external axial load

and n is the number of layers.

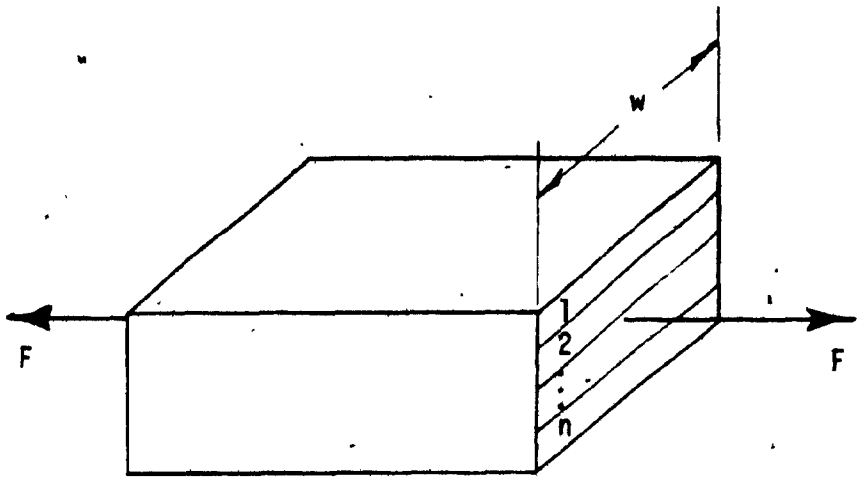

Assuming the layers to deform equally in the axial direction,

$$\varepsilon_1 = \varepsilon_2 = \ldots = \varepsilon_n = \varepsilon_{lam} \qquad \text{(A10.2)}$$

where the subscript "lam" refers to the laminate.

Since $\sigma = \varepsilon E$, (A10.3)

substituting A10.3 into A10.1 and noting A10.2,

$$F = A_1 \varepsilon_{lam} E_1 + A_2 \varepsilon_{lam} E_2 + \ldots + A_n \varepsilon_{lam} E_n \quad . \qquad \text{(A10.4)}$$

Also, we have $$\frac{\sigma_{lam}}{\varepsilon_{lam}} = \frac{F}{A_{lam}\, \varepsilon_{lam}} = E_{lam} \qquad \text{(A10.5)}$$

giving $$F = A_{lam}\, \varepsilon_{lam} E_{lam} \qquad \text{(A10.6)}$$

Equating A10.4 and A10.6, and cancelling ε_{lam},

$$A_{lam}E_{lam} = A_1E_1 + A_2E_2 + \ldots + A_nE_n \quad . \qquad \text{(A10.7)}$$

For unit width of the element sketched (i.e., w = 1), we find

$$A_i = t_i \times 1 \quad , \qquad \text{(A10.8)}$$

where t_i is the thickness of layer i .

Substituting (A10.8) into (A10.7) and rearranging,

$$E_{lam} = \sum_{i=1}^{n} \frac{t_i}{t_{lam}} E_i \quad . \qquad \text{(A10.9)}$$

The thicknesses are available nominally, or by measurement. The axial modulus of a given layer can be found using equation 10. Note that the same can be done for the hoop modulus.